FEASIBILITY STUDY OF ULTRASOUND MEASUREMENTS ON THE HUMAN LUMBAR SPINE

Except where reference is made to the work of others, the work described in this thesis is my own or was done in collaboration with my advisory committee. This thesis does not include proprietary or classified information.

Phani Bhushan Pothuganti Virabadra Venkat

Certificate of Approval:

Ram Gudavalli
Adjunct Associate Professor
National University of Health Sciences
Associate Professor
Palmer Center for Chiropractic Research

P.K. Raju, Chair
Thomas Walter Professor
Mechanical Engineering

Dan Marghitu
Professor
Mechanical Engineering

Joe F. Pittman
Interim Dean
Graduate School

FEASIBILITY STUDY OF ULTRASOUND MEASUREMENTS ON THE HUMAN LUMBAR SPINE

Phani Bhushan Pothuganti Virabadra Venkat

A thesis

Submitted to

the Graduate Faculty of

Auburn University

in Partial Fulfillment of the

Requirements for the

Degree of

Master of Science

Auburn, Alabama
December 15, 2006

FEASIBILITY STUDY OF ULTRASOUND MEASUREMENTS ON THE HUMAN

LUMBAR SPINE

Phani Bhushan Pothuganti Virabadra Venkat

Permission is granted to Auburn University to make copies of this thesis at its discretion, up on request of individuals or institutions and at their expense. The author reserves all publication rights.

____
Signature of Author

____
Date of Graduation

VITA

Phani Bhushan Pothuganti Virabadra Venkat, only son of LaxmiKantham Pothuganti and Vidyavathi Pothuganti, was born in Banswada, Nizamabad District, Andhra Pradesh, India on November 07, 1982. He finished his high school from Dilsukhnagar Public School and later joined in Ideal Junior College for his Intermediate Education. Later he went to Bangalore for pursuing his Bachelor of Engineering in Mechanical at Shirdi Sai Engineering College, Visveswaraiah Technological University. After graduating from Shirdi Sai Engineering College he then entered the Graduate school at Auburn University in the Department of Mechanical Engineering in August 2004. While at Auburn University, he was a teaching assistant for various courses in the engineering and business disciplines. He also worked as a research assistant under the valuable guidance of Dr. P.K. Raju and Dr. Ram Gudavalli and graduated in September 2006 with a Master of Science in Mechanical Engineering.

THESIS ABSTRACT

FEASIBILITY STUDY OF ULTRASOUND MEASUREMENTS ON THE HUMAN LUMBAR SPINE

Phani Bhushan Pothuganti Virabadra Venkat

Master of Science, December 15, 2006
(B.E., Vishveswaraiah Technological University, 2004)

167 Typed Pages

Directed by P. K. Raju

This study is a part of a research project that aims to measure the variation in the intervertebral distance of patients that are subjected to lumbar flexion-distraction chiropractic manipulation. The purpose of this research project is to evaluate the feasibility of using a B-scan image generated by a customized ultrasonic design to measure the distance between the adjacent lumbar vertebrae

Previous research using the same customized ultrasonic design was done and it was found that the reproducibility of the measurement expressed in terms of the coefficient of variation for measurements of the artificial model was found to be better than 0.1% (0.013 mm standard error), whereas for measurements of human subjects it was better than 1% (0.1 mm standard error). The excellent results obtained from the test conducted on the artificial model verify the reliability of the testing instrumentation and methodology. Before this system is routinely used in clinical situations it needs to

undergo further testing process. This system was tested to measure the distance between the lumbar vertebrae of the artificial spine model by scanning the transverse process instead of the spinous process. This experimentation showed us a few drawbacks and certain limitations of using this ultrasonic design equipment.

As a consequence we employed the commercially available high-end ultrasonic device, Philips HDI 5000. Several experiments were conducted on the artificial spine model using this ultrasound machine, such as measuring the distance between the transverse process of the lumbar vertebrae, measuring the depth of the transverse process from the surface of the gelatin solution and measuring the width of each transverse process. Experiments were also made to measure the width of each spinous process of the lumbar vertebrae and these measurements were then compared with the measurements obtained from our customized ultrasound system and also with the physical measurements from the vernier calipers. Measurements obtained from the two ultrasound systems and vernier calipers were very close.

Further tests were conducted on the customized ultrasound system to measure the distance between the lumbar vertebrae (L1, L2 and L3) by imaging the spinous process in a traction conditioned situation. To simulate the traction in the artificial spine, 1 mm rings were used and were placed in-between the vertebral body and the distance was measured. The distance between the lumbar vertebrae was increased by 1 mm for each set of experiments. The results obtained showed that the custom-built ultrasonic system can be used to measure the distance between the lumbar vertebrae by imaging the spinous process in a traction condition. However, a commercially available sophisticated system is needed if the distance between the lumbar vertebrae by imaging the transverse process.

ACKNOWLEDGEMENTS

I would like to express my deepest gratitude towards Dr. P.K. Raju and Dr. Ram Gudavalli for their support, motivation and guidance throughout the research work. I would like to thank Dr. Dan Marghitu for being a positive support throughout my research work and for serving as a committee member. I would also like to thank Dr. David Beale and his student, David Branscomb, for their help in manufacturing the slider.

I would like to thank Dr.Cramer at NUHS on the advice of gel preparation, support of equipment and travel from Cox funds at NUHS and Auburn University. I would also like to extend my appreciation to Dr. Holly McCort and Dr. Hudson for their valuable time and help in conducting the experiments at veterinary school facility, AU.

I wish to express my gratitude to all my family members for being supportive and keeping faith in me at all times. I am highly indebted to my parents, for unconditional love and support, and for always encouraging me to follow my dreams. They have dedicated a great deal of their life to keeping me happy, healthy and successful, and for that I am forever grateful and dedicate this thesis to them.

A special thanks to Sri Harsha, who was always there by my side when I needed the most and provided me with constant support, love and encouragement. Big thanks to all my friends for their support and encouragement. Finally, I want to thank god for guiding me and giving me the encouragement, strength and will to pursue my goal in accomplishing this research work and having the pleasure to see it terminate fruitfully.

Style manual or journal used: *Journal of ASME*

Computer software used: *Microsoft word 2003*

TABLE OF CONTENTS

LIST OF FIGURES

LIST OF TABLES

1. INTRODUCTION

1.1 Overview

Ultrasound has been accepted as a potential imaging utility since the 1940s. Since then, ultrasound has been applied for various medical purposes. Today ultrasound is ranked as a major diagnostic tool in medicine. Its applications are constantly expanding in new diagnostic areas. Obviously, continuous change and continuous improvement are the role in the field of diagnostic ultrasound equipment [1].All the modern clinical ultrasound machines currently in commercial use are based on the construction of an image from the backscattered ultrasound waves [2].

A variety of medical technicians including radiographers, physiological measurement technicians, specialist technicians in ultrasound, medical engineers and physicists play role a in medical diagnostic ultrasound. A well-trained level of expertise in ultrasound is definitely needed for any ultrasound examination procedure.

There are two main types of ultrasonic measurement. First, the Quantitative Ultrasound (QUS), which is a reliable, fast and cost-effective method of determining tissue composition, assess muscle thickness and non-invasively determine bone-mineral-density, risk of fractures, skin pathology, body fat and muscle thickness. In this kind of measurement, ultrasonic waves pass through the site under investigation and reflect back from different kinds of tissue and bone components. The strength of the reflected waves is then correlated to measure tissue composition, bone-mineral-density and body fat [3, 4, 5]. The Second type of measurement is known as Diagnostic Ultrasound (DUS), which covers the imaging aspects of the tissues and skeletal structures [6, 7, 8, 9, 10]. In these types of measurements, a narrow beam of ultrasound is focused onto the tissues, bones, muscles and different body organs, and a pictorial representation of the area of interest can be obtained and used for evaluation and diagnosis purposes [1]. The fundamental mechanism that creates the ultrasound image is the strength of the reflected waves (echoes). The frequency of the ultrasound used for diagnosis depends on a number of factors, including the properties of tissues or organs examined, depth of the tissues or organs from the skin surface, quality of image required and many others.

This research project falls under the diagnostic ultrasound (DUS) measurement. We image the lumbar vertebrae of the human spine and calculate the distance between them before and after the flexion-distraction chiropractic manipulation. In the chiropractic medicine, it is of major importance to calculate the variations in intervertebral distance when patients are treated by the Cox Flexion-Distraction technique.

Figure 1.1: Cox Flexion Distraction Table

Flexion-distraction is an excellent technique for the treatment of middle and lower back pain. It is a gentle and extremely effective technique that helps to decompress the spine and remove pressure on vertebral discs. In addition, it restores range of motion to the spine and realigns the vertebrae. Flexion-distraction is the treatment of choice for many patients suffering with back pain. Most patients experience relief after 3 to 5 treatments. The treatments are comfortable and performed on a fully adjustable ergonomic table that can be fit to all body types including pregnant women. Flexion-distraction should be considered for those whose pain has not responded to other types of care. This treatment can make all the difference in removing and managing your pain permanently [34].

Theoretically, the traction or distraction of the disc combined with isolation and gentle pumping of the involved area allows the central area of the disc, the nucleus pulposus, to assume its central position in the disc. Flexion-distraction is thought to increase the intradiscal height and reduce intradiscal pressures [35]. The largest vertebral mobility under this technique is found in the lumbar and cervical spine section.

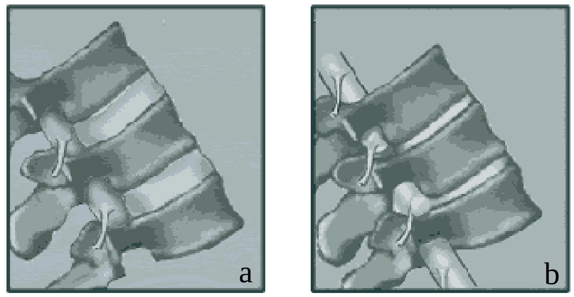

Figure 1.2: Intervertebral distance a) after and b) before flexion-distraction treatment.

To measure the intervertebral distance before and after the flexion-distraction treatment, we can use MRI, X-Ray or Computed Tomography (CT), but these techniques are expensive, ionizing and complex in setup and operations. An inexpensive, sensitive, portable and non-invasive technique for measuring this intervertebral distances. This can be achieved through the application of ultrasound technique.

Literature search revealed a lack of this kind of ultrasound application to calculate the intervertebral distance before, during and after the flexion distraction technique. On the other hand, many investigations were found in measuring the intervertebral distance during the diurnal changes [7, 8] and weight bath therapy [11].

1.2 Main Objective:

The main objective of this research project is to measure the variation in intervertebral distances of patients who are subjected to lumbar flexion-distraction chiropractic manipulation.

The specific goals that will contribute to achieve the objective are:

- Measuring the distance between the vertebrae by scanning the transverse process instead of the spinous process.
- Conducting the experiments on Phillips HDI 5000 CV, ultrasound system and comparing some of the values obtained with our customized built ultrasound system and evaluating the accuracy of our system.
- Simulating the traction condition in the artificial spine using 1mm metal rings and evaluating the reliability of the custom-built ultrasonic design and testing procedure to consistently locate the spinous processes and measure the distance between them.

2. ULTRASONIC WAVE PROPAGATION THEORY

2.1 Evolution of Ultrasonic's

Like so much else in engineering, ultrasonic theory has undergone its greatest and most rapid development in the 19th and 20th centuries. In 240 B.C., the Greek philosopher Chtysippus, speculated that sound took the form of waves. The father of acoustics, Galileo Galilei, and Marin Mersenne developed the first laws governing sound in the 16th and 17th centuries. Sir Isaac Newton developed the first mathematical theory of sound in 1686. Newton's theory allowed for wave phenomena such as diffraction. Later Newton's theory was expanded by Euler, Lagrange, and d'Alembert which led to the development of the wave equation. The wave equation developed by Euler, Lagrange, and d'Alembert allowed sound waves to be represented mathematically [12].

In 1880, Curie discovered the crystals which can convert the ultrasonic energy to electrical energy. The inverse effect known as the piezoelectric effect, converting the electrical energy into ultrasonic energy, was discovered by Lippmann in 1881 [12]. After these discoveries, one of the more practical ultrasonic endeavors was the detection of icebergs at sea, developed in 1912 as a direct response to the sinking of the Titanic. This technique of sending sound waves through water and observing the returning echoes to characterize submerged objects inspired early ultrasound investigators to explore ways to apply the concept to medical diagnosis [37]. In 1929 and 1935, Sokolov studied the use of ultrasonic waves in detecting metal objects. Mulhauser, in 1931, obtained a patent for using ultrasonic waves, using two transducers to detect flaws in solids. Firestone (1940) and Simons (1945) developed pulsed ultrasonic testing using a pulse-echo technique.

Shortly after the close of World War II, researchers in Japan began to explore the medical diagnostic capabilities of ultrasound. The first ultrasonic instruments used an A-mode presentation with blips on an oscilloscope screen. That was followed by a B-mode presentation with a two dimensional, gray scale imaging.

This Japanese achievement in ultrasound was relatively unknown in the United States and Europe until the 1950s. The same researchers then presented their findings on the use of ultrasound to detect gallstones, breast masses, and tumors to the international medical community. Japan was also the first country to apply Doppler ultrasound, an application of ultrasound that detects internal moving objects, such as blood coursing through the heart for cardiovascular investigation.

Ultrasound pioneers working in the United States contributed many innovations and important discoveries to the field during the following decades. Researchers learned to use ultrasound to detect potential cancer and to visualize tumors in living subjects and in excised tissue. Real-time imaging, another significant diagnostic tool for physicians, presented ultrasound images directly on the system's CRT screen at the time of scanning. The introduction of spectral Doppler and later color Doppler depicted blood flow in various colors to indicate speed of flow and direction. The United States also produced the earliest hand-held "contact" scanner for clinical use, the second generation of B-mode equipment, and the prototype for the first articulated-arm hand-held scanner, with 2-D images [37].

2.2 Characteristics of Ultrasonic Waves

Ultrasonic waves are high (“ultra”) frequency sound (“sonic”) waves. They vibrate at a frequency above 20,000 vibrations per second, or 20,000 Hz- too fast to be audible to humans. Our ear can detect frequencies between about 20 Hz (for example, the sound form a bumblebee’s wing) and 17 Khz (the sound from a whistle). Any sound at a higher frequency is ultrasonic and is inaudible.

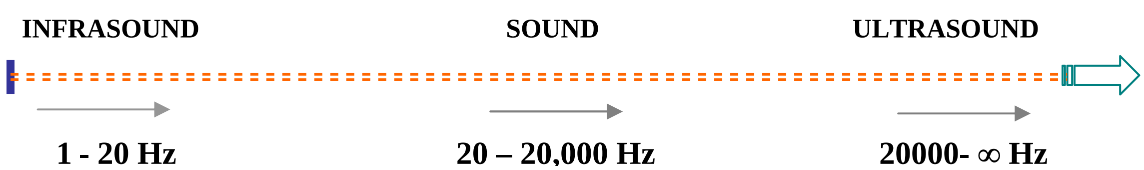

Figure 2.1: Acoustical Frequency Spectrum

Based on the frequency of ultrasound waves, applications can be divided into two groups: (1) applications which use low frequency ultrasound of order 200KHz to 20 MHz, (used to diagnose the physical condition of the material) and (2) applications which use high frequency ultrasound of order 50MHz, (to act on a given material (therapy) to provoke a stimulus or a transformation in the material). Low frequency ultrasound utilizes only as much energy as needed to transmit a sufficiently clear signal through a material. By assessing the behavior and transformation of the wave in the medium, the condition and some characteristics of the material or specimen can be determined.

Among the reasons that justify the use of high frequency waves for the evaluation of materials (instead of using audible frequencies) are:

a) The absorption coefficients of waves at high frequencies are considerably high, thus their use in providing a sensitive parameter for evaluating variations in the internal condition of material.

b) The small wavelength associated with the propagation of high frequencies make the ultrasonic testing sensitive to small heterogeneities along the wave path. Ultrasonic waves can detect heterogeneities equal to or larger than $\lambda/2$; therefore, higher frequencies make the testing sensitive to the presence of smaller singularities (e.g. defects, tiny tissues, air bubbles, and small particles, so on).

Ultrasonic testing is accomplished by introducing electronically controlled pulses into a material from an external surface. The mechanical wave then travels within the material and manifests alterations (attenuation, reflection, scattering, change of propagation mode, etc) as it traverses variations in the mechanical composition (or impedance) in its path. The resulting reflected beam is captured by a transducer, and its features (amplitude, shape, time of flight, etc) are examined for evaluation of the physical characteristics and condition of the material.

Some of the advantages of ultrasonics with respect to other NDT techniques are that defects may be detected in all kind of materials (metallic, nonmetallic, ferromagnetic, wood, ceramics, biomaterial, etc), and it can be also used to locate internal as well as superficial heterogeneities. Ultrasonic technique has rapid testing capabilities, and portable instrumentation is available for field and laboratory testing for a relatively low cost. Conversely, ultrasound is not exempt from limitations; certain physical and technological limitations restrict its use. There may be difficulty in coupling energy to rough surfaces, and it may be impractical to inspect complex shapes. Sometimes it is difficult to detect and measure the length of small, tight cracks or crack-like discontinuities. Also, rather extensive training is required for operators and data evaluators. The resolution of the test is subjected to the utilization of higher frequencies; however, as the frequency is increased, the damping of the wave increases as well. Therefore, a compromise has to be made between resolution and penetration depth.

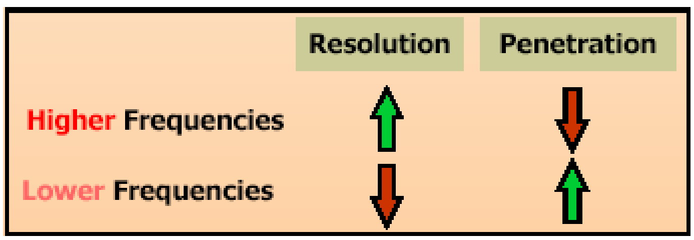

Figure 2.2: Relation between resolution and penetration depth

Many advantages of ultrasonics have led to rapid development in its use. The disadvantages, however, may be formidable, and the diligent NDE engineer must ensure that ultrasonics is the proper technique selection for the required task [13].

2.3 Basic Concepts

The presence of a medium - fluid or solid - is necessary for ultrasonic wave propagation. Wave propagation is the vibration or periodic displacement of successive elements of the medium. These low-energy vibrations (i.e., stress waves) can travel long distances in many liquids and solid materials as compared to travel in gases.

Materials having elastic properties will carry ultrasonic waves as long as their elastic internal forces are capable of holding the particles within their equilibrium position. When the particles of a medium are displaced from their equilibrium positions, internal restoring forces arise. These elastic restoring forces between particles combined with the inertia of the particles, lead to oscillatory motion within the medium.

Ultrasonic waves used for nondestructive testing are periodic and characterized by a central frequency ***"f"*** expressed in cycle-per-second or Hertz [Hz]. The ***frequency*** corresponds to the number of oscillations that a particle experiences in one second, its inverse value is called ***period***, denoted by ***"T"***, and is expressed in time units, see figure 2.3.

$$T = \frac{1}{f} \tag{2.1}$$

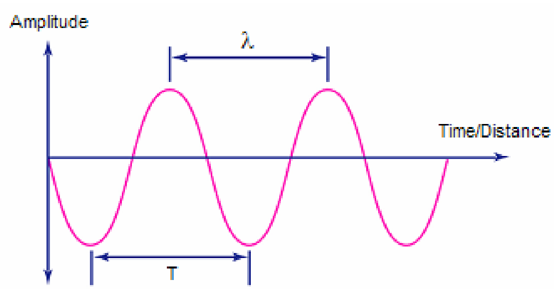

Figure 2.3: Harmonic Oscillation

The ***phase velocity, "c"***, normally expressed in meters-per-second [m/s], is defined as the rate at which any particle amplitude of the perturbation propagates. This parameter is in general determined by the elastic properties of the materials; therefore it is a distinctive characteristic of each medium. If the material is homogeneous and isotropic, the phase velocity will be constant. Both parameters, frequency and phase velocity, are related by the ***wavelength* "λ"**, expressed in longitude units. It represents the least distance between identical particle displacements in the propagation medium, and is given by

$$\lambda = \frac{c}{f} \qquad (2.2)$$

Sound travels through materials under the influence of sound pressure. Because molecules or atoms of a solid are bounded elastically to one another, the excess pressure results in a wave propagating through the solid. The resistance offered by the medium to the particle oscillation exposed to a perturbation is called ***Acoustical Impedance "Z"*** [Kg/m^{2}s]. A material having low impedance will offer slight resistance to deformations if an excitation acts on it and vice versa. It is expressed as

$$Z = \rho \cdot c \qquad (2.3)$$

Where, ρ is the material density.

Acoustic impedance is important in:

1. The determination of acoustic transmission and reflection at the boundary of two materials having different acoustic impedance.
2. The design of ultrasonic transducers.
3. Assessing absorption of sound in a medium.

The normal force applied by a longitudinal wave on a specific surface of a particle plane within the material is called ***Acoustical Pressure "P"***, equation 2.4.

If the wave has a shear propagation mode, it will apply a force parallel to the particle plane, then the pressure will be called shear stress. Both are expressed in Pascal [pa] or [N/m^2].

$$P = Z \cdot c \qquad (2.4)$$

2.4 Types of Ultrasonic Waves

The generation of ultrasonic waves can be done by any means that agitates liquids and gases or high-frequency displacements to surfaces of solid materials. Often, ultrasonic waves are generated using piezoelectric crystals and magnetostrictive materials. Other similar methods of wave generation use electromagnetic and electrostatic generators. Still other high frequency generators include whistle, mechanical vibrators, sirens, and thermal types such as high-energy laser pulses.

The major types of ultrasonic waves are longitudinal, transverse or shear, and surface or rayleigh waves. Most wave types are named according to relationships of particle motions relative to the direction of propagation of the ultrasonic beam [13].

Longitudinal waves: In longitudinal wave mode, particles move parallel to the direction of wave propagation. The longitudinal wave mode is also called a pressure wave or P-wave, because the stress of the periodic compression and rarefaction of the particles is along the direction of propagation (Fig 2.4).

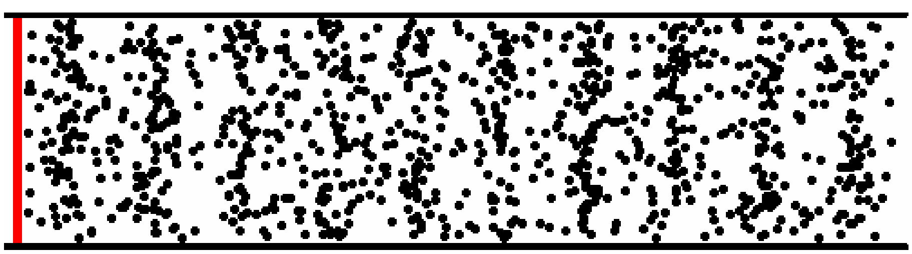

Figure 2.4 - Longitudinal Wave

Longitudinal waves can propagate in solids, liquids and gases and are most widely used for nondestructive testing of materials (Fig 2.5).

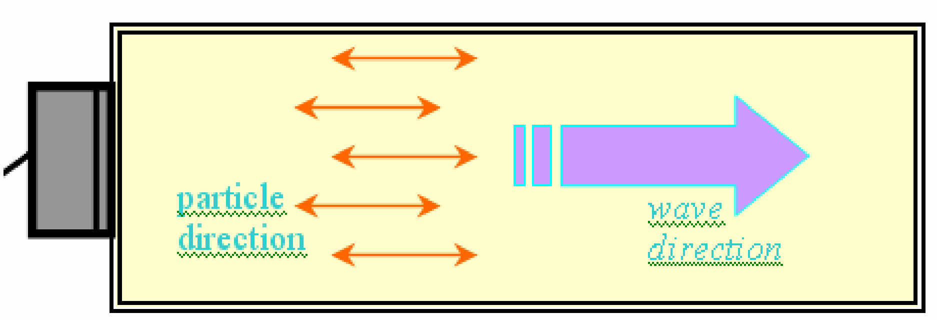

Figure 2.5: Longitudinal wave propagation in a material

Transverse or Shear Waves: The transverse wave mode is often called a shear wave. In these, the particle motion will be perpendicular to the propagation of the wave (fig 2.6). Transverse wave inspection is usually limited to solids, since propagation in liquids occurs only in the very viscous types. Low-viscosity fluids, such as air or water, do not support shear stresses, and thus shear waves cannot propagate through air or water.

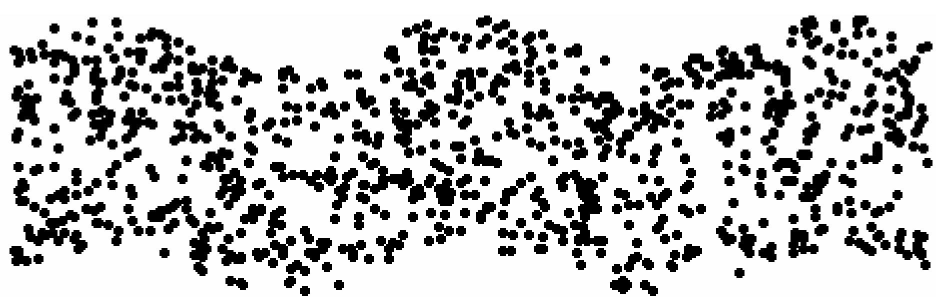

Figure 2.6: Transverse or Shear Wave

A shear wave penetration is normally achieved by using a longitudinal wave transducer attached to an acrylic wedge. According to Snell's Law, the proper selection of the angle of incidence of the beam will help propagate just transverse waves into the material, figure 2.7.

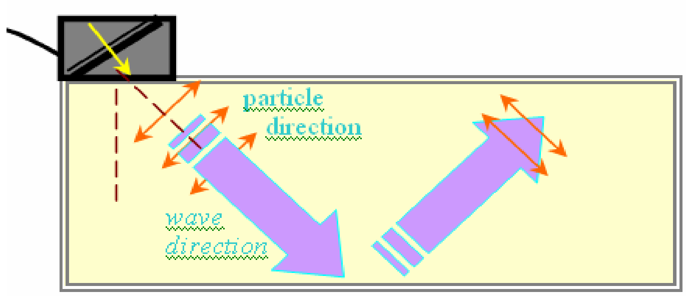

Figure 2.7: Transverse or Shear Wave propagation in a material

Surface Waves: These waves are also called Rayleigh waves. These waves propagate exclusively in the surface of materials to a depth of one wavelength.These waves have an elliptical particle motion in the vertical plane and normally travel undispersed on smooth surfaces (Fig 2.8).

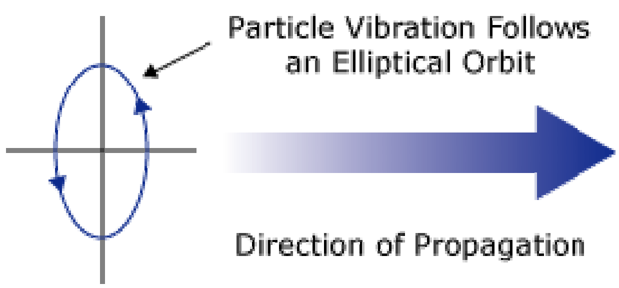

Figure 2.8: Surface Wave

There are other kinds of surface waves known as lamb or plate waves. These are used when the plate in which waves travel is thin compared to the wavelength [13].

Velocities of the various wave types are determined by modulus, density, and Poisson’s ratio of the material in which they propagate. Each type of wave has a different phase velocity, and in each case it depends on the elastic properties of the material and the relative size of the object. The propagation speed or phase velocity of longitudinal (c_L), transverse (c_T), and surface (c_s) waves can respectively be expressed as

$$c_L = \sqrt{\frac{E(1-\mu)}{\rho(1+\mu)(1-2\mu)}} \qquad (2.5)$$

$$c_T = \sqrt{\frac{E}{2\rho(1+\mu)}} = \sqrt{\frac{G}{\rho}} \qquad (2.6)$$

$$c_s = \frac{0.87+1.22\mu}{1+\mu} \cdot \sqrt{\frac{E}{2\rho(1+\mu)}} \qquad (2.7)$$

where “E” stands for Young's modulus, “G” is the Shear Modulus, “μ” is the Poisson’s Coefficient and “ρ” is the density of the propagation material

By relating the first two equations, an expression is found that associates the longitudinal wave velocity with the transverse wave velocity. This is:

$$c_T = c_L \sqrt{\frac{1-2\mu}{2(1-\mu)}} \qquad (2.8)$$

Table 2.1 illustrates the density, longitudinal and transverse wave velocity, and the acoustic impedance of some materials and substances.

MATERIAL	DENSITY [g/cm^3]	VELOCITY [km/s]		ACOUSTIC IMPEDANCE $Z=\rho \cdot c_L$ [Kg/m^{2}s] $\cdot 10^6$
		c_L	c_T	
Steel (structural steel)	7.85	5.82	3.19	45.7
Steel 1018 (Reference Block)	7.85	5.92	3.25	46.4
Aluminum	2.71	6.32	3.08	17.1
Alloy Al-Cu = AI L3120	2.78	6.25	3.10	17.4
Iron Cast	7.2	3.5-5.6	2.2-3.2	25-40
Iron Electrolytic	7.9	5.95	3.22	45
Inconel	8.25	7.82	3.02	64.5
Cooper	8.9	4.7	2.26	41.8
Gold	19.3	3.24	1.20	6.25
Platinum	21.4	3.96	1.67	8.47
Nickel	8.9	5.63	2.96	50
Silver	10.5	3.60	1.59	3.78
Lead 6% antimony	10.90	2.16	0.81	23.6
Brass	8.1	2.12	4.43	35.8
Plexiglas (PMMA, Perspex)	1.18	2.73	1.43	3.2
Zinc	7.1	4.17	2.41	29.6
Araldite	1.15-1.3	2.5-2.8	1.1	2.8-3.7
Quartz Glass	2.60	5.57	3.51	14.4
Rubber (vulcan)	1.2	2.30		2.8
Lithium Sulfate (Li_2SO_4)	2.06	4.72		8.6
Teflon	2.2	1.35		3.0
Oil (SAE 20 a30)	0.89-0.96	1.74		1.5-1.7
Bone	1.62	2.5-4.7		4-7.5
Water	1	1.48		1.48
Blood	1.06	1.57		1.66
Muscle	1.07	1.59		1.7
Fat	0.92	1.45		1.33
Glycerin	1.26	1.92		2.4
Air	0.0012	0.330		$0.389 \cdot 10^{-3}$

Table 2.1: Wave speed, density, and acoustic impedance for some materials

2.5 Behavior of Ultrasonic Waves at Boundaries

The reflection and refraction of the wave front at the boundaries or interface plays an important role in ultrasonic investigations. Voids, cracks, inclusions and coatings can be determined using this effect. Deviation of, or changes in, the wave as it encounters an interface or boundary can lead to one of the following:

- Reflection and/or transmission of the wave
- Propagation of the wave along the boundary or interface
- Change in direction of wave travel (refraction)
- Conversion from one type of wave to another type of wave (mode conversion)

To understand the behavior of the ultrasonic waves at the boundary, we need to understand the:

1) Normal Incidence
2) Oblique Incidence

Here we will discuss only the normal incidence because in our application we deal with the normal incidence of ultrasonic waves on the spinous process of the human vertebra. In normal incidence, a propagating plane wave impinges at 90^o onto a smooth surface separating mediums 1 & 2.

When an ultrasonic beam reaches a smooth boundary one then speaks of reflection; on the other hand, if the reached boundary is rough, i.e. it has irregularities, then the beam gets scattered. In this connection the roughness of the boundary is measured in terms of the wavelength size. When another material is behind the boundary and adherences to the first material so that forces can be transmitted, then the wave may propagate on it.

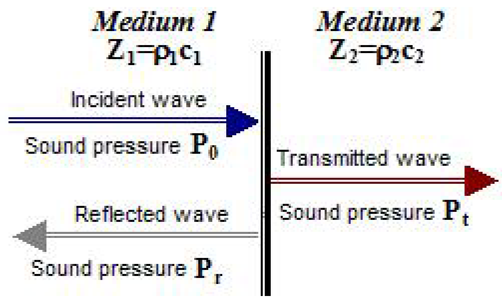

Figure 2.9: Normal incidence of an ultrasonic wave on a smooth boundary

Let's now consider the simple case of a plane wave striking at right angle a plane of smooth boundary that divides two different materials, figure 2.9. A Portion of the wave energy is transmitted to the second medium characterized by an acoustic impedance Z_2 and the remainder is reflected back within the incident medium characterized by an acoustic impedance Z_1. Both waves propagate in a right angle with respect to the boundary.

We now define the **Reflection coefficient** "**R**" as the ratio between the reflected acoustic pressure $\mathbf{P_r}$ and the acoustic incident pressure $\mathbf{P_0}$. The **Transmission coefficient** "**T**" is also defined as the ratio between the acoustic transmitted pressure $\mathbf{P_t}$ and the acoustic incident pressure $\mathbf{P_0}$. Both values are dimensionless.

$$R = \frac{P_r}{P_0} \quad \text{And} \qquad T = \frac{P_t}{P_0} \tag{2.9}$$

By using the relation between acoustic pressure and acoustic impedance, Eq. 2.4, we arrive at

$$R = \frac{Z_2 - Z_1}{Z_2 + Z_1} \tag{2.10}$$

$$T = \frac{2Z_2}{Z_1 + Z_2} \qquad (2.11)$$

From equation 2.10 and table 2.1 it can be inferred that the absolute value of reflection coefficient R tends to 1 (most of the energy is reflected back) when one of the mediums is air. This is a result of the low acoustical impedance of air compared with any other solid or liquid. If the acoustic impedance of the first medium is greater than the second medium, the reflection coefficient will take a negative value. This fact associates a shifting in the phase of the reflected wave with respect to the incident wave. As a consequence, it is concluded that the reflection coefficient is affected by the side where the wave strikes the interface. On the other hand, if the incident wave comes from the medium of less acoustic impedance, then the transmission coefficient will have a value greater than 1. Taking the impedance of PMMA (Plexiglas) Z_p and Aluminum Z_a as an example, and having PMMA as the incident medium, the coefficients R and T can be calculated as:

$$R = \frac{17 - 3.2}{17 + 3.2} = 0.68 \quad , \quad T = \frac{2 * 17}{3.2 + 17} = 1.7 \qquad \text{(e - 2.1)}$$

The transmitted wave has 170% the sound pressure of the incident wave. That is, the incident sound pressure is amplified in the second medium.

As a second example, consider the propagation from human soft tissue (muscle) $Z_s = 1.6 \cdot 10^6$ [kg/m^{2}s], and hard bone $Z_b = 7.5 \cdot 10^6$ [kg/m^{2}s], then R and T result in:

$$R = \frac{7.5 - 1.7}{7.5 + 1.7} = 0.63, \qquad T = \frac{2 \cdot 7.5}{7.5 + 1.7} = 1.63 \qquad \text{(e-2.2)}$$

These results confirm the stress (pressure) relation at the boundary

$$P_o + P_r = P_t \quad or \quad 1 + R = T \qquad (2.12)$$

The energy balance expressed in terms of intensities, calculated on a given boundary for a normal incidence furnishes:

$$I_0 = I_r + I_t \tag{2.13}$$

The expressions for the reflection and transmission coefficients are also valid for transverse waves. However, transverse waves are completely reflected from an interface solid-gas or liquid since shear waves in general do not propagate in these substances [12].

Power ratios are very important in ultrasonic inspection. The power expressions yield the rate at which energy is being transmitted by the wave front. Generally, power can be calculated by:

$$\text{Pwr} = \text{Stress} * \text{Velocity at a point} \tag{2.14}$$

In a similar manner, power expressions for the incident, transmitted, and reflected waves are:

$$Pwr_i = \frac{1}{2}\frac{EA^2{}_i\omega^2}{C_1} \tag{2.15}$$

$$Pwr_t = \frac{1}{2}\rho' C'_1 A^2{}_t\omega^2 \tag{2.16}$$

$$Pwr_r = \frac{1}{2}\rho C_1 A^2{}_r\omega^2 \tag{2.17}$$

Power transmission and reflection ratios can be obtained by algebraic manipulation, using the particle displacement:

$$\frac{Pwr_t}{Pwr_i} = \left[\frac{1 - Z_2/Z_1}{1 + Z_2/Z_1}\right]^2 \tag{2.18}$$

$$\frac{Pwr_r}{Pwr_i} = \frac{4[Z_2/Z_1]}{[1 + Z_2/Z_1]^2} \tag{2.19}$$

The behavior of both the pressure and the power at the boundary are important in nondestructive inspection [14].

2.6 Attenuation of Ultrasonic Waves

The behavior of an acoustic wave to lose energy when traveling through materials is known as attenuation. Attenuation of the waves occurs due to the following mechanisms:

- Absorption: dissipation of energy in the form of heat.
- Scattering: diffraction, reflection, and refraction of the ultrasonic wave due to discontinuities in the medium or at the surface of the medium.
- Beam Spreading: geometric expansion of a nonplanar wave front.
- Dispersion: Difference of velocities of different wave modes [12].

Attenuation is usually expressed in the following form

$$P = P_0 e^{-aL} \tag{2.20}$$

Where

P_0 = Original pressure level at a source or other reference location.

P= Pressure level at second reference location

a = Attenuation coefficient (Nepers per cm)

L= Distance of pulse travel form original source to second reference location.

Ultrasonic pulse attenuation is expressed in units of decibels (dB). This a convenient unit to use when the magnitude of the parameter being measured varies over a large range. Generally, these decibels are based on a logarithmic scale.

The relative sound pressure level (SPL) of a propagating wave is

$$SPL = 20\log\frac{P}{P_0}\,dB \qquad (2.21)$$

Where,

P = Effective Pressure of ultrasonic wave at observation point

P_0= Pressure at an earlier reference point.

If we consider two points in the ultrasonic wave path, then the sound pressure level loss for an ultrasonic wave passing between 1 & 2 is given by

$$SPL_1 - SPL_2 = 20\log\frac{P_1}{P_2}\,dB \qquad (2.22)$$

If the stations are separated by a distance L and the material has attenuation coefficient α , the above equation can be rewritten as

$$\alpha L = 20\log\frac{P_1}{P_2}\,dB \qquad (2.23)$$

Here L is the length and is generally expressed in meters. So, the units of α will be in decibels per meter [14].

The attenuation coefficient increases with increasing frequency. The table below gives the attenuation coefficients for soft tissue.

Frequency (MHz)	Average Attenuation Coefficient for Soft Tissue (dB/cm)
1.00	0.5
2.25	1.1
3.50	1.8
5.00	2.5
7.50	3.8
10.00	5.0

Table 2.2: Average Attenuation Coefficients for soft tissue

A simple proportional approximation is that soft tissue, on average, has 0.5 dB of attenuation per centimeter for each megahertz of frequency [15].

3. TESTING TECHNIQUES AND DATA PRESENTATION FOR ULTRASONIC TESTING

3.1 Introduction

Ultrasonic testing uses high frequency sound energy waves to conduct examinations and make measurements. Ultrasonic inspection can be used for flaw detection/evaluation, dimensional measurements, and material characterization, among other things.

The propagation of the ultrasonic waves in a material depends on the elastic properties of the material and also on the homogeneity of the material's structure. The direction of the waves and measurement of time taken for the waves to pass through the material or reflect from the back surface or defects is very important in the ultrasonic inspection.

A typical UT inspection system consists of several functional units, such as the pulser/receiver, transducer, and display devices. There are two kinds of testing techniques, which are normally used for inspection. They are:

1) Pulse Echo Technique
2) Through Transmission Technique

Our research project deals with pulse echo technique. We image the spinous process of the human lumbar vertebra from the waves reflected back from spinous process tips.

3.2 Pulse Echo Technique:

Pulse Echo technique is also known as the pulse transit-time method. This method has been in use since World War I for locating objects under water. The principle of the pulse echo technique is the simplest of all the ultrasonic testing methods and it is one of the most commonly used techniques.

In this technique a piezoelectric element excited by an extremely short electrical discharge transmits an ultrasonic pulse into a specimen. The probes (emitter-receiver) are coupled to the surface of the test object by a liquid or coupling paste so that the sound waves can transmit into the specimen from the emitter probe and from the specimen into the receiver probe. In some cases, a single transducer acts as both the transmitter and receiver, as shown in fig 3.1. If any flaw is found in its path then it reflects back an echo that is captured by the receiver probe. Another echo is reflected from the back wall but with a certain delay in respect to the first reflection. Observation of the received pulses can provide valuable information about the nature of the defect from which the pulses have been reflected and, perhaps, of the structure of the material being tested.

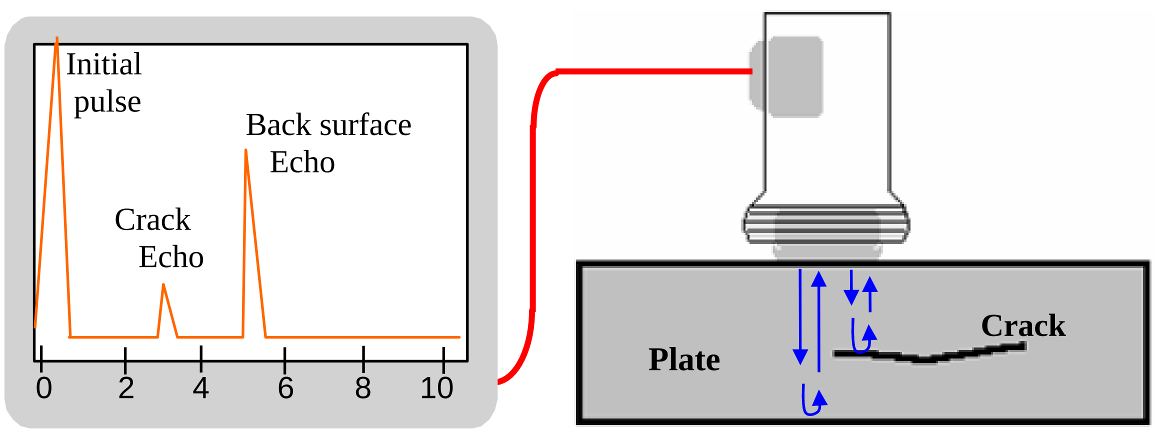

Figure 3.1: Basic schematic of pulse-echo testing technique. In the instrument screen we can see all the echoes received (i.e. back wall, crack echo and initial pulse)

If we know the velocity of the sound in the object, then the time of flight of the pulse obtained from the oscilloscope can be converted into distance or depth in the object. The intensity and shape of the reflected beam depend mainly on the material, attenuation, size of the reflector, frequency of the ultrasonic wave, location of the reflector within the object, defect orientation in respect to the axis of the beam, etc.

The main advantage of this method is that access from only one side of the object is necessary, provided that the back surface of the object is parallel to the surface where the transducer is placed.

3.2.1 Design of Pulse Echo Equipment

The figure 3.2 shows the basic design of the pulse echo method equipment. This is commonly known as the ultrasonic flaw detector, but it can be employed for many other applications. With the aid of this equipment, a trigger can excite simultaneously a time-base control and a pulse generator at regular intervals, usually between 50 and 1000 Hz. Once excited, the time-base control connected to the X-plates of the cathode ray oscilloscope causes the electron beam to sweep in a horizontal direction from left to right. We can use the range control device to vary the time of sweep so that it suites the acoustic path length. A multi-position switch can be used to extend the range of this continuous variation in time of sweep by several orders of magnitude. At the end of the sweep, the electron beam returns to its original position for the next excitation of the trigger. When there is no signal applied to the Y-plate, a bright horizontal trace appears on the oscilloscope screen.

Once excited by the trigger, the pulse generator feeds a direct potential difference, usually from several hundred to thousand volts and for an instantaneous duration to the electrodes of either a transmitting or reversible probe in contact with the material under the test. Pulse energy control can be used to adjust the magnitude of this applied voltage.

A reversible probe is used for a single probe operation and this is connected to an amplifier and rectifier, which can be bypassed if a display of the waveform is required, to the Y-plates of the oscilloscope. The output of the amplifier is usually adjusted by using a sensitivity control. When the probe receives the shock excitation, it generates an ultrasonic pulse, and a large peak known as transmission peak appears at the left-hand extremity on the oscilloscope screen. Returning echoes received by the probe after reflections are converted into electronic pulses and the corresponding peaks appear on the oscilloscope screen.

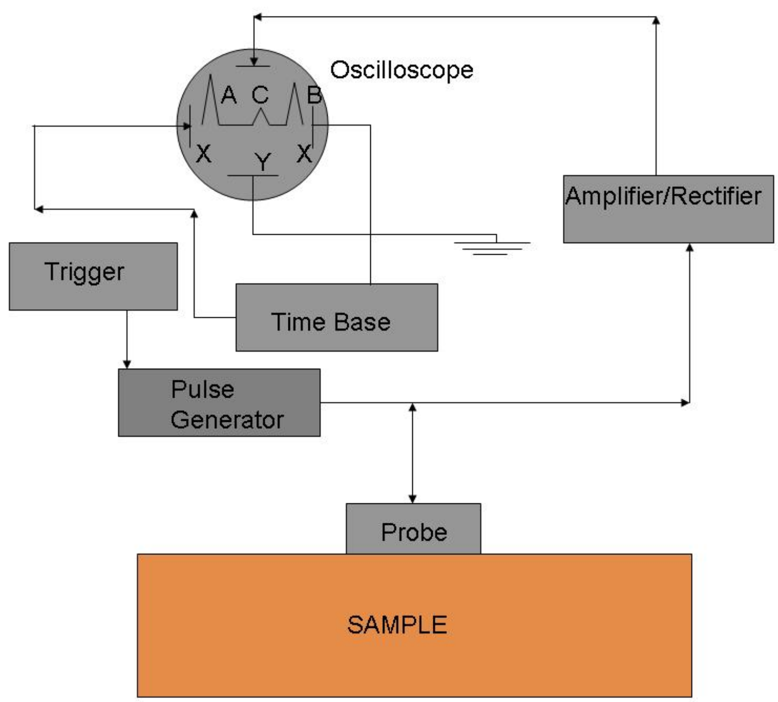

Figure 3.2: Basic Design of Pulse Echo Technique

In a double probe operation the transmitting probe is not directly connected to the oscilloscope; therefore, on transmission of the pulse, the transmission peak does not appear on the oscilloscope screen. However, the received echoes are picked up by the receiving probe and they are converted into electrical pulses and are fed to the Y-plates of the oscilloscope similar to the single probe operation [16].

In the time taken for the sound pulses to travel through the delay, the echo peaks are displaced to the right of point A by distances corresponding to the amount of the delay. Peaks B and C correspond to the first back wall echo and internal defect. Because of the rapidity of the pulse generation as determined by the pulse repetition frequency (PRF), the displayed peaks appear to be steady. The time delay values can be determined by calibrating the time base. If we assume that the time base indications vary linearly with the horizontal distance, then the distance of the indicated defect from the front surface of the test object is equal to the product of its thickness and the ratio AC/AB [16].

3.3 Through Transmission Technique

Through-transmission is used in several cases, particularly for highly attenuate material where a pulse-echo results in significant loss in signal strength. In this technique the transmitter probe is placed on one side of a specimen and a receiver on the opposite side and the specimen is scanned across as shown in figure 3.3, any variations in ultrasonic attenuation in the specimen will be registered.

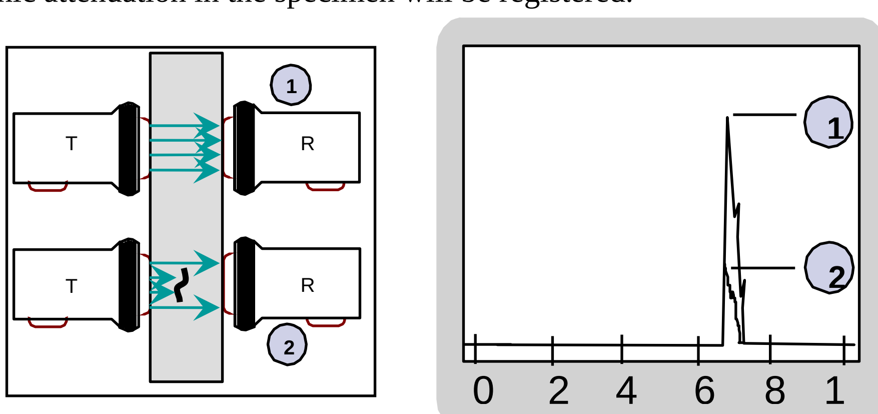

Figure 3.3: Schematic of Through Transmission Technique

An internal flaw in the specimen will reduce the intensity of the transmitted ultrasonic energy as it comes between the probes. Usually this technique is difficult to apply, as the two probes must be maintained rigidly at a fixed distance and angle. Any probe movements relative to one another, or any variation in the specimen surface, will cause a change in the transmitted intensity. This method is sometimes called a Pitch-Catch method or obscuration technique. Through transmission is useful in detecting discontinuities that are not good reflectors and when signal strength is weak. This technique does not provide the depth information of the crack.

3.4 Data Presentation

There are several ways in which the information delivered to the display may be represented. Each presentation mode provides a different way of looking at and evaluating the area of material being inspected. There are four different types of scans or presentation modes in practice. They are

1) A mode scan or amplitude mode scan
2) B mode scan or brightness mode scan
3) C mode scan
4) M mode scan or motion mode scan

3.4.1 A-Scan Presentation

The A mode scan or simply A-scan displays the amount of received ultrasonic energy as a function of time. A mode operation causes a vertical deflection of the spot each time a pulse i.e., reflection, is received by the transducer. The relative amount of received energy is plotted along the vertical axis and elapsed time (which may be related to the sound energy travel time within the material) is display along the horizontal axis. In the

A-scan presentation, relative discontinuity size can be estimated by comparing the signal amplitude obtained from an unknown reflector to that from a known reflector. Reflector depth can be determined by the position of the signal on the horizontal sweep.

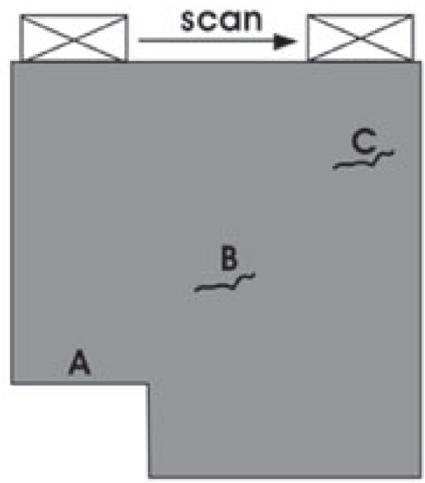

Figure 3.4: Scanning Procedure of the Specimen

In the A-scan presentation shown in figure 3.5, the initial pulse generated by the transducer is represented by the signal *IP*, which is near time zero. As the transducer is moved along the surface of the part as shown in figure 3.4, four other signals will appear on the screen at different times. When the transducer is at the extreme left position, we will see two signals i.e. the *IP* signal and signal *A* (the sound energy reflecting from surface *A***)** will be seen on the trace. As the transducer is scanned to the right, a signal from the back wall *BW* will appear on the screen showing that the sound has traveled farther to reach this surface. When the transducer is over flaw *B*, signal *B*, will appear at a point on the time scale that is approximately halfway between the *IP* signal and the *BW* signal. Since the *IP* signal corresponds to the front surface of the material, this indicates that flaw *B* is about halfway between the front and back surfaces of the sample. When the transducer is moved over flaw *C*, signal *C* will appear earlier in time since the sound travel path is shorter, and signal *B* will disappear since sound will no longer be reflecting from it [16].

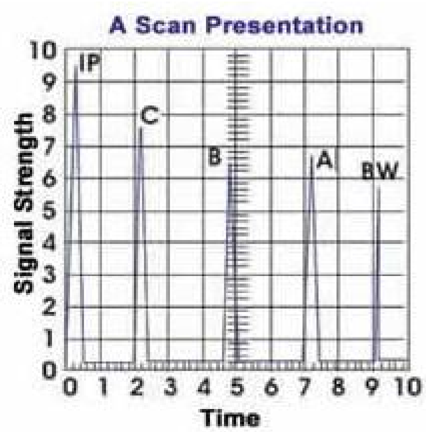

Figure 3.5: A-scan Presentation

3.4.2 B-Scan Presentation

The B-scan presentation as shown in figure 3.6 is a cross-sectional view of the test specimen. In the B-scan, the time-of-flight (travel time) of the sound energy is displayed along the vertical, and the linear position of the transducer is displayed along the horizontal axis. From the B-scan, the depth of the reflector and its approximate linear dimensions in the scan direction can be determined. The B-scan is typically produced by establishing a trigger gate on the A-scan. Whenever the signal intensity is great enough to trigger the gate, a point is produced on the B-scan. The gate is triggered by the sound reflecting from the back wall of the specimen and by smaller reflectors within the material. In the B-scan image above, line *A* is produced as the transducer is scanned over the reduced thickness portion of the specimen. When the transducer moves to the right of this section, the back wall line *BW* is produced. When the transducer is over flaws *B* and *C*, lines that are similar to the length of the flaws and at similar depths within the material appear in the B-scan. A limitation to this display technique is that reflectors may be masked by larger reflectors near the surface [37].

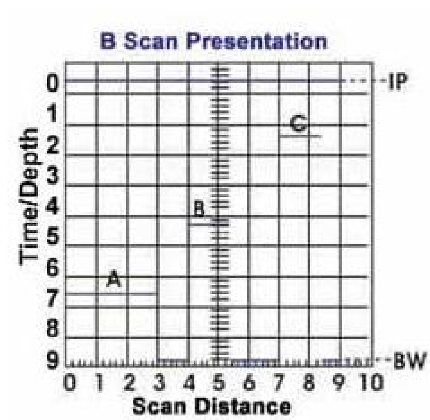

Figure 3.6: B-Scan Presentation

3.4.3 C-Scan Presentation

The C-scan presentation provides a plan-type view of the location and size of test specimen features, as shown in figure 3.7. The plane of the image is parallel to the scan pattern of the transducer. C-scan presentations are produced with an automated data acquisition system, such as a computer controlled immersion scanning system. Typically, a data collection gate is established on the A-scan and the amplitude or the time-of-flight of the signal is recorded at regular intervals as the transducer is scanned over the test piece. The relative signal amplitude or the time-of-flight is displayed as a shade of gray or a color for each of the positions where data was recorded. The C-scan presentation provides an image of the features that reflect and scatter the sound within and on the surfaces of the test piece. High resolution scan can produce very detailed images [37].

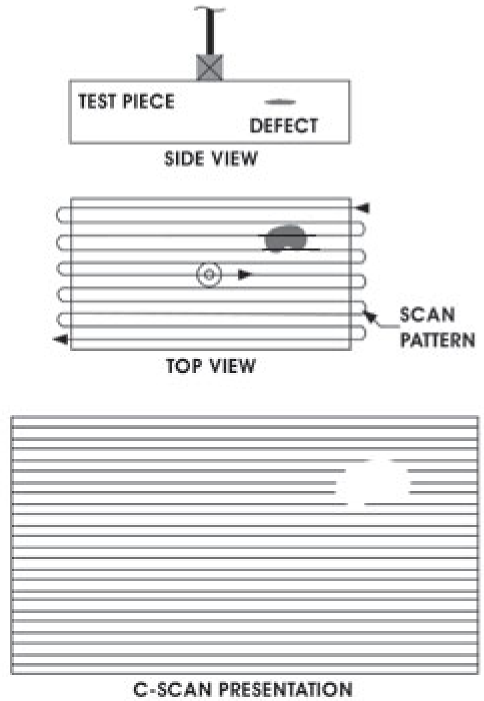

Figure 3.7: C-Scan Presentation

3.4.4 M-Scan Presentation:

M-scan is similar to a B scan presentation, in which the motion of the spots is recorded by a recording medium, usually a strip chart recorder that moves across the face of the display. This results in a recording of the reflector motion. The M-mode scanning is generally used in heart studies.

4. ULTRASONIC TRANSDUCERS

4.1 Introduction

A transducer is a device that converts one form of energy to another, for example, electrical energy to ultrasonic energy or vice versa. Most of the ultrasonic transducers are reversible: the energy conversion is possible in both directions with equal efficiencies.

Ultrasonic transducers may be classified as follows:

1) Piezoelectric transducers
2) Electromagnetic transducers
3) Electrostatic transducers
4) Magnetostrictive transducers
5) Laser and other Optical transducers

Quality of performance, ease of application and cost are the important considerations in selecting the transducers. Piezoelectric transducers are widely used for various inspection processes. However, for proper transmission of ultrasonic waves in the object under test we need a coupling medium which can satisfactorily transmit the ultrasonic waves.

4.2 Construction of a Simple Ultrasonic Transducer:

Three major elements in any ultrasonic transducer construction are: active element, backing and wear plate.

Active element: The active element, normally a piezoelectric material, converts electrical energy such as an excitation pulse into ultrasonic mechanical energy and vice versa. The most commonly used materials are natural piezoelectric as well as polarized ceramics (polycrystalline) such as quartz, barium titanate, lithium sulfate and lead meta-niobate. The active plate is normally 1/2 wavelength thick.

Backing: The backing is usually a highly attenuate material that is used to control the vibration of the transducer by absorbing the energy radiated from the back face of the oscillator**.** When the acoustic impedance of the backing matches the acoustic impedance of the oscillator, the back face of the oscillator transmits a great portion of its vibration into the damping body. As a result, the vibration is absorbed by the backing material, and the vibration of the plate is stopped. This condition describes a heavily damped transducer that displays short pulses (good resolution) but low signal amplitude. On the contrary, if there is a mismatching in acoustic impedance between these two materials, more energy will be reflected forward into the specimen. This is the case of a bad resolution transducer due to the longer wave duration, but may be higher in signal amplitude or sensitivity. Materials such as vulcanized rubber and molded fiber plastic are satisfactory for moderate demands at high frequencies. Composite materials based on curable synthetic resins or rubbers in which other powdery mixtures have been incorporated are preferable. Attempts have also been made to scatter and disturb the waves by using cellular structures and oblique or saw-tooth shaped end faces respectively. Such means can be applied successfully only in combination with an intrinsically effective absorption. Otherwise, the various interfering echoes will produce a background of grass behind the transmitting pulse.

Wear Plate: The wear plate’s purpose is to protect the oscillator plate from the testing environment. In the case of contact transducers, the wear plate must be durable and corrosion resistant in order to withstand the wear caused by the abrasion of the specimen surface. For immersion, angle-beam and delay-line transducers the wear plate has the additional purpose of serving as an acoustic impedance adaptor between the active element and the water, wedge or the delay line respectively [39].

4.3 Principle of Operation

Transducers operating by the principle of piezoelectric effect or magnetostrictive effect are used for producing ultrasonic sound. High intensity ultrasonic sound of frequency 20-40 kHz range can be produced by using magnetostrictive transducers. The high intensity sound of frequency 20-40 kHz is used in ultrasonic cleaning and other mechanical applications. Ultrasound of frequency 1-20MHz is produced by introducing the output of an electronic oscillator to a thin wafer or piezoelectric material like lead zirconate titanate. This type of ultrasound is used in ultrasonic medical imaging. The higher frequencies have shorter wavelengths and thereby provide higher resolution to the imaging process [39].

4.4 Resolution & Sensitivity of Ultrasonic Transducers

Characteristics of an ultrasonic testing system are mainly dependent on the transducer’s features like resolution and sensitivity.

There are two types of resolution, Axial resolution is the ability of the probe to produce simultaneous and distinct indications from reflectors located at nearly the same position with respect to the sound beam. In other words, the minimum distance in the beam direction between two reflectors can be identified as separate echoes. Axial resolution is slightly more than half the **spatial pulse length**, SPL, defined as the product between wavelength and the number of cycles in the pulse. Thus, the axial resolution can be improved in two ways: 1) decreasing the number of cycles in each pulse by manipulating the transducer damping, and 2) decreasing the wavelength of the pulse. The number of cycles per pulse can typically be reduced to a minimum of one. Typically, a frequency range of 2 to 10 MHz is used to meet both resolution and imaging depth requirements. The reason why the minimum reflector distance must be larger than half the spatial pulse length is shown in figure 4.1.

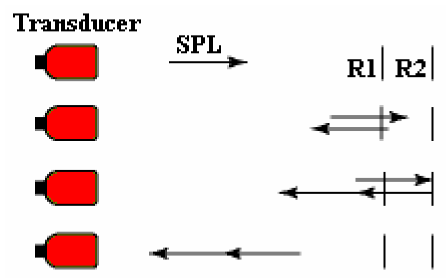

Figure 4.1: Axial Resolution Effect

An ultrasonic transducer and its ultrasound pulse are analyzed at four different times. At time 1, the transducer has just emitted an ultrasound pulse with a spatial pulse length SPL as indicated by the length of the arrow. The pulse encounters two reflectors, R1 and R2, separated by a distance exactly equal to 1/2 SPL in the ultrasound beam direction. At time 2, part of the pulse is reflected from R1; the remainder of the pulse travels on. At time 3, part of the pulse is also reflected from R2. The echoes from R1 and R2 both have lengths equal to the pulse length (SPL). As the "tail" of the echo from R1 leaves this reflector, the "head" of the echo from R2 reaches R1 (time 3). At time 4, both echoes are seen propagating towards the transducer, the "head" of the last echo "biting the tail" of the first one. The transducer therefore cannot separate the echoes. For the two echoes to be resolved, the distance between the reflectors needs to be slightly longer than half the spatial pulse length, which is the maximum axial resolution.

Lateral Resolution refers to the ability to discern two separate objects perpendicular to the ultrasound beam direction. For a single-element transducer, lateral resolution is determined by the ultrasound beam diameter. In order to separate two objects that are closely spaced, the beam must be narrower than the space between them. As the diameter of the beam varies with distance from the transducer so does the lateral resolution. The primary mean to reduce the beam diameter is focusing the beam. Lateral resolution is directly proportional to the frequency, but there always exists the limitation of attenuation as one goes higher in frequency.

Sensitivity: This is the ability of an ultrasonic probe to detect reflectors at a given depth in a test material. The greater the signal that is received from these reflectors, the more sensitive the transducer is. It is a measure of the test system’s ability to detect discontinuities producing relatively low-amplitude signals because of their size, geometry, or distance.

	2.0MHz	**5.0MHz**
Axial Resolution	Decrease	Increase
Lateral Resolution	Decrease	Increase
Sensitivity	Increase	Decrease

Table 4.1: Effect of axial resolution, lateral resolution and penetration of the ultrasonic beam as a function of the frequency

Table 4.1 summarizes the effect of axial resolution, lateral resolution and sensitivity of ultrasonic transducers as a function of frequency.

The variety of transducers used for ultrasonic testing is divided in two main types based on type of waves that they propagate. They are 1) normal incidence or longitudinal wave transducers and 2) angular incidence or transverse wave transducers [17, 18].

4.5 Piezoelectric Transducers

Piezoelectric transducers are the most commonly used for detecting and creating ultrasonic waves. The piezoelectric effect was discovered by Jacques and Pierre Curie in 1880. The piezoelectric effect is the characteristic of single crystals of certain insulators, including lithium sulphate and quartz, and some semiconductors such as zinc oxide and cadmium sulphide. The piezoelectric effect requires the presence of a polar axis, which is present naturally in the single crystal materials used as transducers. When we have a disc made from one of these materials having a polar axis perpendicular to the flat parallel surfaces and subject it to mechanical stress, equal and opposite electric charges appear on these surfaces. This is called as the direct piezoelectric effect.

We can categorize the piezoelectric transducers by the beam orientation, by the environment where it is used, and by the type of wave generated. Most common classifications are:

1) Type of waves generated (longitudinal, shear or surface)
2) Contact, immersion, or air-coupled
3) Normal or angled beam
4) Broadband or narrowband
5) Single or multiple elements
6) Transducer face – flat (normal) or shaped (contoured or focused)
7) Ambient or high temperature

We are next going to discuss about the contact, immersion, normal or angle beamed and single or multiple elements transducers, as these are most directly related to the research work here presented.

4.5.1 Contact, Immersion or Air-Coupled Transducers

Piezoelectric transducers are also classified by their coupling mechanisms: contact, immersion, or air-coupled. Contact transducers, although they appear to come into direct contact with the object under test, in fact require some form of dry couplant or liquid to adequately couple the ultrasound to and from the object under test. A couplant is generally necessary because of the acoustic impedance mismatch between air and solids; for example the test specimen is large and, therefore, nearly all of the energy is reflected and very little is transmitted into the test material. The couplant displaces the air and makes it possible to get more sound energy into the test specimen so that a usable ultrasonic signal can be obtained. There also exist those transducers that transmit the ultrasonic energy normally to the contact surface but use a liquid medium as vehicle; these transducers are known as **immersion** transducers.

Immersion transducers operate in a scanning tank where the specimen and the transducer are fully immersed within the fluid (typically water). Immersion transducers have a design similar to that of contact transducers but the wear plate in its case works as an impedance adapter and are designed to match the acoustic impedance of water [37, 17].

It offers two mayor advantages over the contact transducer:

- Uniform coupling which reduces variation in the sensitivity.
- The focusing feature increases the sensitivity to small reflector.

There are three basic configurations: unfocused (flat), spherical focused (spot), and cylindrical focused (line), figure 4.2. In most transducers the focusing is accomplished by the addition of a lens on the end of the oscillator. A spherical focus beam is normally used to improve sensitivity to small discontinuities while a cylindrical focus is used for inspection of pipes or bars.

The focal length is the distance from the face of the transducer to the point in the sound field where the signal has maximum amplitude. In the case of spherical focus, the focal length depends upon the spherical radius of the lens, as well as the size and frequency of the element. A small radius produces shorter focal length. The same applies for cylindrical lenses.

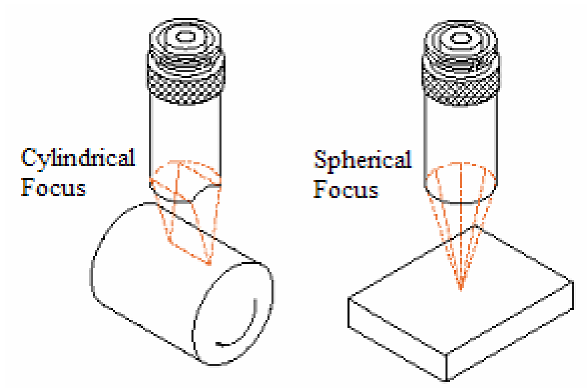

Figure 4.2: Cylindrically and spherically focused transducers

At or near the theoretical focus area, the sound beam maintains shape within a short zone before it again diverges and rapidly spreads out. Since the last signal maximum occurs at a distance equivalent to the near field, a transducer cannot be acoustically focused at a distance greater than N (near field length). The maximum practical focal length for a point target is 0.8N.

The measured focal length of a focused transducer depends on the material in which it was measured. When specifying a transducer focal length, it typically refers to water. Since most of the materials have a higher propagation velocity than water, the focal length is effectively shorter as justified by Snell's Law. The focal length is also affected by the curvature of the surface of the test piece [37, 18].

Because of the high impedance mismatch between the air and the piezoelectric crystal, these air-coupled transducers require a special layer of material for sending the pulse through air to the sample. This layer is called as the impedance matching layer [12].

4.5.2 Normal or Angled Beam Transducers

Transducers can also be categorized on the way the ultrasonic waves transmit from the face of the transducer as normal beam or angled beam. Normal beam transducers, as shown in figure 4.3-a, transmit a wave normal to the face of the transducer, whereas angled beam transducers transmit a wave at an angle (not normal) to the face of the transducer. Angled beam transducers are usually just the normal beam transducers attached with a wedge, as shown in figure 4.3-b, often made of plastic. An important point to be remembered is, due to the Snell's Law, the angle in the wedge is not the same as the angle of the beam created in the sample. When angled beam transducers are manufactured, manufacturers label their transducers based on the angle of injection.

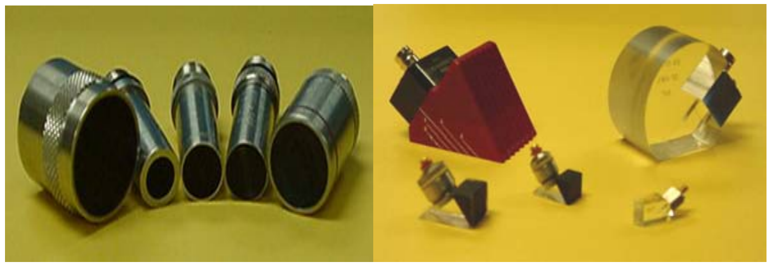

Figure 4.3 - a) Normal Beam Transducers b) Angled Beam Transducers

4.5.3 Single and Multiple Element Transducers

If the transducer has a single element then it is called a single element transducer. The single element of crystal acts as both the transmitter and receiver. The elements of a single crystal transducer are shown in figure 4.4. The external housing is the support of the other elements. The inner sleeve isolates the active (piezoelectric element) element and the backing from the external house. Electrodes attach to both surfaces of the active element and transfer the electric charges to the active element and from the active element to the electrical leads or cables. The electrical network consists in passive elements that work as an impedance matching between the pulse transmitter and the active element. The other three elements, backing, active element, and wear plate, discussed earlier, are the most critical in the design of the transducer.

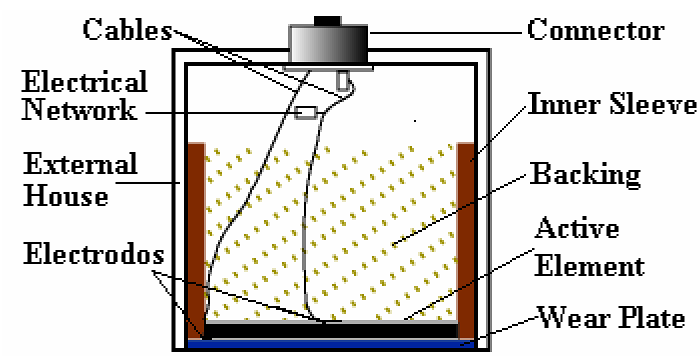

Figure 4.4: Components of a single element transducer

Piezoelectric transducers commonly contain multiple (two or more) elements. In the dual element transducers, we have separate transmitter and receiver elements housed in a common case, as shown in figure 4.5. One of the elements transmits and the other receives. Active elements can be chosen for their sending and receiving capabilities providing a transducer with a cleaner signal, and transducers for special applications, such as inspection of course grain material. Dual element transducers are especially well suited for making measurements in applications where reflectors are very near the transducer since this design eliminates the ring down effect that single-element transducers can produce. (When single-element transducers are operating in pulse echo mode, the element can not start receiving reflected signals until the element has stopped ringing from its transmit function.)

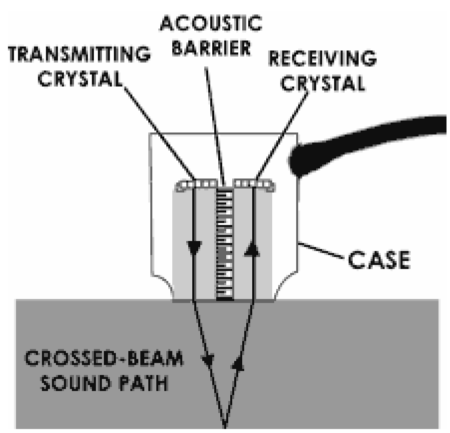

Figure 4.5: Components of a Dual Element Transducer

Dual element transducers are very useful when making thickness measurements of thin materials and when inspecting for near surface defects. The two elements are angled towards each other to create a crossed-beam sound path in the test material. This kind of arrangement allows for improvement in the near surface resolution [12, 37].

A set of several normal piezoelectric transducers acting together is called an array. If the transducers are driven at slightly different times by either electrical or physical means, so that the individual waves interfere constructively and destructively into an angled wave, this is called a ***phased array***. The individual transducers in phased array transducers are usually as small as possible, so that the individual elements appear as point sources.

The phased array concept deals with multi element transducers. Each element of these transducers is connected to a different electronic channel, either directly or through multiplexers, according to electronic device performances. Each element can be activated or not for each shot. The activated elements give the size and the location of the active aperture of a phased array transducer. An electronic delay can be applied to each electronic channel when emitting and receiving the signal to/from the transducer elements. The setup corresponding to all the delays of a given shot is called Delay Law. Each delay law defines a different acoustic beam with particular direction, focusing distance and lateral resolution. This technique requires probes with very low acoustic and electric cross coupling between the elements, so that all the elements can be fired independently [40].

All elements are connected to, and controlled by, a computerized ultrasound system. The system is able to activate each element independently. Typical element size is from 0.02” to 0.1”. Also available are annular arrays, which are circular pieces, divided into donut shaped annular elements. Timing or phasing the individual elements appropriately can be utilized to create different beam profiles. Such is the versatility that the beam can be focused or steered in a wide range of angles.

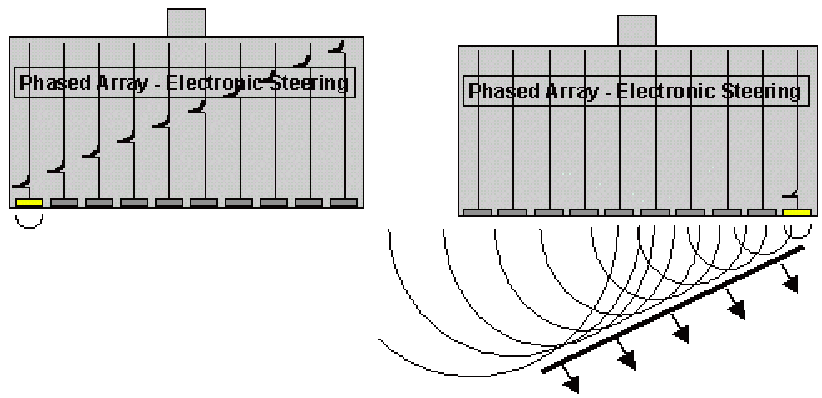

Figure 4.6: Electronic phasing used to steer a sound field

A **steered** angle beam is created by sequentially firing each element in an array to create a wave front following the desired angle, figure 4.6. The angle is set electronically by the instrumentation, and can if necessary be changed pulse by pulse.

The advantages are:

- Only one transducer is required for inspection at variable angle.
- Fast inspection of complex geometry parts.
- The advantage of this technique can be combined with the advantages of electronic focusing.

The creation of a **focused** beam is achieved by a different pulsing cadence, i.e. by selecting the firing order and pulse delays of the array elements. This can be changed pulse by pulse to sweep a focal point through a range of depths in the test material, (Figure 4.7). Note that the beam steering and dynamic focusing can be combined to give a resultant beam which is both focused and angled.

The transducer array can also be used to perform so-called “linear scanning”. It consists in successively fired adjacent groups of elements to create a scanning effect.

The "Virtual Probe" width and scan pitch can be controlled by selecting the number of elements fired in parallel and the number of elements indexed for successive shots. This technique can be combined with both beam steering and dynamic focusing to apply a "scanning motion" to angled and focused beams.

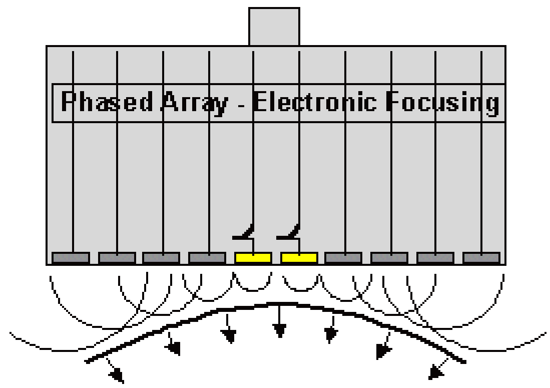

Figure 4.7: Electronic phasing used to create a focused sound field

The advantages are:

- Faster inspection of complete volume of thick pieces with dynamic focusing.
- Electronic focusing can compensate for focusing aberrations due to cylindrical interfaces [18, 40].

An array transducer may be constructed from a wide variety of sources, including piezoelectric elements as well as EMAT (Electromagnetic-Acoustic Transducer) and laser sources. This kind of system is very expensive as each circuit is essentially a separate ultrasonic system controlled by the multiplexer. But the increased speed and versatility of inspection that the array transducers permit, however, may offer advantages that counter the added expense of the system [14].

These phased array transducers are used in inspecting complex geometries such as rotor shafts for turbines and components for nuclear reactors. Figure 4.8 shows some of the commercially available phased array transducers.

Figure 4.8: Commercially available phased array transducers

The adaptability of these kinds of probes reduces the set-up time required for making varied inspections on these geometries, since from one probe placement, different parts of the component can be inspected by just changing the firing scheme of the probe elements.

5. LUMBAR SPINE ANATOMY

The spine works as the main support for the spinal cord and the nerves that carry information from the arms, legs, and rest of the body, and carries signals from the brain to the body. Without a functioning spinal cord, one could not move any part of the body, and the organs could not function. Our back is composed of 33 bones called vertebrae as shown in fig 5.1 [41], 31 pairs of nerves, 40 muscles and numerous connecting tendons and ligaments running from the base of the skull to the tailbone or coccyx.

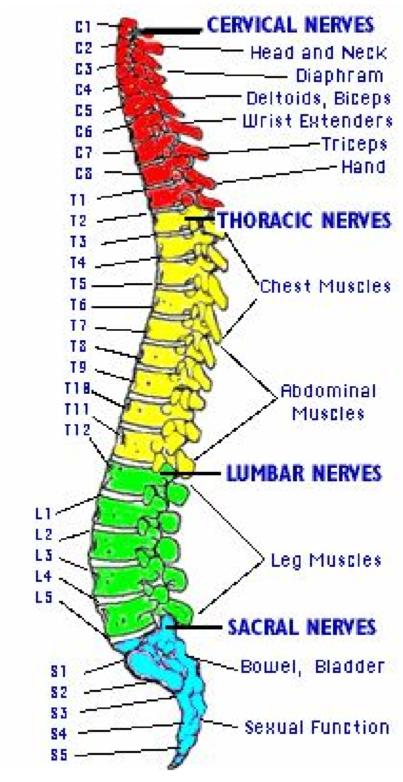

Figure 5.1: Human Spine

5.1 Spinal Column

The spinal column is made up of 33 small bones called vertebrae that are stacked or jointed together to create the spinal column.

The spinal column is separated into 5 specific functional areas:

- Cervical / C 1-7
- Thoracic / T 1 - 12
- Lumbar / L 1 - 5
- Sacral
- Coccyx

The cervical, thoracic and lumbar are the three main segments of the spinal column (Figure 5.1) [41]. The cervical spine is the upper part of the spine, comprised of seven vertebrae (C1 to C7). The cervical bones are designed to allow flexion, extension, bending, and turning of the head. They are smaller than the other vertebrae, which allow a greater amount of movement. The thoracic spine is the center portion of the spine, comprised of twelve vertebrae (T1 to T12). The spinal canal in the thoracic region is relatively smaller than the cervical or lumbar areas. This puts the thoracic spinal cord at greater risk when there is a fracture. The motion that occurs in the thoracic spine is mostly rotational. The ribs prevent bending to the side. A small amount of movement occurs in bending forward and backward. The lower portion of the spine is called the lumbar spine. It usually comprises five vertebrae (L1 to L5); however, some people may have six lumbar vertebrae. Below the lumbar spine is the sacrum. The sacrum is actually a group of specialized vertebrae that connect the spine to the pelvis. At the terminal end of the spinal column is the coccyx, which is composed of four, fused undeveloped vertebrae. The normal spine has an "S"-like curve when looking at it from the side. This allows for an even distribution of weight. The "S" curve helps a healthy spine withstand all kinds of stress.

In all of these vertebrae we have a fibrous, elastic cartilage in between the vertebrae called intervertebral discs. These act as "shock absorbers" which keep our spine flexible and cushion the hard vertebrae as we move, Fig 5.2a [42].

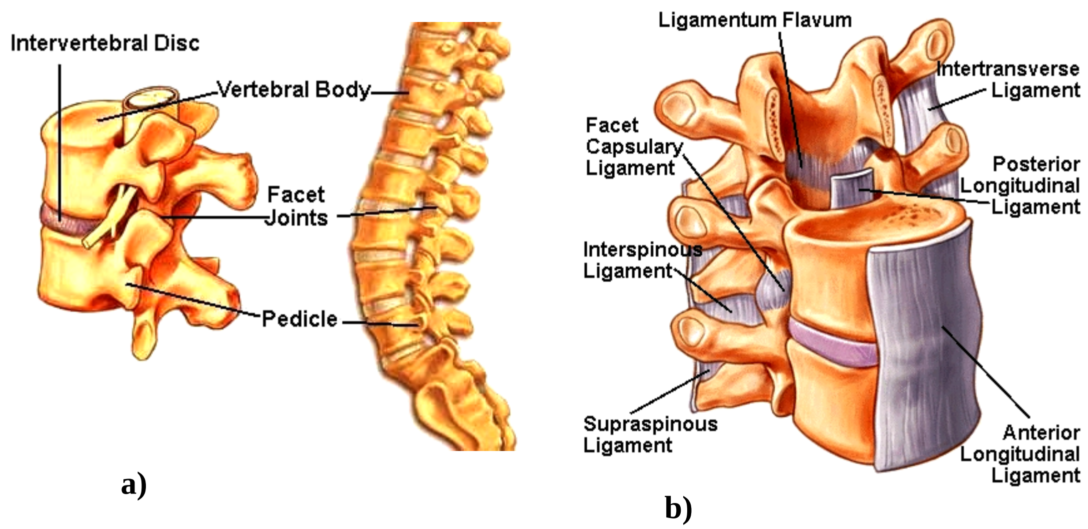

Figure 5.2: Lumbar Spine a) General Structure, b) Ligaments around the vertebrae

There is one disc between each vertebra; each disc has a strong outer ring of fibers called the annulus, and a soft, jelly-like center called the nucleus pulposus. Each vertebra is held to the others by groups of ligaments, figure 5.2b. There are also tendons that fasten muscles to the vertebrae. The spinal column also has real joints (just like the knee or elbow) called facet joints. The facet joints link the vertebrae together and give them the flexibility to move against each other. Each vertebra has an apperture in the center, so when they stack on top of each other they form a hollow tube that holds and protects the entire spinal cord and its nerve roots, figure 5.2a. The spine branches off into thirty-one pairs of nerve roots. These roots exit the spine on both sides through spaces (neural foramina) between each vertebra.

5.2 Vertebrae

Vertebrae are the individual bones of the spine. These are the building blocks of the spinal column. The vertebrae protect and support the spinal cord. They also bear the majority of the weight put upon the spine. The **body** of each vertebra is the large, round portion of bone, figure 5.3. The exterior vertebral body consists of very hard bone (cortical bone), with more spongy bone (cancellous bone) and blood vessels inside.

The body of each vertebra is attached to a bony ring. These rings create the hollow tube through which the spinal cord passes. The bony ring attached to each vertebral body consists of several parts. First, the **laminae** extend from the body to cover the **spinal canal**, or tubular opening in the center of the vertebrae. Second, the **spinous process** is the bony portion opposite the body of the vertebra. We feel this part when we run a hand down a person's back. Then there are two **transverse processes** which attach the back muscles to the vertebrae. Finally, the **pedicle** is a bony projection that connects to both sides of the lamina [43].

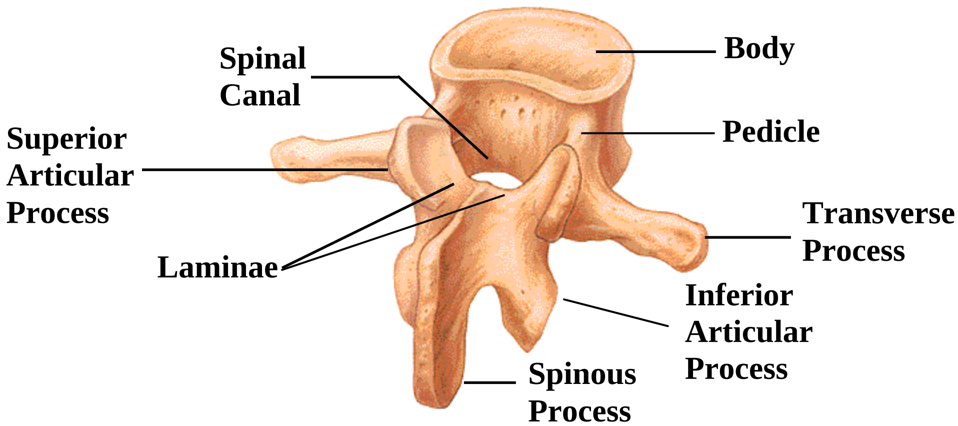

Figure 5.3 – Parts of a Lumbar Vertebrae

5.3 Intervertebral Disc

The intervertebral discs are flat, round "cushions" that act as shock absorbers between each vertebrae in the spine. There is one disc between each vertebra. Each disc has a strong outer ring of fibers called the annulus, and a soft, jelly-like center called the nucleus pulposus, figure 5.4. The annulus is the disc's outer layer and the strongest area of the disc. It also helps keep the disc's center intact. The annulus is actually a strong ligament that connects each vertebra together. The mushy nucleus of the disc serves as the main shock absorber. The nucleus is made up of tissue that is very moist because it has high water content. The water content helps the disc act as a shock absorber - somewhat like a waterbed mattress [43].

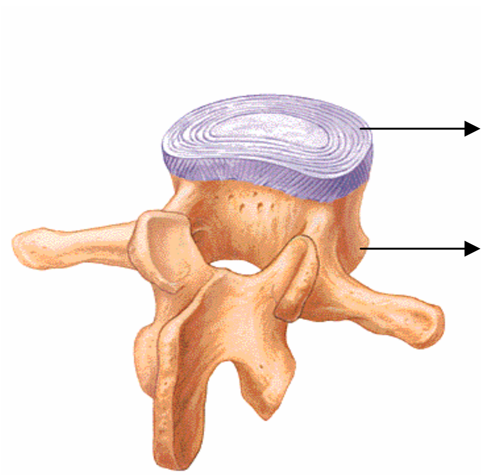

Figure 5.4: Vertebrae with Intervertebral Disc

5.4 Soft Tissue surrounding the lumbar spine

The osseous elements of the lumbar vertebral column are connected by a variety of structures that collectively are known as soft tissue. Ligaments of various types connect the vertebral bodies and the posterior elements of the vertebrae and span one or more segments, depending on the type of ligament and vertebrae level, figure 5.2b.

The paraspinal muscles refer to the muscles next to the spine. They support the spine and are the motor for movement of the spine. The joints allow flexibility and the muscles allow mobility. There are many small muscles in the back - each controlling some part of the total movement between all the vertebrae and the rest of the skeleton. These muscles can be injured directly, such as when you have a pulled muscle or muscle strain of the back muscles. The muscles can also cause problems indirectly, such as when the muscles are in spasm after injury to other parts of the spine.

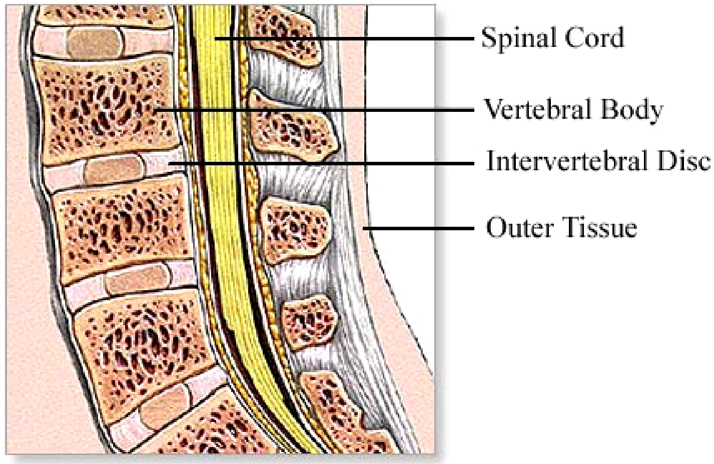

Figure 5.5 – Cross Section of Lumbar Spine Segment

Above the ligaments and muscles associated with the spine, there is outer material composed of connective tissue and layers of skin. The connective tissue, called the hypodermis attaches other tissues of the body to the skin and supports structures such as blood vessels and nerves. This layer is variable in thickness depending on the amount of fat stored in the tissue. Above this layer, there are two layers of skin present: the dermis and epidermis. The dermis is commonly two millimeters in thickness and is composed of fibrous tissue, capillaries, sweat glands, hair follicles and sensory nerve endings. The epidermis is commonly half of a millimeter in thickness, is composed of epithelial tissue and includes sebaceous glands, sweat glands and hair follicles [18].

5.5 Facet Joint

The facets are the "bony knobs" that meet between each vertebra to form the facet joints that join the vertebrae together. There are two facet joints between each pair of vertebrae, one on each side. They extend and overlap each other to form a joint between the neighboring vertebrae facet joints. Without the facet joints, we would not have flexibility in the spine, and we could only move in very straight and stiff motions.

The facet joints are also known as synovial joints. A synovial joint, such as the knee or elbow, is a structure that allows movement between two bones. In a synovial joint, the ends of the bones are covered with a material called articular cartilage. This material is a slick spongy material that allows the bones to glide against one another without undue friction.

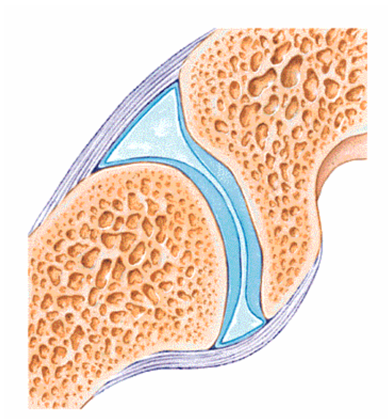

Figure 5.6: Facet Joint

Surrounding the facet joint is a watertight sack made of soft tissue and ligaments. This sack creates what is called the "joint capsule". The ligaments are soft tissue structures that hold the two sides of the facet joint together. The ligaments around the facet joint combine with the synovium to form the joint capsule that is filled with fluid (synovial fluid). This fluid lubricates the joint to decrease friction, just as oil lubricates the moving parts of a machine [43].

6. INSTRUMENTATION AND METHODOLOGY

6.1 Background Information

In the field of chiropractic medicine, it is very important to measure the variations in the intervertebral distance when patients are treated by the Cox Flexion-Distraction technique. Previous research has attempted estimation of the distance between contiguous lumbar vertebrae by identifying specific points in each vertebra to be used as an anatomical reference from which the measurements could be made. The point had to be representative of a singularity that could be very clearly identified in successive trials by recognizing the echo pattern of the pulsed reflected from it. Based on this, the tip of the spinous process was selected as the anatomical reference, viewed from the posterior-anterior orientation. Based on this, a B-scan program was developed and has been used to record the profile of reflections along a trajectory that completely covers two adjacent spinous processes. Distances between the vertebrae has been determined directly by the separation between the indications of the spinous process tips within the image.

Here, we plan on measuring the distance between the lumbar vertebrae by imaging the transverse process instead of the spinous process. The reason behind this is that the distance between the spinous process becomes very small as we move up along the spine into the thoracic and cervical zones, and this makes the measurement of distance between the vertebrae from the spinous process difficult, but there are significant distances between the transverse process in these zones. We have used the same ultrasound equipment as used for previous research. The only change is the frequency of the transducer used. A B-scan program has been used to scan the transverse process and save the recorded image. Another program has been used to read the saved file and rebuild the image for the data analysis.

6.2 Instrumentation

The experiments were carried out in the Litee Laboratory and Veterinary School at Auburn University in Auburn, Alabama.

A computer-controlled ultrasonic testing system, US-Ultratek PCIUT3100, in conjunction with a 3.5 MHz immersion ultrasonic transducer, Panametrics V384, was used to generate the ultrasonic waves and receive the reflections from the specimen. The ultrasonic system includes a pulser/receiver and a high speed analog to digital (A/D) converter board for a PCI bus. It generates a high voltage pulse from the PULSE OUT connector to excite the transducer for the generation of the acoustic signals. The same terminal is used to receive the electric pulse back from the transducer. The analog signal is converted into digital information at a maximum rate of 100MHz (100 millions samples per second), See Appendix B for more technical specifications. The board was housed in external portable bus expansion hardware, Magma 2 Slot CardBus PCI Expansion System, consisting of a CardBus card, expansion bus cable, expansion mother board, and a chassis with power supplier (Figure 6.1).

Figure 6.1: Ultrasonic Testing System

The use of the PCI expansion system was meant to allow the use of a laptop, Dell Inspiron 6000, to operate the ultrasonic system. This configuration provided the portability required to move the whole system to different laboratories and the flexibility to unplug the component as desired, for instance, to use the computer in a different location for data analysis, etc.

The PCIUT3100 board included a software development kit for engineers to write programs to control the different parameters of the pulser/receiver and the A/D converter. Labview, version 6i, National Instrument, was used to write the programs for the different tests. The software development kit provided a dynamic link library with a single function call to control different tasks of the board and get the required data. By setting some features of the function call one can set board parameters such as: receiver gain, sampling frequency, filters, signal rectification, buffer length, pulse width, etc [29]. See Appendix C for details regarding dynamic link library and control of board parameters.

The following is a description of the general functioning of the ultrasonic board. Also refer to figure 6.2.

- The PCIUT3100 board generates a negative high voltage pulse from the PULSE OUT connector and then starts collecting data.
- The pulse excites the ultrasonic transducer with user-defined pulse voltage, pulse width, and damping.
- The receiver on the PCIUT3100 board inputs the ultrasonic signal through RECEIVE IN connector, or (as in our design) directly from the PULSE OUT connector.
- The receiver clips out the high voltage of the signal and then makes the signal go through the amplifier, high pass filter, rectifier, DC offset adjustment, and low pass filter.
- The signal then is directed to the A/D circuit where it is converted to digital data and stored in the memory of the board.
- The data is captured from the memory of the board and saved in the computer RAM for further digital processing and displaying.

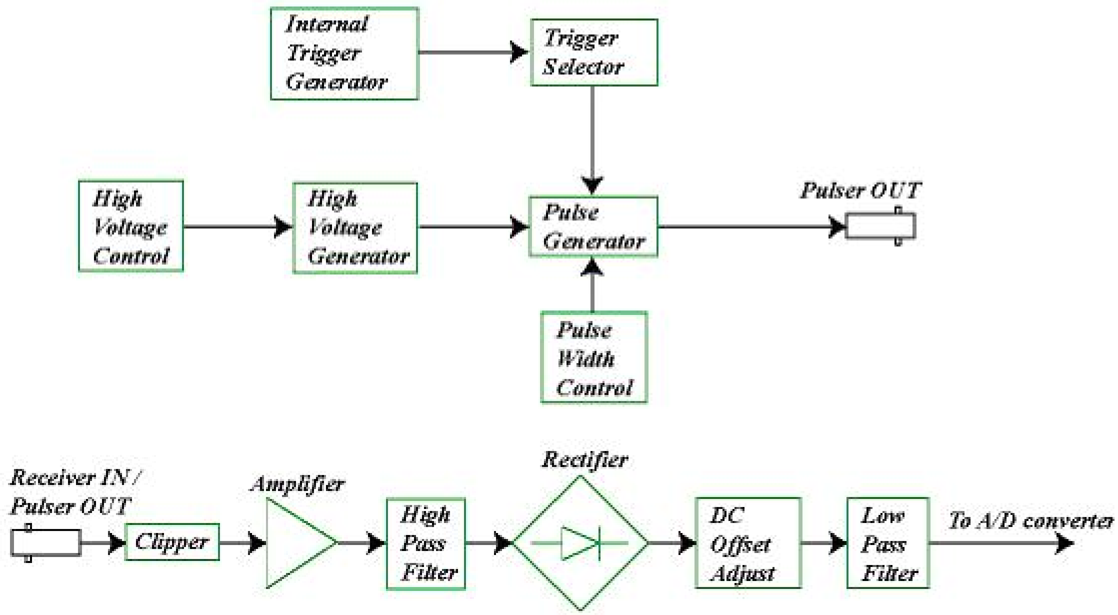

Figure 6.2: Schematic representation of the functioning of the ultrasonic board

6.3 Working of the ultrasonic system

The main four parts of the ultrasonic system are the base, transducer, slider and the encoder.

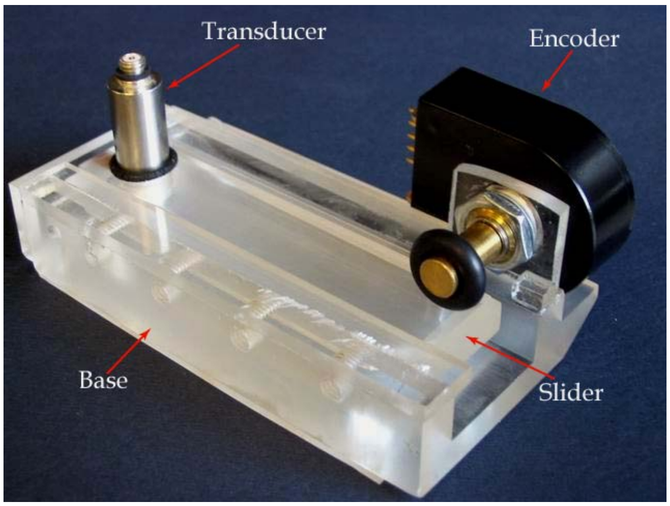

Figure 6.3: Scanning assembly configuration

The ultrasonic system was made out of a translucent acrylic material. As shown in Figure 6.3, the base or main body holds the slider which in turn carries the transducer. The transducer is inserted in the hole of the slider whose diameter is slightly longer than the transducer diameter. The transducer is set in a way that its tip does not touch the bottom level of the base, i.e. its tip is set couple of millimeters above the bottom level of the assembly. This arrangement protects the active element of the transducer, preventing any direct contact between the transducer and the specimen being tested. Once the transducer is adjusted at the desired height, it is fixed by a plastic tip set screw (Figure 6.4).

Figure 6.4: Slider holding the transducer at a fixed position

This design provides a smooth gliding of the slider through the base slot, a desired feature at the time of performing the test. An incremental optical encoder is attached to one of the top corners of the main body (Figure 6.3). This device translates mechanical motion (such as speed, direction, and shaft angle) into electrical signals. Appendix B provides detailed information of the functioning and technical specifications of the encoder.

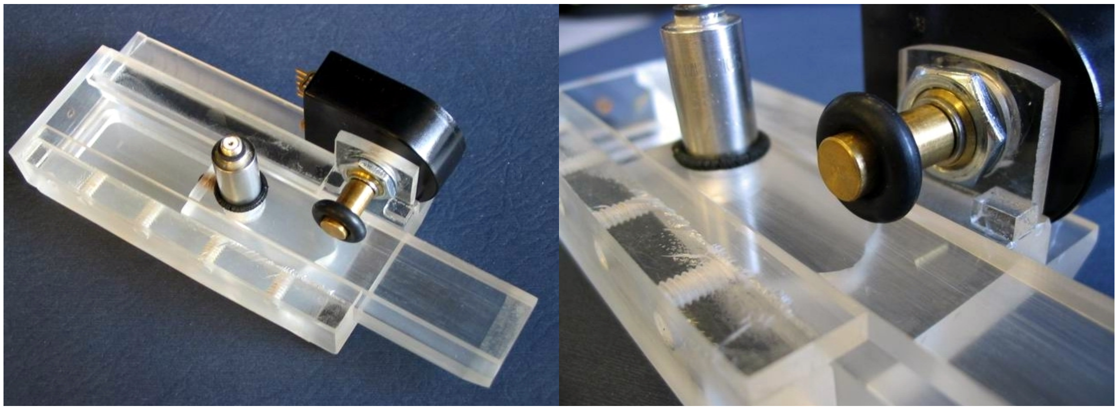

Figure 6.5: Displacement of the slider along the base slot

In this application, the encoder was used to precisely measure the displacement of the transducer along the base slot. A rubber wheel was attached near the tip of the encoder shaft. The wheel is in direct contact with the slider and provides the necessary traction to rotate the encoder shaft as the slider moves, figure 6.5.

As the shaft rotates, the encoder converts real time shaft-angle into digital (square waves) output signals proportional to the number of windows on the optical code disc. An encoder counter was added to the pulser/receiver board to encode the signal received from the encoder output. Two call functions were then used to properly read and manipulate the counter data. The first of them sets the starting value of the encoder counter and the second one simply gets the values from the encoder counter. The counter delivers integer numbers from -8388608 to 8388607. If the encoder wheel is moved in counter clockwise direction, the values will be positive and vice versa.

The rectangular groove in the base of the assembly was covered by a thin rubber-type sheet creating a small air volume under the slider, (Figure 6.6). During tests, the volume is partially filled with water to provide the acoustic coupling necessary to propagate the ultrasonic energy from the transducer to the test specimen. The rubber sheet was glued to the base to avoid any water leaking.

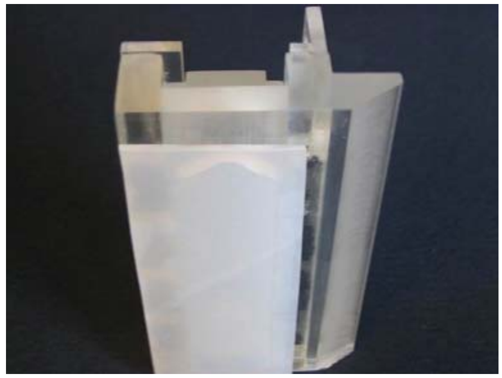

Figure 6.6: Rubber sheet glued at the bottom of the base

6.4 Scanning Procedure

Test preparation begins with setting the transducer and encoder on the assembly and plugging up their outputs to the respective input connectors on the board. The maximum displacement of the transducer before it touches the encoder shaft (physical limit) is approximately 6.2 cm.

As noted above, a call function was set to read the data from the encoder counter. The starting value of the encoder counter was set at zero. This means that once the program has been run, the zero reference point is automatically set in the position where the slider begins rotating the encoder. Accordingly, if the slider is placed somewhere between the origin of the slot and the encoder shaft (as in figure 6.5), the point exactly below the center of the transducer will be the zero reference point. In general, the slider will be positioned touching the back edge of the assembly to provide the maximum coverage along the assembly.

Once the program has been run, no measurements are made unless the encoder wheel rotates. The Labview program, also called virtual instruments, was programmed in such a way that the encoder counts trigger the testing protocol. This means that when the counter advances the first positive digit from zero to one, the whole measurement and storing protocol begins.

As the transducer is moved, the counter keeps delivering values, and the scanning continues up to the point where the slider is stopped by the encoder shaft. A command in the program was set in such a way that as the slider is glided back up to a predetermined position (couple of millimeters back from the encoder shaft), the program automatically builds an intensity plot containing the information stored in a preset buffer. The denominated **B-scan** screen is shown in Figure 6.7.

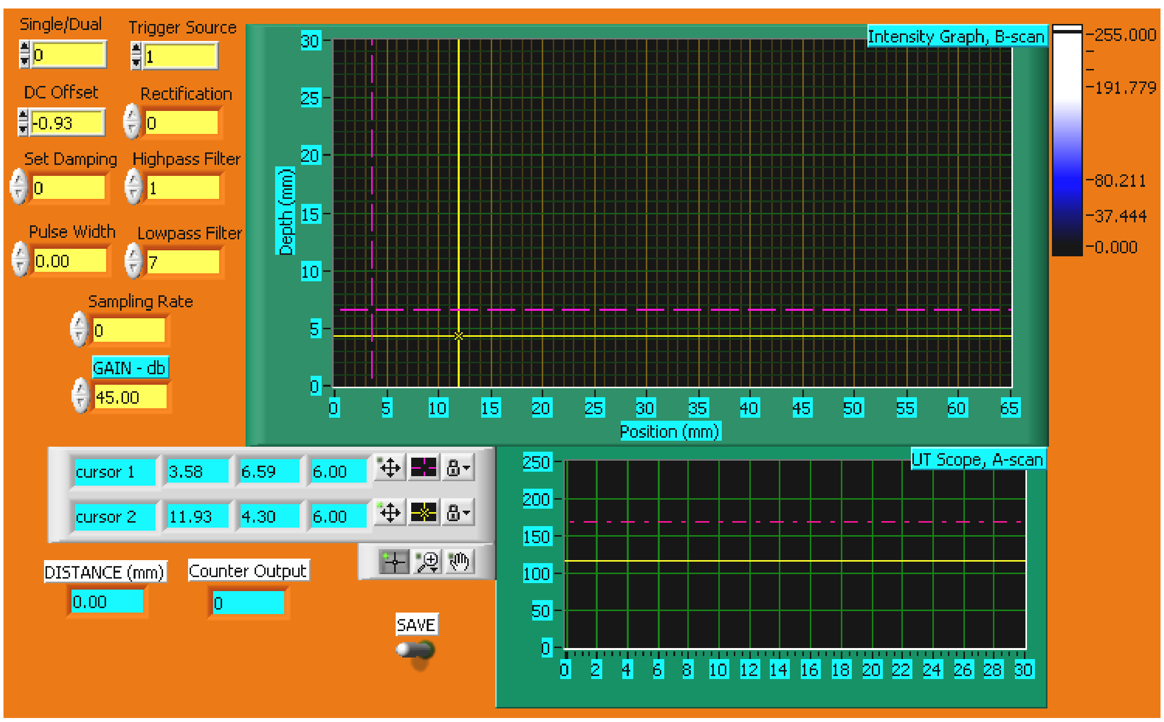

Figure 6.7: B-scan (intensity plot) representation and instrumentation settings

Once the image has been generated, one can decide to save it using the “SAVE” switch or to reset the screen to run another scanning. The new scanning is carried out just by gliding the slider back until it reaches the position chosen as starting point (back edge of the assembly). At that point the counter will read zero again, “Counter Output”, and a command will reset the image instantaneously. If the slider is moved forward again, the encoder counter will start counting positive counts back. This in turn will start a new data acquisition process without clicking any button. This feature allows an agile scanning.

The front panel of the “virtual instrument” allows adjustment of important parameters, for instance, signal rectification, high and low pass filters, pulse width, sampling rate, gain, etc [29]. In addition, it provides other capabilities such as multiple zoom, and two positioning cursors to compute the distance between any pair of points, cursor coordinates reader, etc. More details about of the operation and features of the front panel may be found in any help-tutorial of Labview software. Appendix C provides more details regarding the B-scan program.

6.5 Data Analysis

The ultimate goals of the data analysis procedure are to determine the distance between the transverse processes and evaluate the correlation between the images as well as the reliability of the measurements. In some parts we have the figures of the spinous processes to explain the data analysis and about the B-scan program. Each B-scan is created from a two-dimensional data array saved as a text string file for further analysis. The text files are loaded by a program written in labview, and an identical to the original B-scan display is re-built (Figure 6.8). As in the former program, the display has multiple imaging enhancement features such as different types of zooms, two cursors to compute the distance between any pair of points within the image, adjustment of different intensity thresholds to emphasize or disguise specific levels of amplitudes (brightness), distance-reading indicator, etc.

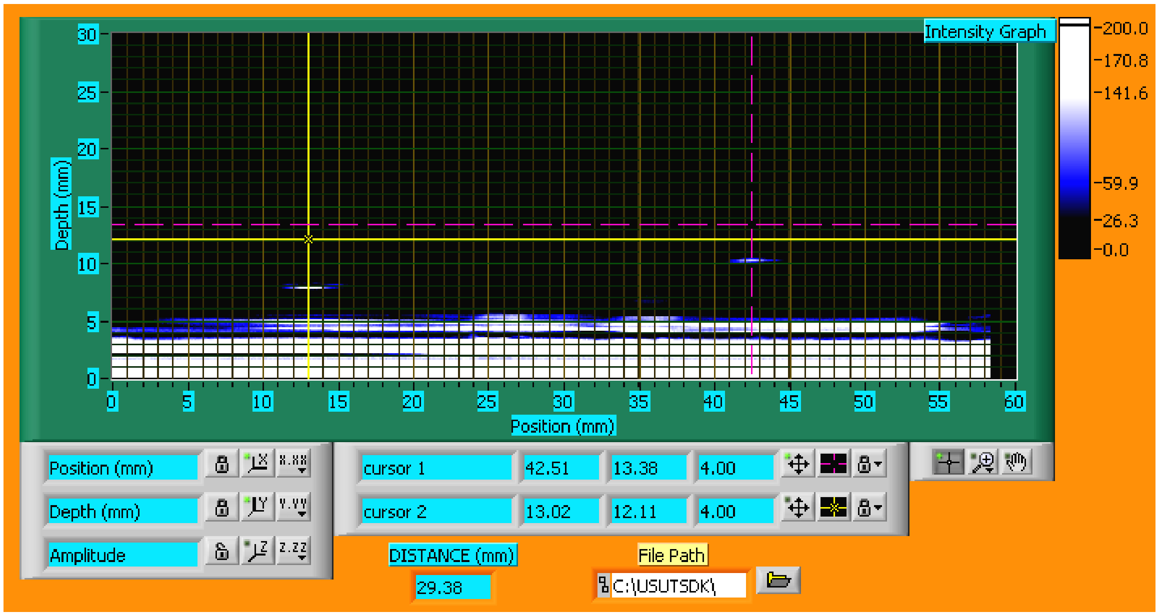

Figure 6.8: Front panel of the data analysis program

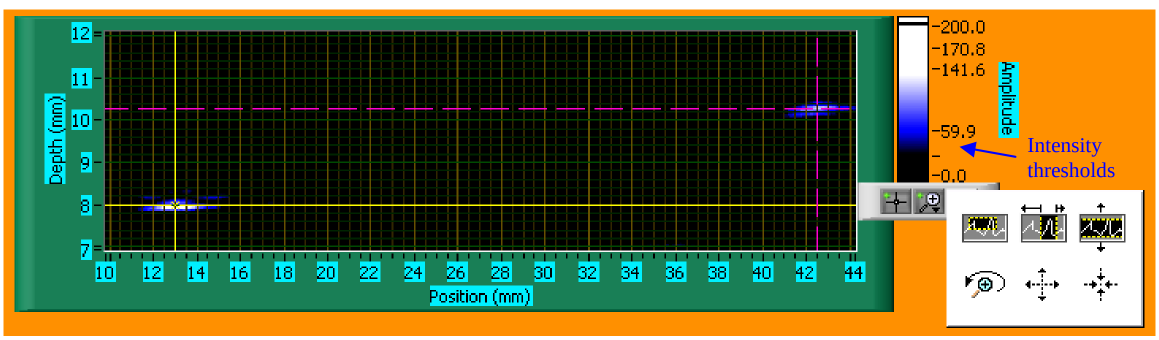

Figure 6.9: Zoom in image of Figure 6.8

Once an image has been loaded the intensity thresholds can be adjusted to improve the image definition of the spinous process indications regardless of the quality of the rest of the image. In fact, one could select a smaller area of the image containing just the spinous process indications (Figure 6.9), to obtain a better view of the shape and boundaries of each singularity. The measurement of the distance is achieved by positioning the cursors in the center of each spot. The "DISTANCE" meter of the front panel shows the distance between the X-coordinate of each cursor, which represents the distance between the spinous process tips.

6.6 Spatial Resolution, Encoder Resolution

The spatial resolution of the scanning refers to the number of excitations of the ultrasonic system, or, in other words, the number of samples taken for every millimeter that the transducer advances along the assembly. The greater the number of excitations, the better is the resolution of the system, which in turn implies a better accuracy in the scanning. This feature was restricted by the encoder resolution since the ultrasonic pulse generator was triggered as the encoder counter generated an output count. By experimental measurements it was established that 1972 counts were generated as the transducer displaced 56.8 mm. Dividing this distance by the number of counts one obtains that the separation at which every measurement is taken is $56.8/1972 = 0.028\,mm$. The proper performance of the ultrasonic system and computer diminished each time the transducer was moved fast along the assembly. Each time the encoder triggered the system, a complex and long procedure (excitation and reception of the ultrasonic pulse, analog to digital conversion of the information, data acquisition and processing, etc.) was carried on. The vast amount of data being acquired and processed by the computer in each excitation (due to the high sampling frequency) demanded a minimum time that can be exceeded if the encoder is rotated too fast. When this minimum time is surpassed, the computer is unable to consistently synchronize the data collection with the data storing, resulting in the creation of incoherent images. To ensure the usefulness of the scanning it was necessary to apply a delay to the scanning excitation rate. This was achieved by setting the program to start the scanning (excitation of the pulse generator) every increment of 4 of the encoder counter. In other words, four counts were skipped at every excitation. This fact in turn decreased the spatial resolution to one fourth the original resolution which corresponds to 0.112 mm. This rate is still excellent considering the order of magnitude of the separation between the center of the S.P. tips (experimentally found to be between 25 to 40 mm, depending on the size of the subject) and the size of their tip sections (between 5 to 20 mm depending on the size of the subject) [18].

6.7 Selection of the Transducer

The selection of the transducer obeyed geometrical and performance criteria. Sensibility and resolution of several probes acting on a human bone target (radius of a human arm) and on the artificial model were evaluated. The best results were achieved by immersion transducers since those are designed to match the acoustic impedance of water which is very close to that of soft tissue, $1.5{\cdot}10^6$ [Kg/m^{2}s] and $1.6{\cdot}10^6$ [Kg/m^{2}s] respectively. The 2.25MHz - 1/4" element size and 1.0MHz - 1/2" element size immersion transducers from Panametrics are selected for this purpose.

6.8 Test Sessions

Several testing sessions were conducted in LITEE Laboratory and the Veterinary School at Auburn University. The tests were carried out on artificial spine model. Each of the test sessions followed specific goals and procedures as it will be detailed next.

6.8.1 Tests on the Artificial Spine Model Using Customized Ultrasound System

The lumbar plastic spine segment is immersed in an unflavored gelatin solution, and left till it solidifies as shown in figure 6.10. A thin layer of gelatin covers the spinous process tips.

Figure 6.10: Artificial lumbar spine in the gelatin solution

The gelatin simulated the soft tissue surrounding the bone. Several samples of different concentration were tested in order to find the texture and flexibility that better matches soft tissue characteristics. The final concentration was of about 100 ml of water for every 7.06 g of gelatin powder.

The average wave propagation speed in the gelatin solution was, c= 1517 m/s, which correlates very well with the wave propagation speed of tissues such as fat (1450 m/s), muscle (1590m/s), and water (1480 m/s). This result added to the similitude in texture and flexibility and made gelatin a good approximation of the vertebrae-surrounding tissue without offsetting the effect of the heterogeneous nature of real tissue.

Tests of the artificial model were meant to measure the distance between the lumbar vertebrae by imaging the transverse process instead of the spinous process. Imaging the transverse process is important because the distance between the vertebrae is very small as we move up along the spine, and it really becomes difficult to measure the distance between the vertebrae by imaging the spinous process. The spinous process image in the cervical and thoracic zones will not be sufficiently clear to measure the distance between the vertebrae, but the distance between the transverse process will be significant which makes distance measurement easy.

Two immersion transducers of frequencies 2.25 MHz and 1 MHz were obtained from the leading manufacturer Olympus for this experimentation. The diameter of these two transducers was ½ inch. We had a new slider manufactured (as shown in Figure 6.11), especially for holding these two transducers, as the early slider had a small hole which was not sufficient to hold the new transducers. Translucent acrylic was used as the material for the slider.

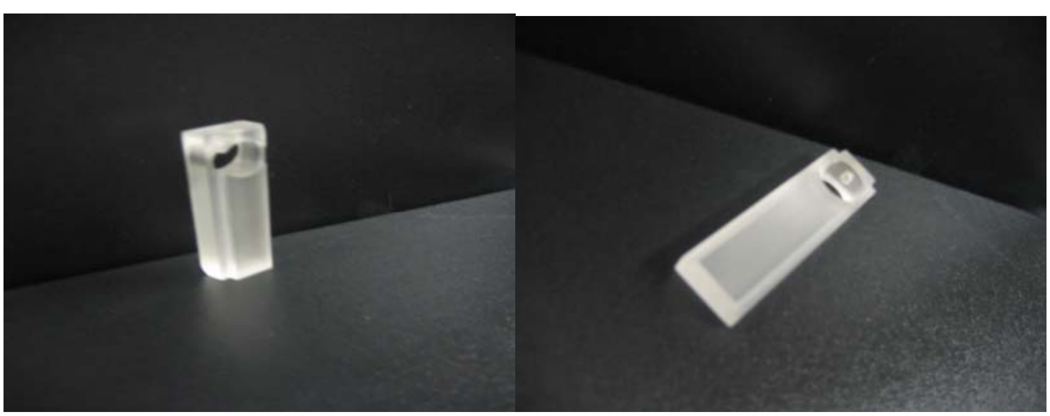

Figure 6.11: New slider with large diameter hole

For conducting experiments on the plastic lumbar spine, the necessary gel was prepared and the plastic spine was immersed in it and allowed to solidify. With this done, the assembly was carefully placed on the top of the different segments of the spine covering at least two contiguous transverse process tips in each scanning (as shown in Figure 6.12). A thin layer of water was spilled on the surface of the gelatin to allow the propagation of sound from the rubber film to the specimen. Provision was taken to remove any air bubble between the rubber film and the specimen surface as well as to fully cover the transducer tip with water during the whole test. An air bubble would obstruct the propagation of the wave to the specimen which would result in unexposed zones invalidating the test or leading to data interpretation error.

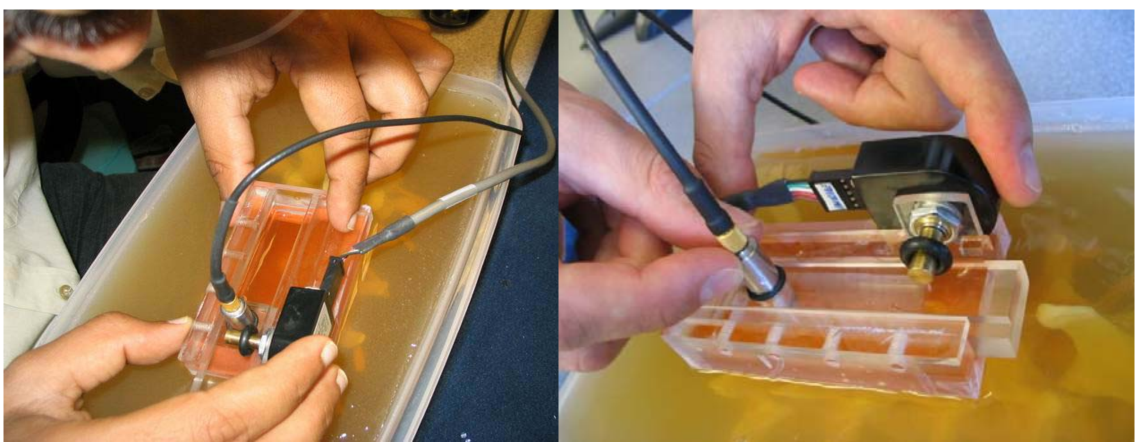

Figure 6.12: Scanning procedure of artificial sample

It was necessary to search for the best position above the transverse processes so that good reflections were received from their tips. The translucent nature of the gelatin eases this task making it possible to complete the data collection in a few minutes depending on the experience of the operator.

The LabVIEW B-scan program was used for this data acquisition. In general, the occurrence of a well defined and isolated peak would characterize the presence of a bone in the trajectory of the beam. The 2.25 MHz and 1 MHz immersion transducers were used for this scanning, but we did not get any reflections from the transverse process. Some reasons for not getting the image of the transverse process may be:

1) Due to the depth of the transverse process from the surface of the gelatin solution. Physical measurement showed that the transverse processes are 35 mm to 40 mm deep from the surface.
2) Due to the contour of the transverse process. The shape of the transverse process is very curvilinear which makes the ultrasonic wave to deflect from their path; thus waves may not reflect back.
3) Due to the immersion transducers which did not have enough energy to transmit the ultrasonic waves deep enough.

These shortfalls of the customized ultrasonic system required us to go to other ultrasonic devices to scan the transverse process. Thus we conducted the same experiments in the Veterinary School at Auburn University using the highly sophisticated ultrasound system, Philips HDI 5000, at that facility.

6.8.2 Tests on the Artificial Spine Model in VET School – Auburn University

Tests were next conducted on the artificial spine model using the Philips HDI 5000, ultrasonic system. These tests were conducted to check for the feasibility of measuring the distance between the lumbar vertebrae by imaging the transverse processes.

6.8.2.1 Specifications of the Ultrasonic System – Philips HDI 5000

The physical dimensions of the ultrasonic system shown in Figure 6.13 are:

- Weight – 380 lbs
- Height – 62 in (including the monitor)
- Width – 28.35 in
- Depth 39.35 in

Figure 6.13: Philips HDI 5000 Ultrasound System

This machine offers the different imaging modes:

- Gray-Scale 2D
- M-Mode
- Doppler
- Color 2D
- Color M-Mode
- Tissue Doppler Imaging (TDI)

The 2 Dimensional expresses a measurement with two dimensions on a flat plane. It is a cross-sectional representation of anatomical structures. 2D images also display motion. The position, texture, shape and dynamics of the anatomy displayed in the 2D image are presented in real-time. The 2D image is also used to orient the scanhead for M-Mode, Doppler, Color, and Power imaging. The 2D image allows us to locate the area of interest for magnification during the M-mode zoom. During the Doppler imaging, the 2D image provides a reference for sample volume, depth and size, and Doppler angle correction. The 2D image also provides the reference for the color display during the color and power imaging.

Using this 2D display, the scrolling Doppler display provides blood flow direction, speed, timing information and quality. An understanding of hemodynamics (i.e. study of the forces involved in the circulation of blood) and timing of normal and abnormal blood flow allows one to diagnose pathology using the Doppler display. M-Mode or Motion Mode is used with the 2D display. A line within the 2D image represents the M-line. Over time the movement of the anatomy along the M-line creates a scrolling display. M-mode is primarily used for cardiology imaging.

Color flow imaging uses Doppler principles to generate a color image. Color is related to velocity and direction in the color flow imaging. This information is then used to overlay a color image onto the 2D gray scale display. The color flow image provides information about blood flow direction, speed, quality and timing. Color flow imaging helps you locate blood flow disturbances. Tissue Doppler Imaging (TDI) is a color Doppler imaging technique used primarily in cardiology to display ventricular wall motion.

It can be used for diagnosis of abdominal, adult Cardiology, advanced breast imaging, cardiology contrast specific imaging (CSI), gynecological and Ffertility, musculoskeletal, neurology, obstetrical, pediatric/fetal cardiology, peripheral vascular, prostate and transcranial doppler [20].

6.8.2.2 Experiments Using Philips HDI 5000 Ultrasound System

These experiments were also conducted in the Veterinary School at Auburn University. The purpose of conducting these experiments was to find a suitable system for future work. The artificial lumbar spine model was set up in the gelatin solution before the experimentation (shown in Figure 6.14).

Figure 6.14: Artificial Lumbar Spine in Gelatin Solution

The Philips HDI 5000 system was equipped with three kinds of transducers. We have used the Linear Array Transducer having a varying frequency from 5 to 12 MHz. It has 128 elements and 38mm effective aperture length. This can be used to image vascular, small parts, breast, and musculoskeletal areas.

We started with imaging the transverse process of the L1 vertebrae using the linear array transducer. For proper coupling between the transducer and the gelatin surface, ultrasound gel was used. This coupling allowed for proper transmission and receiving of ultrasonic waves to and from the transducer. We were able to get the image of the L1 transverse process which was very difficult to image using our customized ultrasound system.

Using this highly sophisticated ultrasound system, Philips HDI 5000 we then measured:

1. The width of the transverse process on both sides of the vertebral body
2. Distance between the two contiguous transverse process
3. Depth of the transverse process from the surface of the gelatin surface
4. Width of the spinous process
5. Distance between the spinous process vertically along the body of the spinous process.

We began with measuring the width of the transverse process on the right side of the vertebral body. Once the linear array transducer was placed exactly on top of the transverse process, we obtained the real time 2D image on the screen. The transducer was moved until we get a better quality image of the transverse process. While doing this we could change the frequency of the transducer in real time. Once we saw the good quality image we were able to freeze the image on the screen and then measure what ever was needed using the cursors available to measure the distance. The distance measured could be seen on the lower left side of the picture. We also labeled the parts as shown in Figure 6.15. Once we made all the necessary measurements and labeling we saved the image on the machine. These saved images can then be transferred to the computer and later used for analysis purpose. The Figure 6.15 shows the width of the transverse process of the L1 vertebra. The width of the L1 transverse process was found to be 6.8 mm (or 0.68 cm).

Figure 6.15: Width of the L1 Transverse process on the right of the vertebral body

We did similar experiments on both sides of the vertebral body to measure the width of the transverse process. Figure 6.16 shows the width of the L1 transverse process.

Figure 6.16: Width of the L1 transverse process on the left of the vertebral body

Afterwards, the scans were performed covering all the transverse processes of the lumbar vertebra and making necessary measurements and labeling to identify them.

Our next activity was to measure the distance between the transverse processes. A procedure similar to the imaging the width of the transverse process was followed to get the image of the two transverse process in one image and thereby measure the distance between them (Figure 6.17). The figure below shows the distance between the L1 and L2 transverse process on the right of the vertebral body. The distance was found to be 3.29 cm from the top tip of the first transverse process to the top tip second transverse process and 3.26 cm when measured at the same level.

Figure 6.17: Distance between the L1 & L2 transverse process

Similarly the scans were performed to measure the distance between the other lumbar vertebra transverse process.

Our next step was to measure the depth of each transverse process from the surface of the gelatin. Scans were performed to measure this, and Figure 6.18 shows the depth of the L4 and L5 transverse process from the top surface of the gelatin.

Figure 6.18: Depth of L4 and L5 transverse process from the gelatin surface

We then planned on measuring the length of each spinous process as shown in Figure 6.19, and comparing the value with the value obtained by our customized ultrasound system. Following the same procedure, we then measured the length of all the five spinous lumbar vertebrae using the linear array transducer. Figure 6.19 shows the length of the L4 spinous process, and it was found to be 0.82 cm (or 8.2 mm).

Figure 6.19: Length of the L4 Spinous process

The same spinous process has been imaged using our customized ultrasound system and the length was found to be 0.84 cm (or 8.41 mm). Figure 6.20 shows the length of the L4 spinous process obtained using our ultrasound system.

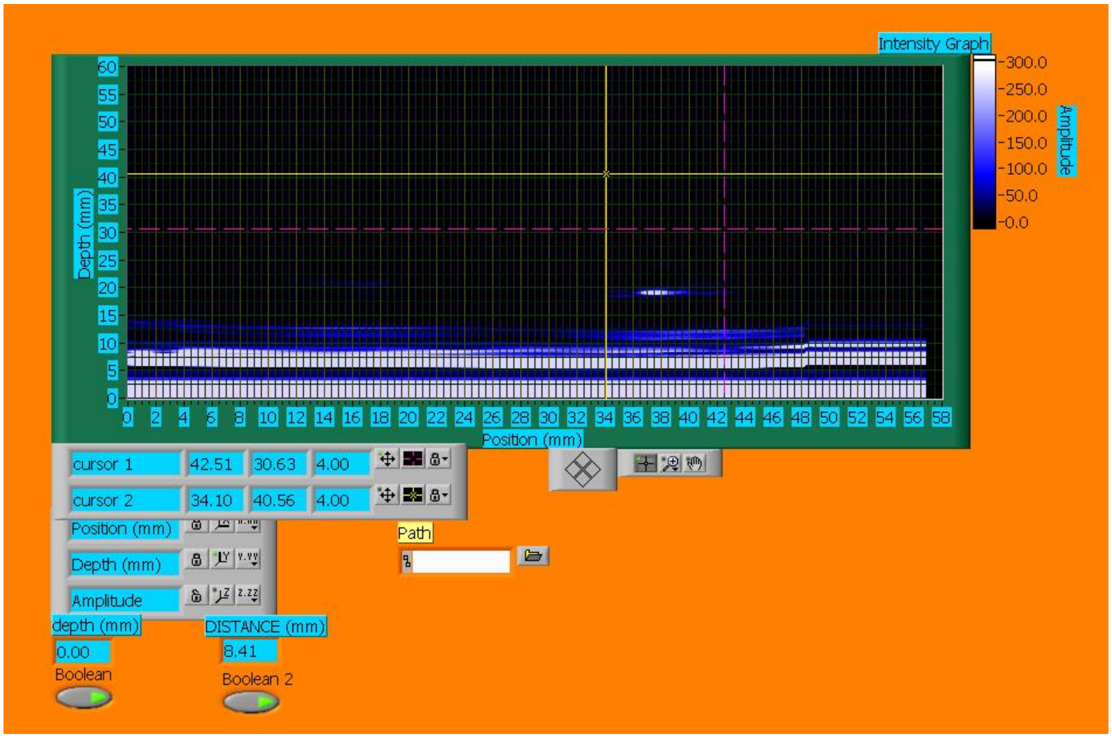

Figure 6.20: Length of the L4 spinous process

Finally scans were performed measuring the distance between the contiguous lumbar vertebrae vertically along the spinous process element as shown in Figure 6.21. Four to five measurements were made vertically along the spinous process. The figure below shows the four measurements made between the L3 and L4 lumbar vertebra.

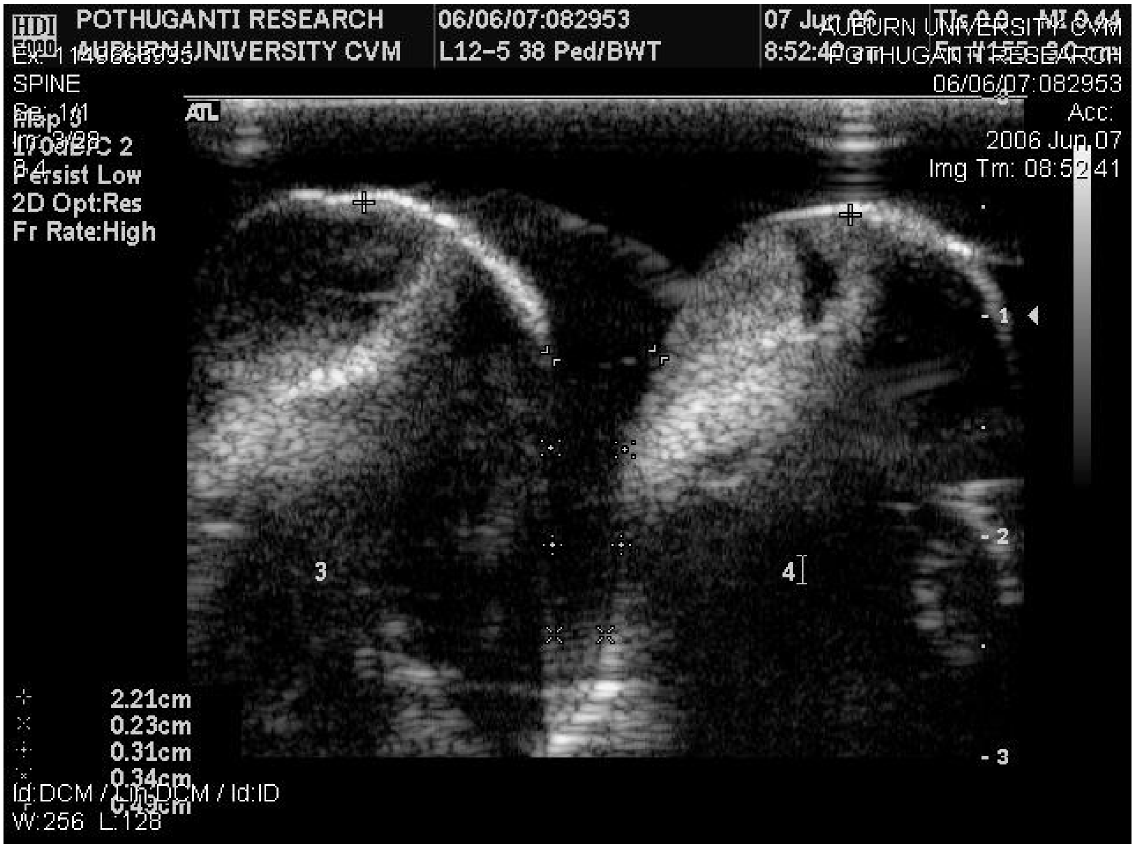

Figure 6.21: Vertical Measurements between the L3 and L4 lumbar vertebra

Another important features of this HDI 5000 system is the dual image capability. The length of the transducer was not enough to image three lumbar vertebrae at once, so, we used the dual imaging control to get the three vertebrae in a single image as shown in figure 6.22. The dual image control displays two 2D images side by side on the screen. Initially, after the first scan was made we could freeze the image and scan again for the second image, and then we could overlap the second image on the first image as shown in Figure 6.22.

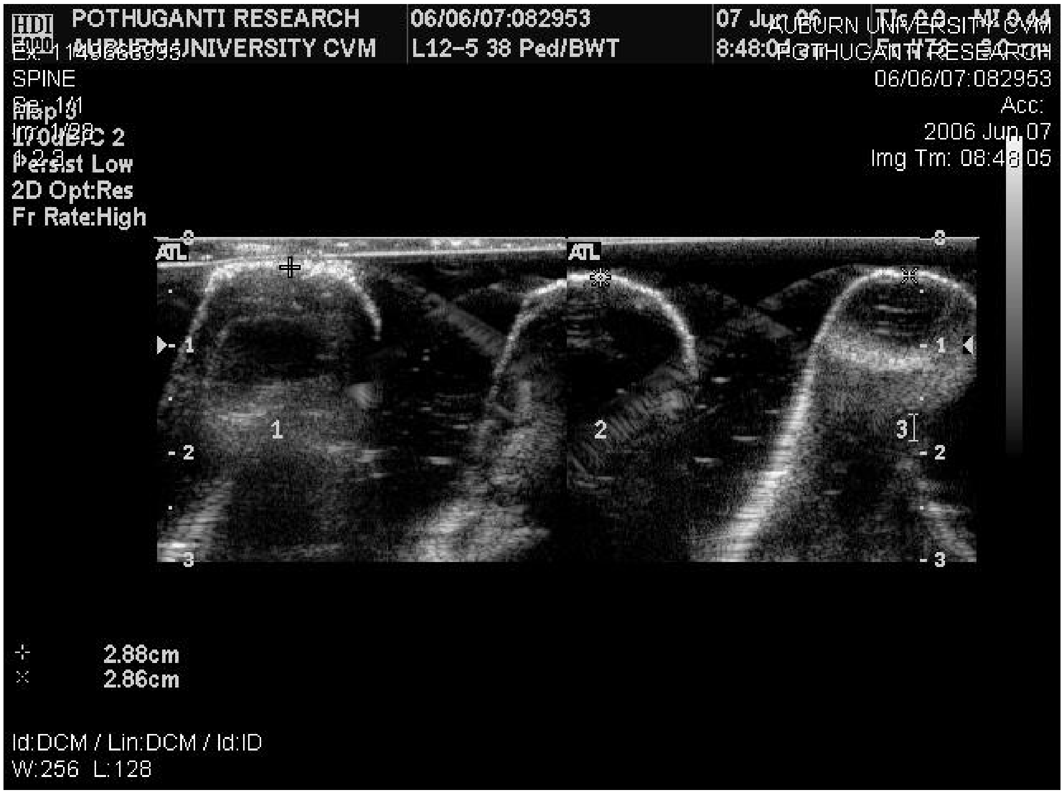

Figure 6.22: Dual Image of L1, L2 and L3 vertebrae

There is a disadvantage in using this dual image capability. We may not always be able to exactly attach the second image onto the first image where it has been cut. There will definitely some error in doing this. The only way to image three spinous processes is to use a linear array transducer having a long effective aperture length of around 50mm.

As our customized ultrasound system had certain limitations, we had to look for other sophisticated ultrasound systems which could serve our purpose. Using this ultrasound equipment, HDI 5000, we were able to measure what we had planned, and it had all features what we needed. We also compared some of the values obtained from

HDI 5000 system with our customized ultrasound system and evaluated our system's accuracy.

6.8.3 Simulating the Traction in the Artificial Lumbar Spine

Flexion -Distraction is an excellent technique for the treatment of middle and lower back pain. It is a gentle and extremely effective technique that helps to decompress the spine and remove pressure on the vertebral disc. In addition, it restores range of motion to the spine and realigns the vertebrae. Theoretically, the tractioning or distraction of the disc combined with isolation and gentle pumping of the involved area allows the central area of the disc, the nucleus pulposus, to assume its central position in the disc. In simple words, traction is like a pulling or stretching force to remove the pressure from the discs and increase the distance between them.

We have simulated the traction condition in the artificial lumbar spine using the 1 mm rings in between the vertebral body. First, we calculated the distance between the L1, L2 and L3 lumbar vertebrae without any 1 mm rings (as shown in Figure 6.23) in between them, and for the second set of scanning we inserted 1 mm rings in between the vertebral body and took the readings using our customized ultrasound system. Similarly we increased 1 mm more for the next set of experiments and so on until we had put 5 mm rings in between the lumbar vertebrae (as shown in Figure 6.24). This kind of setup simulates exactly what happens during the traction of the lumbar vertebrae.

Figure 6.23: L1, L2 and L3 Vertebrae with no 1mm rings

Figure 6.24: L1, L2 and L3 vertebrae with 5 mm rings in between

7. RESULTS AND DISCUSSION

7.1 Tests on the Artificial Spine Model

The real time images obtained from the Philips HDI 5000 were very clear for analysis providing reliable information relating to the spinous and transverse processes. It also enabled us to make all necessary measurements and labeling on the image (as shown in Figure 7.1). This Figure shows the image of the L4 vertebra and transverse process of L5 vertebra.

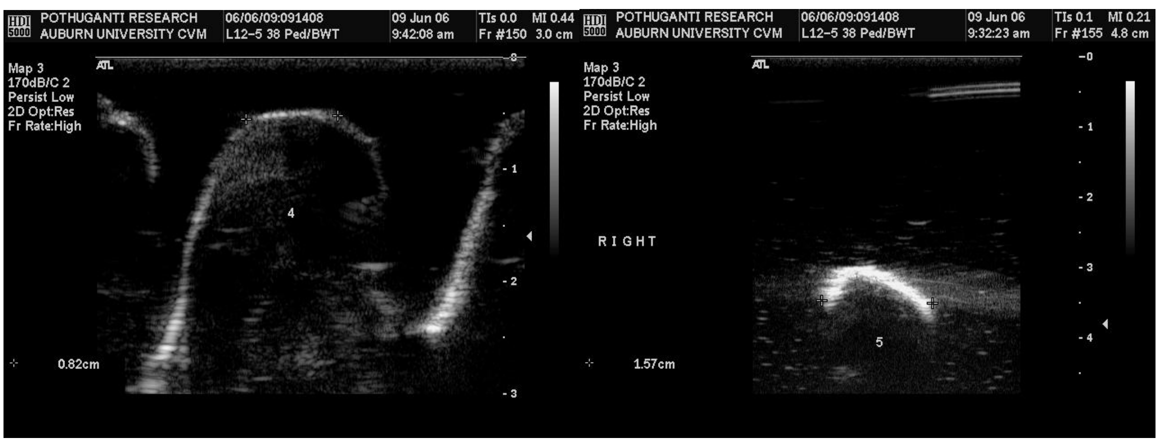

Figure 7.1: Image of L4 Vertebra and transverse process of L5 Vertebra from Philips HDI 5000 Ultrasound System

In the above Figure, whenever we make any measurement, the value appears on the lower left hand corner of the image. When we make 2 or more measurements, each measurement has a different symbol to identify the measurement; this symbol can be seen to the left side of the measurement value (as shown in Figure 7.2). The units of the measurement are shown to the right side of the value as shown in Figure 7.2.

Figure 7.2: Depth measurement of L4 and L5 transverse processes

Experiments were conducted to measure the depth of the transverse process from the surface of the gelatin solution. Table 7.1 shows the depth measurements of the transverse process.

Transverse Process	Left (mm)	Right (mm)
L1	29.9	24.1
L2	34.9	20.8
L3	34.2	27.4
L4	44.8	31
L5	34	26.9

Table 7.1: Depth of the Transverse Process

The next activity was to measure the width of each transverse process on both sides of the vertebral body. Table 7.2 shows the width of each transverse process in millimeters.

Transverse Process	Left (mm)	Right (mm)
L1	9.7	6.8
L2	11.6	8.6
L3	10.3	7.7
L4	8.7	11.3
L5	16.5	15.7

Table 7.2: Width of the Transverse Process

There was significant difference between the widths of the transverse process on the left and right side of the vertebral body. This explains the complicated shape of the transverse process and difficulty in imaging them. Moreover the shape of the transverse process is very curvilinear which makes the ultrasonic waves to deflect and makes it difficult to image using a single element immersion transducer.

We also measured the distance between the transverse process on both sides of the vertebral body. Table 7.3 shows the distance between the transverse process.

Transverse Process Section	Left (mm)	Right (mm)
L1-L2	28.9	32.6
L2-L3	34.4	29.2
L3-L4	31.3	32.9
L4-L5	28.1	29.5

Table 7.3: Distance between the Transverse Process

The shape of the lumbar vertebrae is very complicated as evidenced by the difference in measurements of the transverse process on both sides of the vertebral body.

The length of the spinous process was also imaged and the Table 7.4 shows the values of it.

Spinous Process	Length (mm)
L1	10.9
L2	10.7
L3	9.9
L4	8.2
L5	8.0

Table 7.4: Length of the Spinous Process from Philips HDI 5000

The same spinous processes length was measured using our customized ultrasound system. Figure 7.3 shows the length of the spinous process of L4 vertebra.

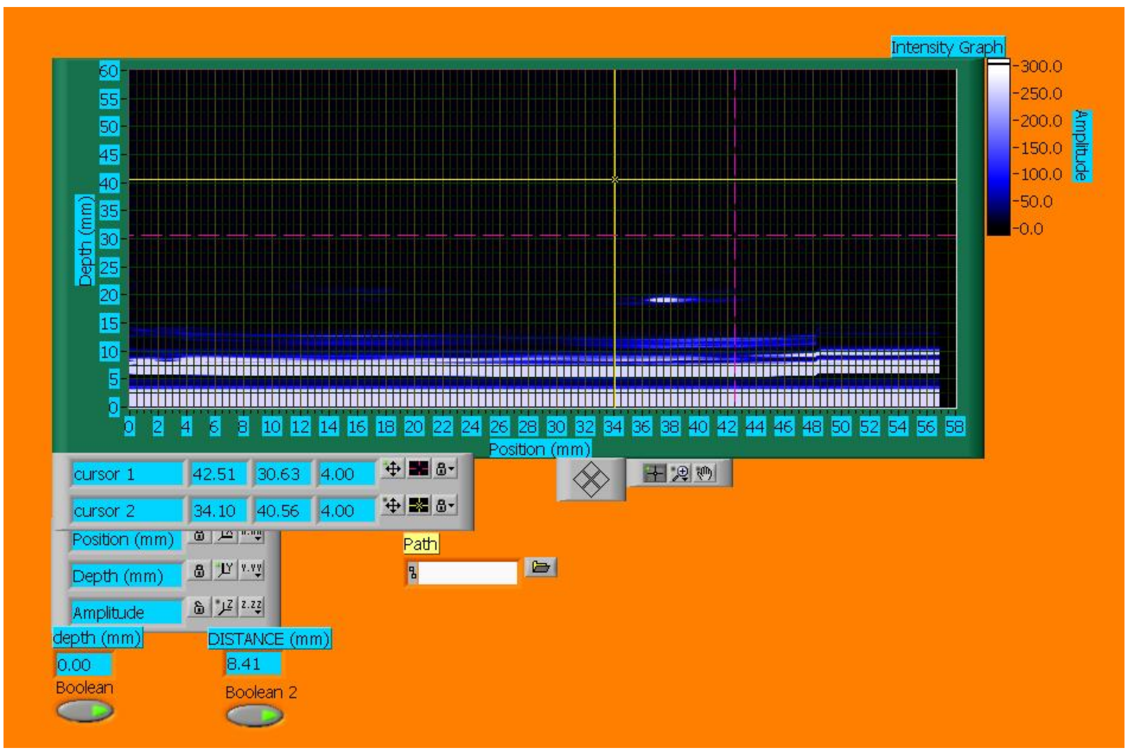

Figure 7.3: Image of the spinous process of L4 vertebra using our ultrasound system

Table 7.5 below shows the values obtained from our customized ultrasound system.

	L1	L2	L3	L4	L5
Trial 1	11.29 ± 0.11	10.60 ± 0.11	10.14 ± 0.11	8.41 ± 0.11	7.60 ± 0.11
Trial 2	11.40 ± 0.11	10.71 ± 0.11	10.14 ± 0.11	8.64 ± 0.11	7.83 ± 0.11
Mean (mm)	11.34 ± 0.11	10.65 ± 0.11	10.14 ± 0.11	8.52 ± 0.11	7.72 ± 0.11

Table 7.5: Length of spinous process from our ultrasound system

This spinous process length obtained from the two ultrasound systems was compared with the values obtained by vernier caliper. Table 7.6 shows the comparison of the spinous process length from the two ultrasound systems and the vernier calipers.

Spinous Process	Phillips HDI 5000 CV (mm)	OUR SYSTEM (mm)	Vernier Caliper (mm)
L1	10.9	11.34 ± 0.06	11 ± 0.1
L2	10.7	10.65 ± 0.06	10.4 ± 0.1
L3	9.9	10.14 ± 0	9.8 ± 0.3
L4	8.2	8.52 ± 0.12	8.5 ± 0.2
L5	8.0	7.72 ± 0.12	8.2 ± 0

Table 7.6: Comparison of Spinous Process Length

The three kinds of measurement were compared and a graph plotted using those values (shown in Figure 7.4).

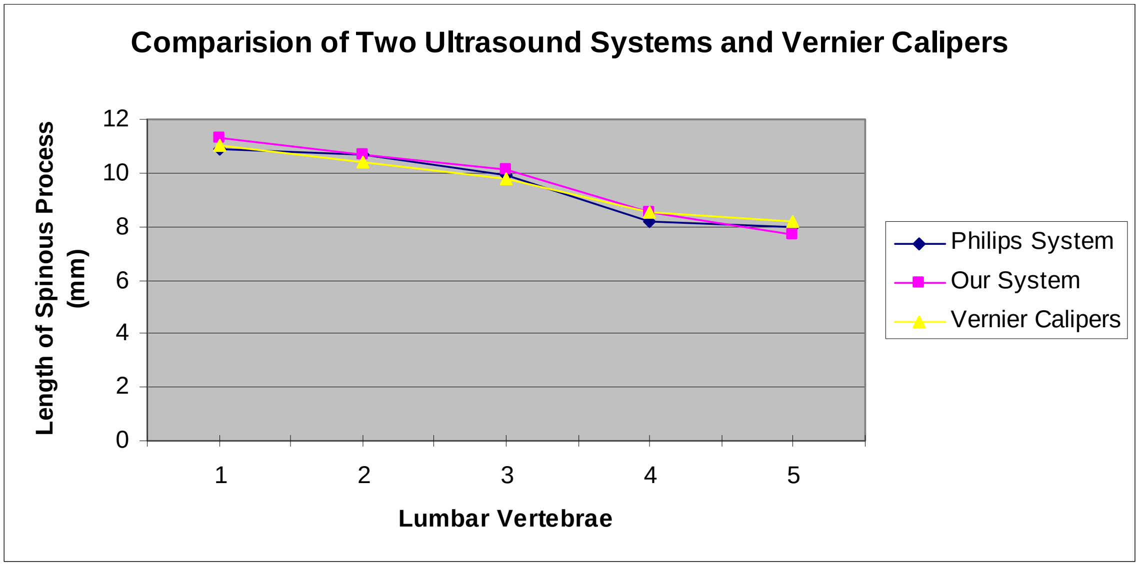

Figure 7.4: Comparison Graphing two ultrasound systems and vernier calipers

The values obtained from the vernier calipers were considered as a standard and the difference in values from the customized ultrasound system and Philips ultrasound system has been calculated and shown in table 7.7 and table 7.8.

Spinous Process	Vernier Caliper (mm)	Phillips HDI 5000 CV (mm)	Difference in Values (mm)
L1	11 ± 0.1	10.9	0.1
L2	10.4 ± 0.1	10.7	0.3
L3	9.8 ± 0.3	9.9	0.1
L4	8.5 ± 0.2	8.2	0.3
L5	8.2 ± 0	8.0	0.2

Table 7.7: Difference in spinous process length obtained from vernier calipers and philips system

Spinous Process	Vernier Caliper (mm)	OUR SYSTEM (mm)	Difference in Values (mm)
L1	11 ± 0.1	11.34 ± 0.06	0.34
L2	10.4 ± 0.1	10.65 ± 0.06	0.25
L3	9.8 ± 0.3	10.14 ± 0	0.34
L4	8.5 ± 0.2	8.52 ± 0.12	0.02
L5	8.2 ± 0	7.72 ± 0.12	0.48

Table 7.7: Difference in spinous process length obtained from vernier calipers and the customized ultrasonic system

The experiments conducted on the Philips HDI 5000 ultrasound system confirmed a lot of information and helped us to a better analysis of the lumbar vertebrae. The same ultrasound machine can be used to image the whole human spine with no difficulty.

7.2 Tests on Artificial Spine Model – Simulating the traction in the model.

The traction conditioned has been simulated in the artificial lumbar vertebra by placing the 1mm rings in between the vertebral body.

The most important sources of error linked to the testing system and procedure of scanning were imprecision in the data collection and data interpretation. Data were collected at points that were assumed to be right above the spinous process tips. The center of the tips was displayed by well defined shades and their mid points were used to compute the distance between the bone tips. To have consistent measurements the same reference points needed to be picked in all measurements, which obligate one to follow the same trajectory over the tips during every scan. This requirement was hard to comply with since there was no way to assure the probe was exactly in the same position above the bones.

For the first set of experiments there were no 1mm rings placed in between the lumbar vertebral body; this simulates the human vertebra before the traction treatment.

The Table 7.9 shows the values distance measured between the L1, L2 and L3 vertebra. We have calculated the Mean ($\tilde{x}$), Standard Deviation (SD) and Coefficient of Variation (CV) using the formulas:

$$\tilde{x} = \frac{\sum_{i=1}^{n} x_i}{n} \qquad 7.1$$

$$SD = \sqrt{\frac{\sum_{i=1}^{n} (x_i - \tilde{x})^2}{n}} \qquad 7.2$$

$$CV = \frac{SD}{\tilde{x}}.100 \qquad 7.3$$

Where x_i represents the elements of the sample of size n, i = 1, 2…..n.

Trials	L1-L2 Segment (mm)	L2-L3 Segment (mm)
1	27.30	29.84
2	27.30	29.84
3	27.30	29.84
4	27.42	29.84
Mean	27.33	29.84

Table 7.9: Distance between the Lumbar Vertebra with no 1mm rings

Second set of experiments was conducted by inserting the 1mm rings in between the vertebral body. This kind of setup simulates the little traction applied to the lumbar vertebra. Four measurements of the distance between L1, L2 and L3 spinous processes were recorded, and the mean, standard deviation and coefficient of variation has been calculated. Figure 7.5 shows the distance between the L2 and L3 spinous process. In the Figure you can notice the 2 clear reflections from the two spinous processes and the distance between them.

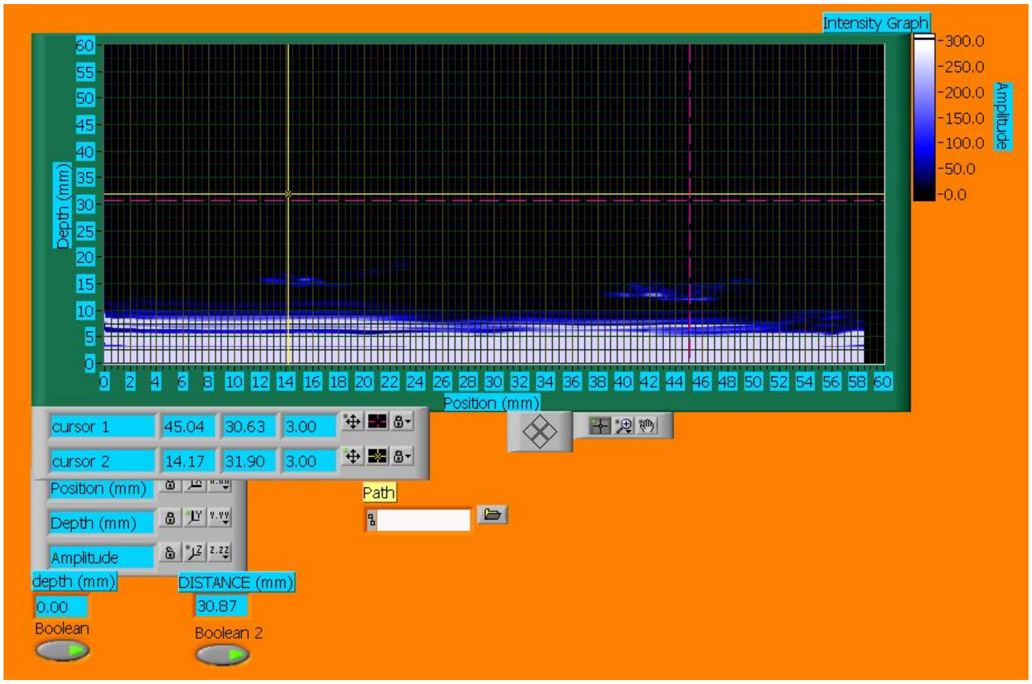

Figure 7.5: Distance between the L2 and L3 spinous process

Table 7.10 shows the distance measured between the vertebras when 1mm rings are placed in between.

Trials	L1-L2 Segment	L2-L3 Segment
1	28.34	30.87
2	28.11	30.87
3	28.11	30.87
4	28.34	30.87
Mean	28.23	30.87

Table 7.10: Distance between the lumbar vertebra with 1mm rings

For the next set of experiments we placed 2 mm rings in the vertebral body. Table 7.11 shows the distance measured between the L1, L2 and L3 lumbar vertebras when 2 mm rings are placed in between.

Trials	L1-L2 Segment	L2-L3 Segment
1	29.26	31.80
2	29.49	31.80
3	29.26	31.80
4	29.26	31.80
Mean	29.32	31.80

Table 7.11: Distance between the lumbar vertebrae with 2 mm rings

Similarly we placed 3 mm, 4mm and 5mm rings in between the lumbar vertebral body and measurements were made. All these measurements were conducted to simulate the traction applied to the human lumbar vertebrae. In the traction mechanism also, we gradually stretch the vertebrae there by increasing the distance between the lumbar vertebrae and decreasing the pressure in between them. Tables 7.12, 7.13 and 7.14 show the distance measured between the L1, L2 and L3 vertebrae when 3mm, 4mm and 5mm rings are placed in between the lumbar vertebral body respectively.

Trials	L1-L2 Segment	L2-L3 Segment
1	30.30	32.83
2	30.30	32.83
3	30.30	32.83
4	30.30	32.83
Mean	30.30	32.83

Table 7.12: Distance between the lumbar vertebrae with 3 mm rings

Trials	L1-L2 Segment	L2-L3 Segment
1	31.33	33.98
2	31.33	33.87
3	31.33	33.75
4	31.33	33.75
Mean	31.33	33.84

Table 7.13: Distance between the lumbar vertebrae with 4 mm rings

Trials	L1-L2 Segment	L2-L3 Segment
1	32.37	34.68
2	32.26	34.68
3	32.26	34.79
4	32.37	34.79
Mean	32.31	34.74
SD	0.06	0.06
CV %	0.19	0.17

Table 7.14: Distance between the lumbar vertebrae with 5 mm rings

Once all the experiments were done by simulating the traction condition in the artificial lumbar spine, all that remained was to calculate the differences between the measurements for analysis and for calculating how accurately our customized ultrasound system had imaged the spinous process in each set of experiments. Table 7.15 shows the difference between the spinous processes distances when there are no 1mm rings to the distance when there are 1 mm rings in between the vertebral body. The calculated difference is very close to 1mm, which shows that the customized ultrasound system can accurately image the spinous process.

	L1-L2 (mm)	L2-L3 (mm)
0 mm	27.33	29.84
1 mm	28.23	30.87
Expected Difference	1	1
Obtained Value	0.9	1.03
Error (mm)	0.1	0.03

Table 7.15: Difference in the spinous processes distance when 1 mm rings are used

Similarly the differences in the spinous processes distance were calculated when 1 mm rings and 2 mm rings are placed. The values are shown in table 7.16. Even these values were very close to 1mm difference.

	L1-L2 (mm)	L2-L3 (mm)
1 mm	28.23	30.87
2 mm	29.32	31.80
Expected Difference (mm)	1	1
Obtained Value (mm)	1.09	0.93
Error (mm)	0.09	0.07

Table 7.16: Difference in the spinous processes distance when 2 mm and 1mm rings are used

Similarly, differences in spinous processes were calculated when 2 mm, 3 mm, 4 mm and 5 mm rings are placed in between the vertebral body. Table 7.17, 7.18 and 7.19 show the differences respectively.

	L1-L2 (mm)	L2-L3 (mm)
2 mm	29.32	31.80
3 mm	30.30	32.83
Expected Difference (mm)	1	1
Obtained Value (mm)	0.98	1.03
Error (mm)	0.02	0.03

Table 7.17: Difference in the spinous processes distance when 2 mm and 3 mm rings are used

	L1-L2 (mm)	L2-L3 (mm)
3 mm	30.30	32.83
4 mm	31.33	33.84
Expected Difference (mm)	1	1
Obtained Value (mm)	1.03	1.01
Error (mm)	0.03	0.01

Table 7.18: Difference in the spinous processes distance when 3 mm and 4 mm rings are used

	L1-L2 (mm)	L2-L3 (mm)
4 mm	31.33	33.84
5 mm	32.31	34.74
Expected Difference (mm)	1	1
Obtained Value (mm)	0.98	0.90
Error (mm)	0.02	0.10

Table 7.19: Difference in the spinous processes distance when 4 mm and 5 mm rings are used

Finally, calculations were made by keeping the normal distance, with no 1 mm rings in between the spinous processes, as a reference or base line for calculating the difference for 1 mm, 2 mm, 3 mm, 4 mm, and 5 mm rings as shown in Tables 7.20, 7.21, 7.22, 7.23 and 7.24. Table 7.20 shows the differences calculated between the L1 - L2 and L2 – L3 when 1 mm rings are placed. The calculated differences were 0.9 and 1.03 mm, which are very close to the increased 1 mm distance.

	L1-L2 (mm)	L2-L3 (mm)
0 mm	27.33	29.84
1 mm	28.23	30.87
Expected Difference (mm)	1	1
Difference (mm)	0.9	1.03
Error (mm)	0.1	0.03

Table 7.20: Difference in normal spinous processes distance and when 1 mm rings are used

The table below shows the normal distance between the L1, L2 and L3 spinous process and when 2 mm rings are place in between them. The differences calculated were 1.99 and 1.96 mm, which are very close to the increased 2 mm distance.

	L1-L2 (mm)	L2-L3 (mm)
0 mm	27.33	29.84
2 mm	29.32	31.80
Expected Difference (mm)	2	2
Obtained Value (mm)	1.99	1.96
Error (mm)	0.01	0.04

Table 7.21: Difference in normal spinous processes distance and when 2 mm rings are used

The difference calculated when 3 mm rings are used is 2.97 and 2.99 mm, which is very close to the increased 3 mm distance.

	L1-L2 (mm)	L2-L3 (mm)
0 mm	27.33	29.84
3 mm	30.30	32.83
Expected Difference (mm)	3	3
Obtained Value (mm)	2.97	2.99
Error (mm)	0.03	0.01

Table 7.22: Difference in normal spinous processes distance and when 3 mm rings are used

Similarly the tables below show the differences calculated when 4 mm and 5 mm rings are used.

	L1-L2 (mm)	L2-L3 (mm)
0 mm	27.33	29.84
4 mm	31.33	33.84
Expected Difference (mm)	4	4
Obtained Value (mm)	4	4
Error (mm)	0	0

Table 7.23: Difference in normal spinous processes distance when 4 mm rings are used

	L1-L2 (mm)	L2-L3 (mm)
0 mm	27.33	29.84
5 mm	32.31	34.74
Expected Difference (mm)	5	5
Obtained Value (mm)	4.98	4.9
Error (mm)	0.02	0.1

Table 7.24: Difference in normal spinous processes distance when 5 mm rings are used

All the values calculated were very close to the increased distance between the spinous processes. This proved that our customized ultrasound system can be used for measuring the distance between the spinous processes very effectively and accurately.

8. CONCLUSIONS AND POTENTIAL FOR FUTURE DEVELOPMENT

The reliable, agile and inexpensive ultrasound based testing system developed for this project was tested and used to measure the distance between the lumbar vertebrae in a human spine by imaging the spinous process under simulated traction conditions in an artificial spine model by inserting a series of rings between the vertebral components. The results obtained were both effective and accurate; for example, the standard deviation (SD) was 0.05 mm and the coefficient of variation (CV) was 0.18% for the distance between L1 and L2 when no rings were inserted, and the SD was 0 mm and CV was 0% for distance between the L2 and L3 vertebrae. Similarly, when 5 mm rings were inserted, an SD of 0.06 mm and a CV of 0.06% were obtained for the L1 and L2 segment, with an SD of 0.19 mm and a CV of 0.17% for the L2 and L3 segment.

Moreover, the difference in the individual values was consistently in the range of ±0.05 mm. An extensive literature review revealed no previous reported use of ultrasound to measure the intervertebral distance between adjacent lumbar vertebrae using the spinous process tips as the anatomical reference in flexion distraction chiropractic manipulation or under traction conditions alone.

In continued testing experiments were conducted to measure the intervertebral distance between adjacent lumbar vertebrae by imaging the transverse process as an anatomical reference. For this experiment 2.25 MHz and 1 MHz immersion transducers were used to image the transverse process in an artificial spine model and a slider was constructed specifically to support these large diameter transducers. However, although multiple attempts were made, it was not possible to image the transverse process of the lumbar vertebrae, which represents a severe limitation of the new ultrasound system. The main reason for this inability to image the transverse process is thought to be the shape of the transverse process itself, which is very curvilinear. This causes the ultrasonic wave to be deflected in different directions and thus makes it impossible to collect the reflected ultrasonic waves using conventional immersion transducers. The literature search failed to reveal any previous reports of the use of ultrasound to measure the intervertebral distance of the adjacent lumbar vertebrae between transverse process tips as the anatomical reference in either flexion-distraction chiropractic manipulation or in the traction condition. However, the transverse process tips were used as the reference to measure the intervertebral distance in the lumbar zone during diurnal changes by Ledsome and Lessoway [31].

Another potentially serious limitation of this system is the magnitude of the error inherent in the testing system and the scanning procedure. Data were collected at points that were assumed to be immediately above the spinous process tips. The center of the tips was displayed by well defined shades and their mid points were used to compute the distance between the bone tips. However, in order to obtain reproducible measurements, the same reference points must be selected consistently in every measurement, which makes it imperative to follow exactly the same trajectory above the tips for every scan. This requirement was difficuly to comply with under the conditions of this study since there was no way to ensure that the probe was in exactly the same position above the bones for each run. This led to significant imprecision in both the data collection and data interpretation steps.

This inability to scan the transverse processes in the lumbar zone due to limitations in the scanning procedure, data collection and data interpretation made it necessary to seek a more sophisticated ultrasound system. The Auburn University School of Veterinary Medicine kindly made available their Philips HDI 5000 ultrasound system and this was used to gather a large number of additional measurements of the width of each transverse process and the distances between the adjacent transverse processes of the lumbar vertebrae. The length of the spinous process was also measured and compared with the values obtained using the ultrasound system constructed for this study. These two sets of values were also compared with vernier caliper measurements and the values obtained from all three data sources were found to be in good agreement.

This comparison, as well as the experiments conducted to simulate traction conditions in the artificial spine, verified that the new system can be used to measure the distance between the adjacent lumbar vertebrae by imaging the spinous process. It is not, however, suitable for measurements of the transverse process.

This research revealed that there is a great deal of potential for this new approach and it seems likely that many different kinds of experiments would benefit from the application of the customized ultrasound system developed for this study.

Although the customized ultrasound system was not used on human subjects who were being treated by the flexion distraction technique for this study, future research should examine its use on human subjects to measure the intervertebral distance before and after the flexion distraction technique. An additional set of experiments should be conducted on the artificial spine model to simulate the traction condition, with experiments repeated on consecutive days to confirm the repeatability and reliability of the system.

For further work, a highly sophisticated ultrasound system is needed. Using such a system will make it possible to image both the transverse processes and spinous processes in the lumbar zone and accurately measure the intervertebral distance. Other measurements of the artificial spine model can also be made, including:

1) Measuring the width of the transverse process by taking 10 measurements along the contour of the transverse process and comparing the results with those obtained using vernier calipers.
2) Measuring the vertical distance gap between the adjacent lumbar vertebrae and again comparing the results with those obtained using vernier calipers.
3) Measuring the intervertebral distance by imaging the spinous and transverse processes.

All these experiments should be performed at least twice to enable proper evaluation of the ultrasound technique in making these kinds of measurements. Once the principle has been established using the artificial spine model, the work can be extended to similar experiments on human subjects.

This system can also be used to image the intervertebral disc height by applying conventional transabdominal ultrasound imaging techniques.[33] The effectiveness of the flexion distraction intervention can be determined by imaging the surrounding tissue around the lumbar vertebrae, particularly the supraspinous and interspinous ligaments, to reveal exactly how their properties change as a result of flexion distraction chiropractic manipulation.[23]

REFERENCES

1. Matthew Hussey. Basic physics and technology of medical diagnostic ultrasound. *Elsevier Science Publishing Co., Inc. 1985*

2. Z.H. Cho, Joie P. Jones, Manbir Singh. Foundations of Medical Imaging. *John Wiley & Sons, Inc. 1993.*

3. D. Hans, T. Fuerst, F. Duboeul. Quantitative ultrasound bone measurement. *European Radiology.7 (Suppl. 2), S43-S50 (1997). Springer – Verlag 1997*

4. Y. Ishida, J.f. Carrol, M.L. Pollock, J.E. Graves, S.H. Leggett. Reliability of B-Mode ultrasound for the measurement of body fat and muscle thickness. *American journal of human biology 4:511-520 (1992).*

5. D.Wayne Rhodes, D.C. and Philip A. Bishop, Ed. D. A review of diagnostic ultrasound of the spine and soft tissue. *Journal of Manipulative and Physiological Therapeutics, volume 20, number 4, may 1997.*

6. Jason C. Birnholz. Fetal lumbar spine: Measuring axial growth with ultrasound. Department of diagnostic radiology and nuclear medicine, *Rush-Presbyterian-St.Luke's Medical Center, Chicago. 1985.*

7. Zeynep Siklar, Efgan Sanli, Yildiz Dallar and Gulten Tanyer. Diurnal variation of height in children. *Pediatrics International (2005) 47, 645-648*.

8. John R. Ledsome, Vickie Lessoway, Lark E. Susak, Faith A. Gagnon, Roy Gagnon, Peter C. Wing. Diurnal changes in lumbar intervertebral distance, measured using ultrasound. *Spine Volume 21, Number 14, pp 1671-1675. 1996.*

9. Claudia Naish, Richard Mitchell, John Innes, Mike Halliwell, Donal McNally. Ultrasound imaging of the intervertebral disc. *Spine Volume 22, number 2, pp 107-113. 1996.*

10. R Gosling. Medical Imaging with ultrasound: Some basic physics. *Phys. Educ. 24 (1989).*

11. Kurutzne KM, Bene E, Lovas A, Molnar P, Monori E. Biomechanical experiments for measuring traction lengthening of the lumbar spine during weight bath therapy. *Orv Hetil 2002 Mar 31 ; 143 (13) : 673- 84.*

12. Peter J. Shull. Nondestructive Evaluation. Theory, Techniques, and Applications. 2002.

13. Don E. Bray & Don McBride. Nondestructive Testing Techniques - 1992.

14. Don E. Bray & Roderic K. Stanley. Nondestructive Evaluation – A Tool in Design, Manufacturing, and Service. Revised Edition – 1997

15. Frederick W. Kremkau. Diagnostic Ultrasound - Principles, Instruments, and Exercises. Third Edition – 1989.

16. Jack Blitz and Geoff Simpson. Ultrasonic Methods of Non-destructive Testing, First Edition – 1996.

17. Josef Krautkramer. Ultrasonic Testing of Materials. Springer-Verlag, 1969.

18. Determination of the distance between adjacent lumbar vertebrae by an ultrasonic based image system, Ariel M Medina.

19. PCIUT 3100 – SDKLV, Software Development Kit for LabVIEW, User's Guide, UsUltratek, May 2002.

20. Philips HDI 5000, ATL Ultrasound– Reference Manual- 1998.

21. P H F Nicholsont, M J Haddaway: and M W J Daviet. The dependence of ultrasonic properties on orientation in human vertebral bone. Phys. Med. Biol. 39 (1994) 1013-1024. Printed in the UK

22. Marta Kurutz, Eva Bene, Antal Lovas, Erika Monori and Peter Molnár. Experimental Biomechanics of Human Lumbar Spine Segments.

23. Seong-Hwan Moon, MD, Moon-Soo Park, MD, Kyung-Soo Suk, MD, Jin-Suk Suh, MD, Sang-Hoon Lee, MD, Nam-Hyun Kim, MD, and Hwan-Mo Lee, MD. Feasibility of Ultrasound Examination in Posterior Ligament Complex Injury of Thoracolumbar Spine Fracture. Spine 2002;27:2154–2158

24. James W. Murakani, Bernadette L.Koch, Brian D.Coley, William E.Shiels, Gregory Bates and Mark Hogan. Diagnostic and interventional ultrasound of the pediatric spine. Pediatr Radiol (2001) 31: 775 – 785, Springer-Verlag 2001.

25. Dan Nemet, Tzipora Dolfin, Baruch Wolach and Alon Eliakim. Quantitative Ultrasound Measurements of Bone Speed of Sound in Premature Infants. Eur J Pediatr (2001) 160: 736 – 740.

26. Jason C. Birnholz, MD. . Fetal Lumbar Spine: Measuring Axial Growth with Ultrasound. Radiology 807, Volume 158, Number 3.

27. Gretchen A. W. Gooding, MD, Mitchel S. Berger, MD, Gregory D. Linkowski, MD, William P. Dillon, MD, Philip R. Weinstein, MD, James E. Boggan, MD. Transducer Frequency Considerations in Intraoperative US of the spine. Radiology 273, Volume 160, Number 1.

28. Claudia Naish, Richard Mitchell Et Al. Ultrasound Imaging Of The Intervertebral Disc. Spine, Vol 28, N° 2, Pp 107-113, 2003.

29. Weiss Gary. Spinal Ultrasound: Clinical Correlation Of Spinal Ultrasound And MRI. AJPM, Vol 6, N° 4, October 1996.

30. Osmo Tervonem Et Al. Ultrasound Diagnosis Of Lumbar Disc Degeneration. Spine, Vol 16, N° 8, 1991.

31. John Ledsome,Vickie Lessoway. Diurnal Changes In Lumbar Intervertebral Distance, Measured By Using Ultrasound. Spine, Vol 21, N° 14, Pp 1671-1675, 1996.

32. PCIUT 3100 – SDKLV, Software Development Kit for LabVIEW, User's Guide, USUltratek, May 2002.

33. Osmo Tervonen, MD, Seppo Lahde, MD, and Heikki Vanharanta, MD. Ultrasound Diagnosis of Lumbar Disc Degeneration. Comparison of computer tomography/discography.

APPENDICES

APPENDIX A

LITERATURE REVIEW ON IMAGING OF LUMBAR VERTEBRAE AND THE INTERVERTEBRAL DISTANCE USING THE ULTRASOUND

The following is a literature review of the most significant investigations done in the area of diagnostic and quantitative ultrasound as well as in the biomechanics of lumbar spine. The review consists in a summary of the articles describing their objective, methodology used and the results.

A.1 Review of Research Papers

1. *The dependence of ultrasonic properties on orientation in human vertebral bone*

Speed of sound (SOS) and broad-band ultrasound attenuation (BUA) were measured in cubes of human trabecular bone from lumbar venebrae, in the three major anatomical axes. The three major anatomical axes are:

1) Cranio-caudal (cc)
2) Antero-posterior (AP) axes,
3) Lateral (LT)axes

There were significant differences in the SOS and BUA when measured across the different axes. SOS was approximately 500 m s^{-1} greater than in either the lateral (LT) or antero-posterior (AP) axes, and BUA was approximately 23 dB MHZ^{-1} cm^{-1} greater. Small, but significant, differences existed between the AP and LT axes for both SOS and BUA. In the AP and LT directions, strong linear correlations existed between SOS and apparent density (correlation coefficient, r = 0.90), and between BUA and apparent density (r = 0.96). In the cc axis, correlations with density were poorer [21].

2. *Experimental Biomechanics of Human Lumbar Spine Segments*

The aim of research was to clear the biomechanical background of traction bath therapy curing low back pain problems, moreover, to obtain the mechanical characteristics of human lumbar segments for the FEM model of human spine in tension. The authors developed a special subaqual ultrasound method for measuring the deformations of the lumbar segments of human body suspended in water. Special software has been used for analyzing the ultrasound pictures. In vivo deformations of segments L3-L4, L4-L5 and L5-S1 have been measured. Experiments were conducted on 155 adult patients taking around 3000 ultrasound pictures of 400 segments.. Biomechanical parameters like sex, age, weight, height of the body and the viscoelastic behaviour of segments have been analyzed. Just after being suspended in water, 30-50% of patients shows instant elastic tensile deformation, by registering a mean value of 1, 0-1,1 mm elongation per segments. At the end of the 20 minutes long weightbath treatment, elongation of lumbar segments have been registered practically in 55-60% of patients without any extra weights, and in 70-85% of patients with 20-20N extra lead loads applied on the ankles. The total mean viscoelastic elongation of human lumbar segments is about 1,2-1,7 mm in average of deformable segments. As for the biomechanical parameters, a significant difference has been demonstrated in reaction time of men and women. Women react more slowly, however, after 20 minutes the deformations are equal to that of the men [22].

3) *Feasibility of Ultrasound Examination in Posterior Ligament Complex Injury of Thoracolumbar Spine Fracture*

A study was done one 12 patients with thoracolumbar spinal fractures, to assess the feasibility of ultrasound examination for posterior ligament complex injury in thoracolumbar spinal fractures. In posterior ligament complex injury of thoracolumbar spine fracture, the reliability of magnetic resonance imaging (MRI) for diagnosis has been reported. Nevertheless the usefulness of ultrasound for diagnosis has not been studied, whereas diagnostic ultrasound has been applied in the musculoskeletal system.Two healthy volunteers without a history of spinal trauma were recruited for pilot examination of the ultrasound procedure to access normal findings of the posterior ligament complex. This study investigated 12 thoracolumbar spine fractures. Four were flexion distraction injury, six were stable or unstable burst fractures, and two were simple compression fractures. Ultrasound was performed over the injured area by an experienced musculoskeletal radiologist in addition to radiography and MRI. Five patients underwent operative procedures to stabilize the fractured spine. Imaging data and operative findings were correlated with ultrasound examination. In the patients who did not undergo surgery, agreement in diagnosis between MRI and ultrasound was moderate (5 of 7) and in the patients who underwent surgery, correlation between MRI, ultrasound, and operative findings was excellent, especially in diagnosing the status of the supraspinous and interspinous ligaments. Nevertheless, it is impossible to visualize deep seated structures (i.e., ligamentum flavum, deep muscles of the spine, and facet joint) with ultrasound. This study demonstrated the excellent diagnostic ability of ultrasound to detect the status of the supraspinous and interspinous ligaments, especially in patients who undergo surgery. Although ultrasound examination appears to be less sensitive than MRI in predicting ligament status, the cost effectiveness of ultrasound and its use as an alternative to MRI in special situations (i.e., patients with pacemaker, ferromagnetic implant, or severe claustrophobia) should be emphasized [23].

4) *Spinal Ultrasound: Clinical correlation of spinal ultrasound and MRI*

The objective of this study was to determine the clinical utility of spinal ultrasound by demonstrating its sensitivity to patient clinical history and neurological examination and to compare its findings to the findings of MRI. Ultrasound was found to have an increased sensitive when compare with MRI in detecting injuries and inflammation of the spinal structures, it was more highly consistent with patient's history and clinical examination. The study confirms the usefulness of spinal ultrasound especially in soft tissue application. This raises the conclusion that less expensive ultrasound should be used as a screening test prior to a more expensive MRI for low back pain. There exist the needs of statistically validate studies [29].

5) *Diagnostic and interventional ultrasound of the pediatric spine*

Research was done to show that the ultrasound can be used as a diagnostic tool in the evaluation of the pediatric spine. MRI is the primary modality for spine imaging in children and adults, ultrasonography is an important and useful modality in the neonate and infant. The non-ossified posterior elements of the infant offer an excellent acoustic window for evaluation of the spine. With ultrasonography, exposure to ionizing radiation is avoided, no patient sedation is required and accurate diagnoses are generated. High resolution linear array transducers up to 15MHz are used for getting the excellent detail of the spine from a posterior approach. They were successful in imaging children up to 1 year of age, although the quality of ultrasound images often decreases markedly after approximately 6 months of age due to increased posterior element ossification. The ultrasound has been used for diagnosing various other kinds of diseases related to the human spine. At the end it was concluded that, despite MRI being the definitive modality for imaging the spine, ultrasound remains a powerful and viable tool for imaging the neonatal and pediatric spine and can successfully guide interventional procedures [24].

6) *Quantitative Ultrasound Measurements of Bone Speed of Sound in Premature Infants.*

Experiments were conducted to measure the bone speed of sound in premature infants by quantitative ultrasound. Experiments were conducted on a total of 44 neonates which included 29 premature infants and 15 full term infants. The left tibial speed of sound (SOS) was measured by quantitative ultrasound. Bone SOS was successfully measured in all infants. A significant correlation between tribial SOS and gestational age ($r=0.78$, $P<0.0005$), but a significant inverse correlation between tibial SOS and post-natal age ($r = - 0.78$, $P<0.0005$). But bone SOS was significantly higher in full term infants compared to premature infacts. In conclusion, the results indicate that the tibial speed of sound was reduced in premature infants compared to full term infants [25].

7) *Fetal Lumbar Spine: Measuring Axial Growth with Ultrasound*

Ultrasound (US) can be used to visualize vertebral segments, suggesting a quantitative means of studying vertebral column growth in utero and thus a means of detecting developmental abnormalities. US images of the lumbar spine were obtained in 128 clinically normal fetuses between the gestational age of 11 through 41 weeks. A large-aperture, dynamically focused US system capable of regional magnification was used. Lateral coronal, transverse, and sagittal views of the lumbar spine were obtained with a large-aperture, dynamically focused array system, operated at a 3.5- on 5.0-MHz center frequency (Acuson 128; Mountain View, Calif.). The focal zone was placed at the depth of the spine, and selective magnification was used so that the lumbar spine occupied half or more of the horizontal extent of the display matnix (which is allocated dynamically over 1,024 pixels horizontally and 486 TV lines vertically). Preprocessing amplification was logarithmic, with a 30- on 40-dB plateau and mildly sigmoidal gray-scale assignment for slight accentuation of upper- level reflectors. Images were made with integration of four to ten successive video frames. Average lumbar spacing was calculated from distance between centrums of at least four lumbar bodies. The average distance between lumbar centrums increased nearly linearly throughout the second and third trimesters 2

0.98). Enhanced anatomic display implies new capabilities for recognizing developmental abnormalities antenatally [26].

8) *Ultrasound Imaging of the Intervertebral Disc*

The main concern of this article is to determine the reliability of ultrasound imaging in the detection of structural changes associated with disc pathology. An In Vitro ultrasound imaging of dog intervertebral disc was performed. The discs of several dogs were stripped of all surrounding tissue and scanned using ultrasound before being sectioned and photographed. The ultrasonic images were compared with the photographs, which were graded previously in order to allow an evaluation of the progressive stage of the disc degeneration. Ultrasonic imaging of several disc demonstrated echo patterns that matched, in both location and appearance, real structural defects identifiable on the sectioned disc. This initial study shows that ultrasound images can contain a high degree of structural information, relate well with the pathologic condition of the disc, and is able to locate specific pathologic defects [28].

9) *Ultrasound Diagnosis Of Lumbar Disc Degeneration*

The purpose for this study was to evaluate the accuracy of ultrasound for imaging internal disc changes, and to asses its value as a screening method for symptomatic disc prior to CT/discography. A total of 56 discs in 29 patients were examined by both methods. The sensitivity of ultrasound for recognizing a discographically painful and deteriorated disc was 0.95, and its specificity was 0.38. Correspondingly, the predictive value of a positive US finding was 1.53, and that of the negative finding was 0.13. The reproductively of the US depend on the experience of the examiner to a great extent more than in other radiologic examination, and the system of classification has to be simple in order to keep the interobserver error at a reasonable level. Nevertheless, US proved a reliable method for detecting structural changes in intervertebral disc. It provides a cost effective method for screening prior to discography; if a disc is normal in US, a clinical significant lesion is improbable, and CT discography can be omitted. If US shows locally or generally increased the echogenicity, an intradiscal lesion is probably, and CT/discography needs to be perform to evaluate the clinically significance of the finding [30].

10) *Diurnal Changes In Lumbar Intervertebral Distance, Measured By Ultrasound*

The study measure the distances between the tips of the transverse processes of adjacent lumbar vertebrae (L1-L4) in the same subjects after one day of normal activities and again the next morning. Its objective was to evaluate the feasibility of directly measure the lumbar intervertebral distance using ultrasonography and to determine the magnitude of the diurnal change. Measurements were made on six occasions in each of six patients after 6:00 PM at evening and the following morning before rising. The results show that the measurements were done in an individual with a coefficient of variation of 7.5%. The reproducibility of the measurements of the total distance was better than ± 4%. The intervertebral distances between L1 to L4 were significantly greater in the morning than in the evening. These results shown that the measurement of the change in the distances between the lumbar vertebrae is feasible to perform by using ultrasonography [31].

11) *Transducer Frequency Considerations in Intraoperative US of the spine*

Intraoperative spinal ultrasound has been used on 15 patients to determine the effect of transducer frequency. Fourteen men an one women underwent intraoperative US studies of the spine immediately after a spinal laminectomy had been performed. All patients but one had spinal stenosis and/or disk disease that affected the cervical cord (n=5), the thoracic cord (n=1), or the lumbosacral area (n=8). Three different commercial real-time units were available. Both 5 MHz and 10 MHz transducers were used on one patient and the transducer with the option of 3.5, 5 or 7.5 MHz was used in ten, and a 10 MHz transducer was used on four other patients. A 10 MHz frequency transducer produced images superior to images produced with either 5 MHz or 7.5 MHz transducers, as determined by characterization of fine morphologic detail of the spine with magnification of the image. The 3.5 MHz transducer frequency was suboptimal for diagnostic detail. Intraoperatively, the 10 MHz transducer, which had superior spatial resolution, produced the most detailed images of spinal cord, the surrounding subarachnoid fluid, the radicular arteries, and the dural sheath [27].

APPENDIX B

TECHNICAL SPECIFICATIONS OF THE ULTRASOUND SYSTEM

B.1 PCIUT3100 - Ultrasonic Pulser/Receiver and 100 MHz A/D Board for PCI Bus

PCIUT3100 is a combination of a pulser/receiver and a high-speed analog to digital converter on a single PCI board as shown in figure B.1. The board generates an electrical pulse with user-defined pulse voltage and pulse width. The pulse is transmitted to an ultrasonic transducer, which converts the electrical excitation pulse into an ultrasonic pulse. The pulse is then propagated into couplant or the material to be tested. The transducer receives the echoes that are reflected from the interface and converts the ultrasonic pulse back into an electrical signal. The on-board receiver processes the signal with the user defined parameters, and the A/D converter converts analog signals into digital data at a rate of 100 million samples per second. In addition, the digital data is transferred to a computer's RAM at about 10 MB per second. The resolution of the conversion is 9 bits, which can scale from 0 to 511. The memory depth can reach up to 256 kilo samples [51].

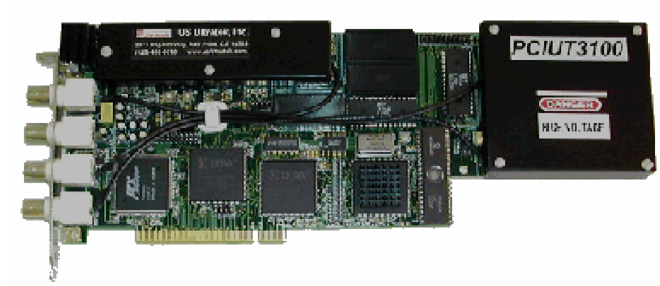

Figure B.1: PCIUT3100 board

B.1.1 Technical Specifications of PCIUT Board

Pulse Voltage	-40V to -300V, 256 steps. Higher voltages are available upon request.
Pulse Width	50 ns to 484ns, 256 steps Optional 15 ns is available upon request.
Damping	620?, 340?, 200?, 160?, 60?, 55?, 50?, or 47?
Internal Trigger	10 Hz to 5000 Hz in 10 Hz increments when internal trigger is selected.
Receiver Gain	0 dB to 80 dB in 0.1dB increments.
DC Offset	-2.5V to +2.5V in 5mV increments
Low Pass Filter	All, 48MHz, 28MHz, 18MHz, 8.8MHz, 7.5MHz, 6.7MHz, or 5.9MHz
High Pass Filter	4.8MHz, 1.8MHz, 0.8MHz, or 0.6MHz
Waveform	Full rectify, + half rectify, - half rectify, or RF
Sampling Rate	100MHz, 50MHz, 25MHz, 12.5MHz, 6.25MHz, 3.125MHz, 1.5725MHz, and external clock < 100MHz
Transducer Mode	Single (Pulse/Echo) or dual (through transmission)
Resolution	8 bits (0 to 255) or 9 bits (0 to 511)
Memory	16 kilo samples and 256 kilo samples
Waveform Length	16 to 16382 in 4 sample steps
Trigger Source	external, internal or software
Connectors	3 BNC connectors: Pulse out, receiver in, and external trigger in
Post Trigger delay	2 to 32764 samples in 2 sample step
Dimensions	12.5"x4.25" not including BNC and PCI edge connectors
Add-on Options	- BNC external clock connector - BNC trigger sync output connector - Logarithmic amplifier - Distance amplitude correction - Up to 4 encoder counters and connectors - Two additional 14-bit A/D converters - 256K sample memory upgrade - Windows software development kits - Hardware security key module - Hardware key development kit - Multi-channel control option

Table B.1: Technical specifications of PCIUT3100 board

B.2 2 Slot CardBus PCI Expansion Systems

MAGMA’s 2 slot CardBus PCI Expansion System is general purpose bus expansion system for the PCI local bus. MAGMA's 2 Slot Cardbus-to-PCI Expansion Systems provide two full-length 32-bit or 64-bit PCI slots in a separate enclosure (chassis) that connects to a PC notebook or Apple PowerBook (which do not have built-in PCI slots) through a 32-bit CardBus slot, figure B.2. With MAGMA's patented PCI Expansion Technology, everything installed in the enclosure actually acts as if it's inside the notebook. The PCI expansion system consists of CardBus card, an expansion bus cable, an expansion motherboard and a chasis with the power supply.

Figure B.2: MAGMA's 2 Slot Cardbus-to-PCI Expansion Systems

B.2.1 General Specifications:

- Backplane: Two standard PCI slots and One non-standard PCI slot (32-bit/33MHz or 64-bit/33MHz)
- Standard Expansion Cable Length: 1 meter (1.5 meter is optional)
- PCI Local Bus Specification: Revision 2.2
- PCI Bridge Architecture Specification: Revision 1.1
- Interconnect Bandwidth: 132 MB/sec (Theoretical Max. of PCI 33/32)
- MTBF: 25,000 hours
- Operating Environment: 0º to 50º C Operating Temperature, -20º to 60º C Storage Temperature , 5% to 85% Relative Humidity, Non-condensing
- Supported Operating Systems: Win XP, Win 2000, Win NT, Win ME, Win 98SE, Mac OS X (version 10.2.2+), Mac OS 9.x, and Red Hat Linux 9 [52].

B.3 Ultrasonic Transducer

Panametrics Slim Line V384, 3.5 MHz immersion ultrasonic transducer, Figure B.3. This Video Scan series transducer is an untuned device that provides heavily damped broad band performance. This type of transducer are the best choice in applications where good axial and distance resolutions are necessary or in test that require improved signal-to-noise ratio in attenuating or scattering materials. Figure B.4 shows the Video Scan performance of a 5MHz transducer.

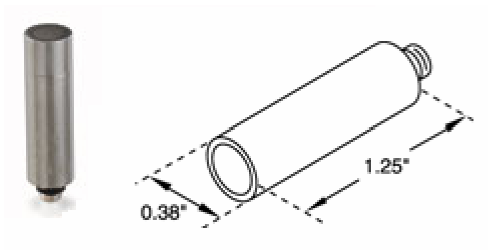

Figure B.3: Immersion Ultrasonic Transducer

B.3.1 General Specifications:

- Stainless steel case is only 0.38 in (10 mm) in diameter, ideal for limited access areas.
- Standard connector style is Straight Microdot Connector (SM)
- Available in 0.25 in (6 mm) and 0.125 in (3 mm) element diameters.

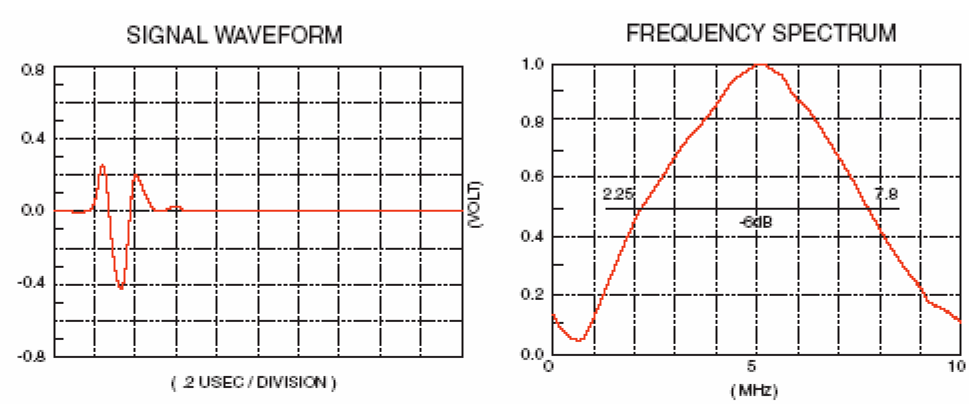

Figure B.4: Signal waveform and frequency spectrum of a Video Scan 5 MHz transducer

B.4 Assembly

The assembly is the component where encoder and transducer are held, figure B.5. It has two principal elements, the base body and the slider. Both are made out of reluctant high density acrylic. The base body was assembled bonding 5 machined parts together as shown in figure B.5.

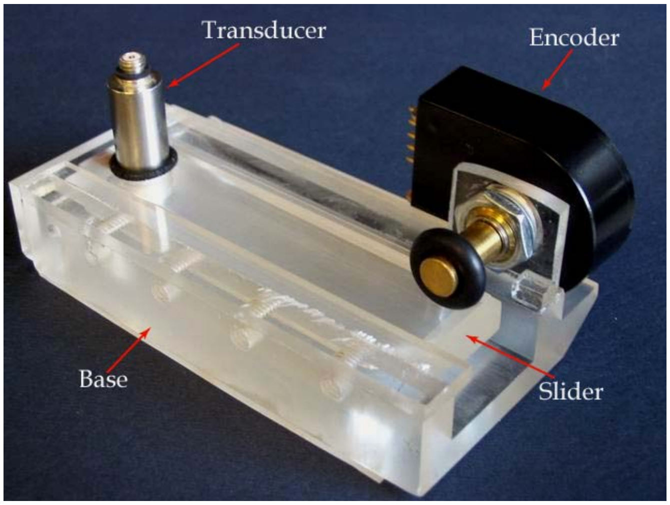

Figure B.5: Final Assembly

APPENDIX C

LABVIEW PROGRAMS AND DLL

C.1 Dynamic Link Library

A dynamic link library **PCIUTDLL.dll** is provided with this software development kit to give a user an access to PCIUT3100 pulser/receiver and analog to digital converter board from a LabVIEW program. There is only one function call in the dynamic link library **PCIUTParms()** to send the parameters to the board and get acquired data as well as encoder information from the board. There are four parameters for the function call **PCIUTParms()**.

int PCIUTParms(int mode, int board, DWORD wParam, int lParam);

Parameter **mode** is a number starting from 1000 that defines the purpose of the function call. Different number specifies different control tasks. The values of this parameter are defined in the pciut.h file.

Parameter **board** is the board number. A 0 specifies the first PCIUT3100 board in the computer. If an invalid board number is specified, the parameter will be downloaded to the active board. A function call with a valid **board** number will set the active board.

Parameters **wParam** and **lParam** are the additional information past to the function. They have different meanings depending on the parameter **mode**.

The modes of the Dll function used for the programming of the B-scan program are described next. For a complete description of all modes refer to reference 19.

ISDATAREADY (mode = 1000), Get data status

Get the status of the data acquisition process.

wParam: not used

lParam: not used.

Return: 0 if no data in the memory yet. Otherwise there are data in the memory.

SOFTWARETRIGGER (mode = 1001), Generate a software trigger

Generate a software trigger. After this function call the board will generate a pulse from the PULSE OUT connector, and the analog to digital converter will start converting analog signal to digital data with the user-specified parameters. The digital data will be saved in the -board memory.

To generate a software trigger, the trigger source needs to be set to software trigger. See the section.

mode=1016 below for details.

wParam: not used

lParam: not used.

Return: 1 if successful.

SETSAMPLINGRATE (mode = 1002), Set Sampling Rate

Set sampling rate.

wParam: index which is from 0 to 7. Default is 0.

0 - 100 MHz

1 - 50 MHz

2 - 25 MHz

3 - 12.5 MHz

4 - 6.25 MHz

5 - 3.125 MHz

6 - 1.5725 MHz

7 - external clock

lParam: Not used, Return: 1 if successful.

SETLOWPASSFILTER (mode = 1004), Set Low Pass Filter

Set receiver low pass filter.

wParam: index which is from 0 to 7. Default is 0 which means no filter.

0 - No filter

1 - 148 MHz

2 - 28 MHz

3 - 18 MHz

4 - 8.8 MHz

5 - 7.5 MHz

6 - 6.7 MHz

7 - 5.9 MHz

lParam: Not used

Return: 1

SETHIGHPASSFILTER (mode = 1005), Set High Pass Filter

Set receiver high pass filter.

wParam: index which is from 0 to 3. Default is 3 which means 0.6 MHz.

0 - 4.8 MHz

1 - 1.8 MHz

2 - 0.8 MHz

3 - 0.6 MHz

lParam: Not used

Return: 1

SETRECTIFIER (mode = 1006), Set Rectifier

Set receiver signal type.

wParam: index which is from 0 to 3. Default is 3 which means RF signal (no rectification).

0 - Full wave rectify

1 - positive half rectify

2 - negative half rectify

3 - RF signal (no rectification)

lParam: Not used

Return: 1

SETDAMPING (mode = 1007), Set Damping Resistor

Set the pulser damping resistor value on a single channel PCIUT3100 card. Use SETMCHANDAMPING or SETCHANDAMPING to set the damping resistors on a multi-channel board DT16B (or DT8B.)

wParam: index which is from 0 to 7. Default is 0 which is 620 ohms.

0 – 620 ohms

1 – 339 ohms

2 – 202 ohms

3 – 159 ohms

4 – 60 ohms

5 – 55 ohms

6 – 50 ohms

7 – 47 ohms

lParam: Not used

Return: 1

SETTRANSDUCERMODE (mode = 1008), Set Transducer Method

Set the transducer method, pulse/echo or through transmission on single channel PCIUT3100 card. Use SETCHANTRANSDUCERMODE or SETMCHANTRANSDUCERMODE to set the transducer mode on a multi-channel board DT16B (or DT8B.)

wParam: index which is 0 or 1. Default is 0 which is pulse/echo.

0 – pulse/echo. In this case the board connects PULSE OUT and RECEIVE IN together.

1 – through transmission

lParam: Not used

Return: 1

SETBUFFERLENGTH (mode = 1009), Set Buffer Length

Set the buffer length that specifies how many data samples that the next acquisition will collect data.

wParam: number of samples to take. It ranges from 16 to 16382 in step of 4 samples. Default

value of the buffer length is 4000 samples.

lParam: Not used

Return: 1

SETPULSEVOLTAGE (mode = 1011), Set Pulse Voltage

Set pulse voltage.

wParam: index which is from 0 (-300V or –350V with –350V option) to 255 (-40V). The default is 255 which is -40V. Section 3.35 describes how to get the information about the –350V pulse voltage. Pulse voltage can be set from -40 V to -300 V. The formula is pulse voltage (V) = -(4 + 4000 / (0.392157 x Index + 13.5)).

Use the following formula to calculate the pulse voltage for –350V option pulse voltage (V) = -(4 + 4000 / (0.392157 x Index + 11.56))

lParam: Not used

Return: 1

SETPULSEWIDTH (mode = 1012), Set Pulse Width

Set pulse width.

wParam: index which is from 0 to 255. Default is 0 which is the minimum pulse width. The minimum pulse width Wmin can be obtained by using function call mode=1025. Normally it is 50 ns or 28 ns with special order. Pulse width can be set from minimum pulse width to 480 ns. The formula is Pulse width (nanoseconds) = 18 + (760.8 x index) / (161.67 + Index). If the result is less than Wmin, Wmin should be used.

lParam: Not used

Return: 1

SETGAIN (mode = 1013), Set Gain

Set the receiver gain. This function sets the gain of both fixed gain amplifier and the DAC amplifier. If DAC is on, this function sets the fixed amplifier only. The DAC gain can be set by using function call mode=1015. When the gain is a negative number, the amplifier acts like an attenuator. At this point the attenuation is not linear to the calculated value. So the attenuation value is not reflecting the true attenuation. The number is just for reference.

wParam: index which is from 0 to 1023. It specifies the total gain from -20 dB to 80 dB for both amplifiers, or -10 dB to 40 dB for the fixed gain amplifier along. Default is 511 which is 30 dB of the global gain. Receiver gain can be set from -20 dB to 80 dB with about 0.1 dB resolution. The formula is Receiver gain (dB) = 0.0978 x (Index – 204)

lParam: Not used

Return: 1

SETDCOFFSET (mode = 1014), Set DC Offset

Set the receiver DC offset.

wParam: index which is from 0 to 1023. Default is 511 which is 0V.

DC offset can be set from –2.5V to 2.5V with 5mV resolution. The formula is DC offset = 0.005 x Index

lParam: Not used

Return: 1

GETENCODERCOUNTER (mode = 1017), Get Encoder Counter

Get the encoder counter from one of the counters.

wParam: index of the counter.

0 – first encoder (X axis)

1 – second encoder (Y axis)

2 – third encoder (Z axis)

3 – forth encoder (W axis)

lParam: Not used

Return: counter value from -8388608 to 8388607.

SETENCODERCOUNTER (mode = 1018), Set Encoder Counter

Set the value of an encoder counter.

wParam: index of the counter.

0 – first encoder (X axis)

1 – second encoder (Y axis)

2 – third encoder (Z axis)

3 – forth encoder (W axis)

lParam: counter value from -8388608 to 8388607.

Return: 1

GETDATA (mode = 1019), Get Digitized Data from Memory

Get the digitized data from the memory on the board after the data acquisition.

wParam: pointer of the receiving buffer: (unsigned char *)

lParam: number of bytes to move from the board memory to the buffer. It should be multiple of 4.

Return: -2 if wParam is NULL or 1 if successful.

RESETCOUNTER (mode = 1020), Reset A/D Board

Use this function call to reset the analog to digital converter before acquiring data.

wParam: not used

lParam: not used

Return: 1

RESETMEMORY (mode = 1021), Reset Memory

Use this function call to clean up any data in the memory. It should be called before acquiring data.

wParam: not used

lParam: not used

Return: 1

SETOFFSETADJUSTMENT (mode = 1022), Reset DC Offset Adjustment

Use this function call to set DC offset adjustment which can make the signal smoother.

wParam: 0 - change the adjustment value and download it to the board 1 – do the task above and save the adjustment value in the Non-Volatile memory on the board. So it can be retrieved when the program starts running again.

lParam: adjustment value fro –127 to 127.

Return: 1

GETMODELNUMBER (mode = 1023), Get Board Model Number

Get the model number of the board. Normally it is PCIUT3100.

wParam: pointer of the receiving buffer: (char *). It should have enough room for at least 20 characters.

lParam: not used

Return: -2 if wParam is NULL or 1 if successful.

GETSERIALNUMBER (mode = 1024), Get Serial Number

Get the serial number of the board. The serial number can be used to verify which board you are talking to.

wParam: pointer of the receiving buffer: (char *). It should have enough room for at least 20 characters.

lParam: not used

Return: -2 if wParam is NULL or 1 if successful.

GETMEMORYSIZE (mode = 1025), Get Memory Size

Get the size of the memory. The returned value could be 16384 or 262144.

wParam: not used

lParam: not used

Return: size of the memory.

C.2 Labview Programs

The B-scan program developed in Labview is presented in the next pages. In order to understand the elements of the diagram and the sequence of the operations the readers need to be familiar with Labview programming. Structures such as the one next to the symbol "*"in the next page, are called sequences and contain multiple substructures. The subsequences are depicted in subsequent pages.

C.2.1 Labview Diagram of B-scan Program

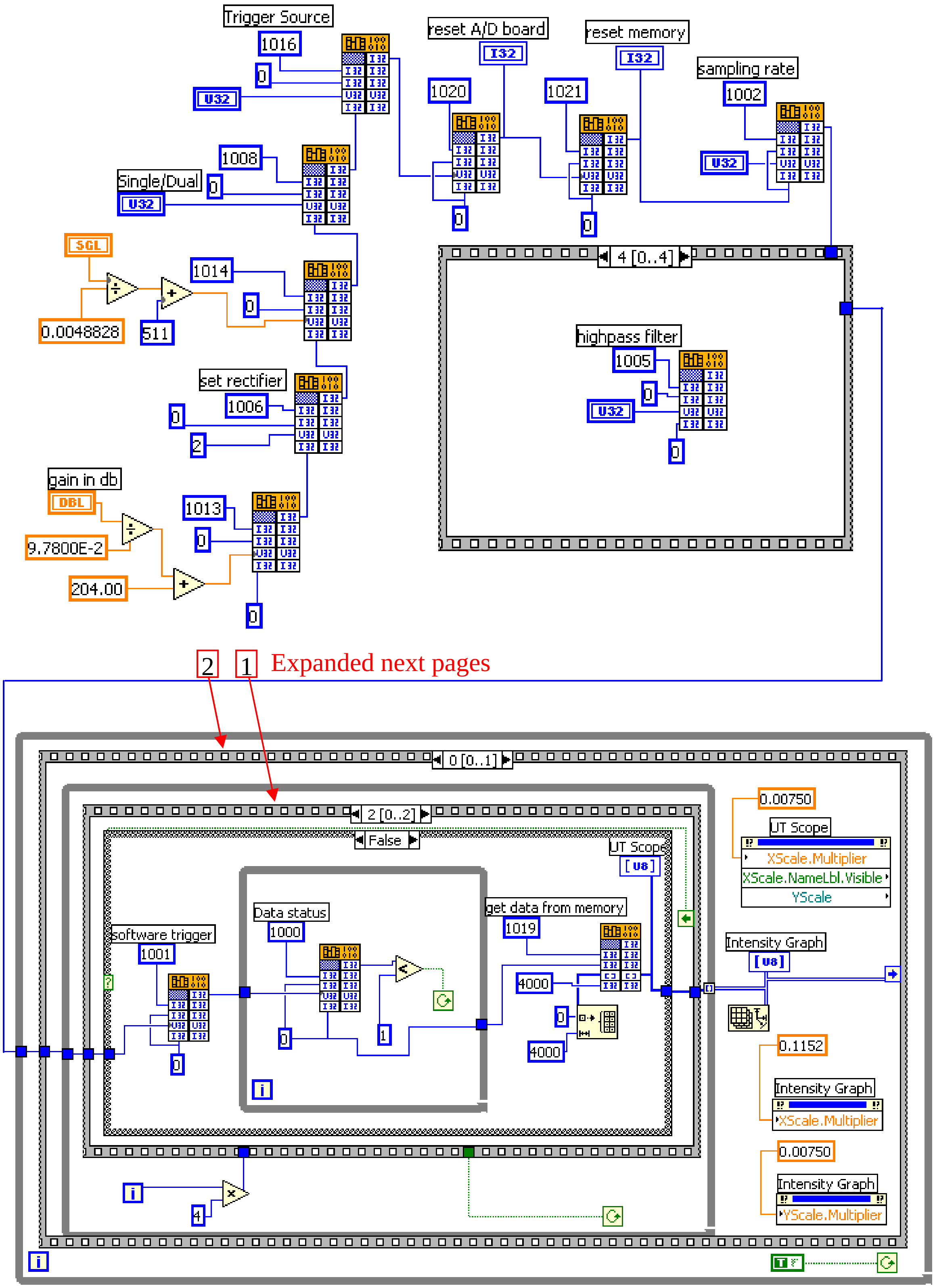

Sequence 1

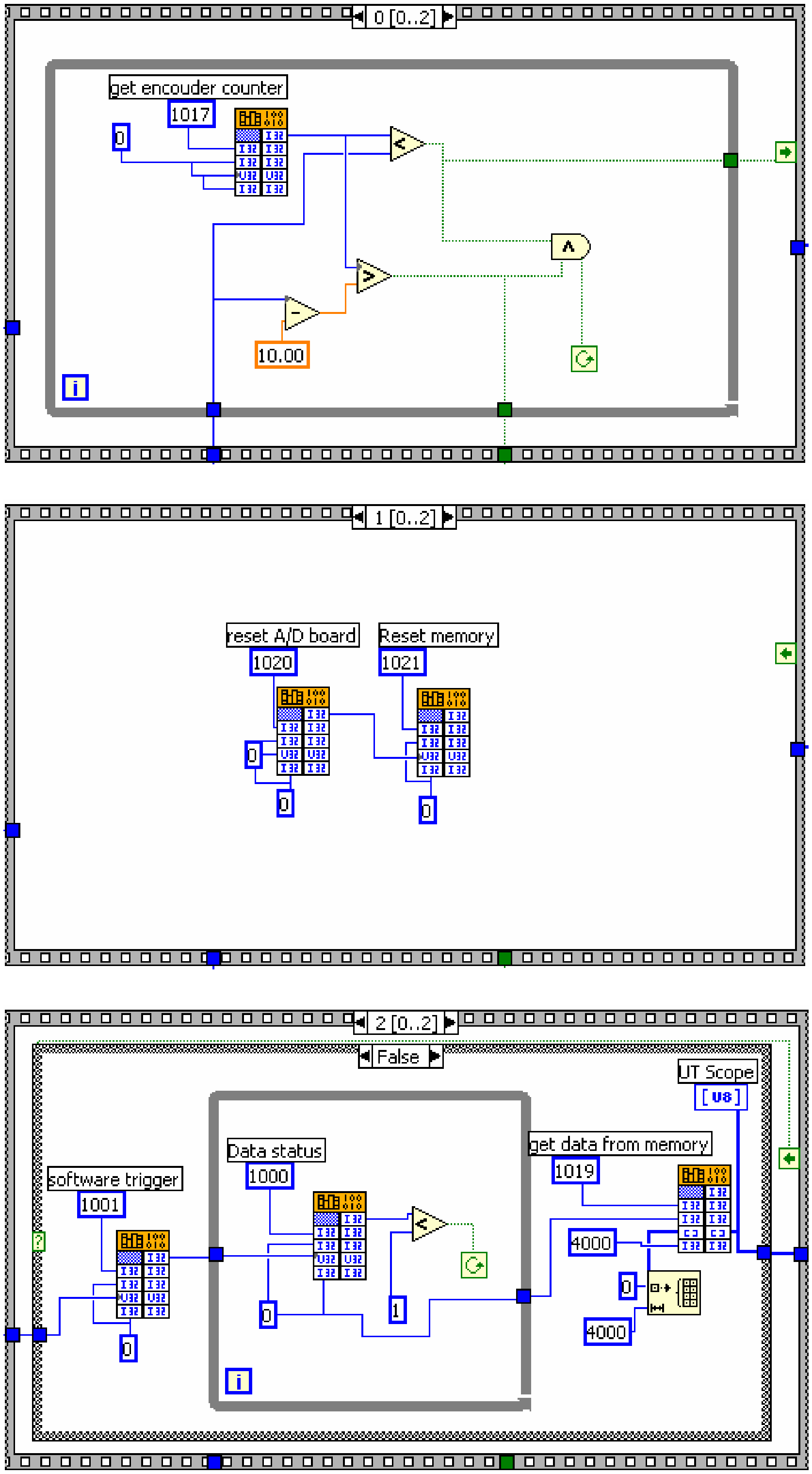
0 [0..2]
get encouder counter
1017
0
10.00
1 [0..2]
reset A/D board
1020
0
0
Reset memory
1021
0
2 [0..2]
False
software trigger
1001
0
Data status
1000
0
1
get data from memory
1019
UT Scope
[U8]
4000
0
4000

Sequence 2

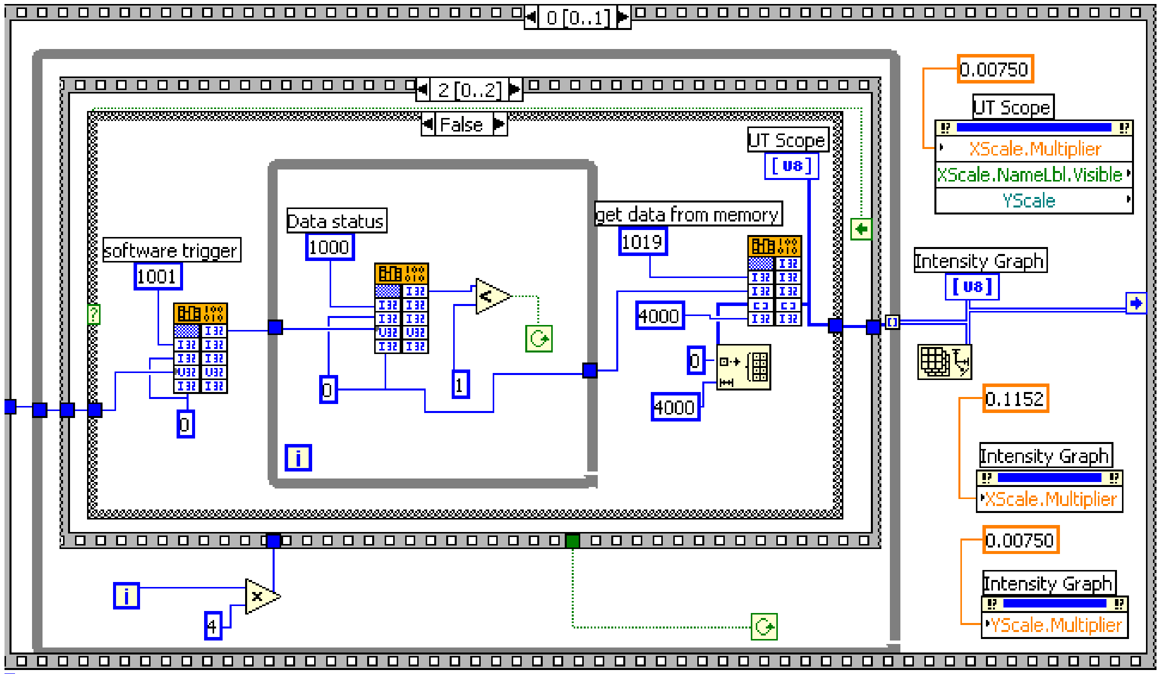
0 [0..1]
2 [0..2]
False
software trigger
1001
0
Data status
1000
0
1
i
get data from memory
1019
4000
0
4000
UT Scope
[U8]
0.00750
UT Scope
XScale.Multiplier
XScale.NameLbl.Visible
YScale
Intensity Graph
[U8]
0.1152
Intensity Graph
XScale.Multiplier
0.00750
Intensity Graph
YScale.Multiplier
i
4

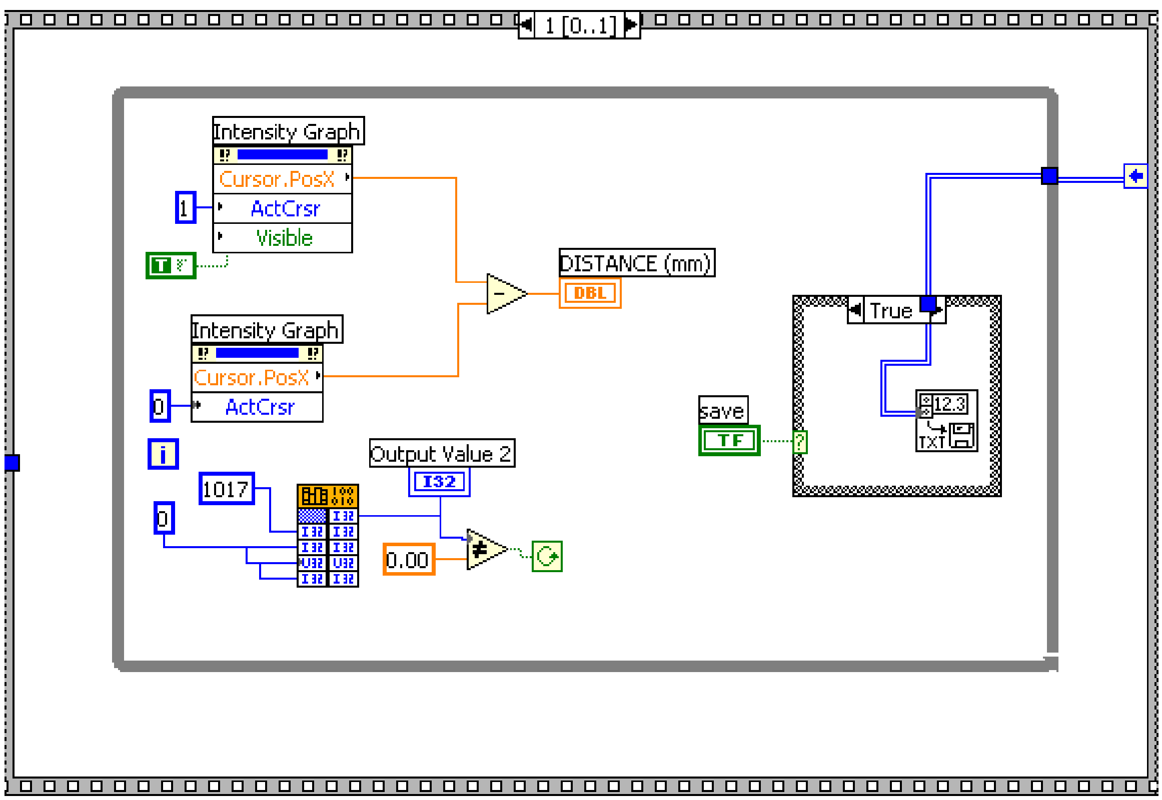
1 [0..1]
Intensity Graph
Cursor.PosX
ActCrsr
Visible
1
Intensity Graph
Cursor.PosX
ActCrsr
0
i
DISTANCE (mm)
DBL
Output Value 2
I32
1017
0
0.00
save
TF
True
12.3
TXT

APPENDIX D
COMMERCIAL ULTRASOUND SYSTEMS

D.1 Introduction

There are many highly sophisticated and multipurpose ultrasound systems available in today’s market.
Some of the major companies developing these systems are

1) Siemens
2) General Electric
3) Philips
4) Aloka
5) Pyramid
6) TeraRecon

D.2 General Electric (GE) Ultrasound System

GE Healthcare's broad range of products and services enable healthcare providers to better diagnose and treat many diseases and disorders with ease.
GE Healthcare has 15 major products grouped into four families in its global Ultrasound business:
1) **Leadership Ultrasound –** High end ultrasound systems like LOGIQ9, LOGIQ7, Voluson 730 and LOGIQWorks.
2) **Value Ultrasound –** Mid-range and portable ultrasound systems like LOGIQ5, LOGIQ3, LOGIQBook.
3) **Echo Cardiology Systems –** Ultrasound products related to Cardiac application like Vivid 7, Vivid 4, Vivid 3 and Echopac.
4) **Primary Care Diagnostic Systems –** Products related to bone densitometry 42.

After a little research it was found that the LOGIQ Book XP which can be used for musculoskeletal imaging matches our requirement.
The LOGIQ Book XP as shown in figure D.1[45], is a high performance multipurpose color hand-carried imaging system designed for abdominal, obstetrics, gynecology, vascular, musculoskeletal, small parts, pediatric and neonatal applications.

Figure D.1: LOGIQ Book XP from GE

D.2.1 Specifications

Dimensions and Weight

- · Height: 78 mm(3.07 in)console only 99.5 mm (3.92 in)with handle
- · Width: 350 mm (13.78 in)
- · Depth: 280 mm(11 in) console only 430 mm (12.6 in) with handle
- · Weight: approx. 4.2 kg (9.2 lb.)

Console Design

- Laptop Style
- Integrated HDD (20GB)
- Wireless LAN Support
- 1 probe p ort with micro-connector
- Rear handle

Scanning Methods

- Electronic Convex
- Electronic Linear with slant scanning

Transducer Types

- Convex Array
- Microconvex Array
- Linear Array

Operating Modes

- B-Mode
- M-Mode
- Color Flow Mode (CFM)
- Power Doppler Imaging (PDI)
- Pulse Wave Doppler(PWD)

Standard Features

- High Resolution 10.4 inch Color LCD
- 435 Frames (15 sec) Standard CINE
- Memory (64MB)
- 20GB(over 4,000 images) Hard Drive
- Loops storage-from'on the fly' scanning and from memory
- Automatic Optimization [45]

D.2.2 Price:

The total cost of the equipment is $39,040.00. This includes:

1) LOGIQ BOOK XP Compact Digital Ultrasound Console
2) 8L-RS Probe: This is a wide band liner probe 4 – 10 MHz which supports small parts, vascular, musculoskeletal, pediatrics and breast imaging. It has a 39 mm aperture.
3) 3S-RS Phased array transducer: Wide band multi-frequency transducer with bandwidth between 1.5 and 3.6 MHz. This can be used for imaging and screening, abdominal, trauma, and Transcranial imaging.

More information can be found on the official website of GE, http://www.gehealthcare.com/usen/ultrasound/products/logiq.html

D.3 Philips HD11 XE Ultrasound System

The Philips HD 11 XE Ultrasound System is shown in Figure D.2. From its digital broadband beamformer with proven SonoCT imaging, to its powerful XRES image processing, every HD11 XE system is built for High Definition performance. This means enhanced edges and margins for more sharply defined structures, with reduced noise and speckle, for better visibility and contrast of even the smallest structures. Clinicians are demanding smaller, higher performing systems specifically designed to meet their clinical and operational challenges. The new Philips HD11 XE system provides a powerful architecture for superb High Definition performance; elegant design for ergonomics, mobility and ease-of-use; and a versatile suite of applications and options for highly-flexible configurations [50].

Figure D.2: Philips HD 11 XE Ultrasound System

D.3.1 Specifications:

The HD11 XE system provides the foundation for an ergonomic environment that adapts to virtually any scanning condition for optimal user comfort and convenience.

- Its independent adjustment of monitors and controls, specifically monitor and control panel height and articulation, meet Industry Standards1 for the prevention of WRMSD, facilitating neutral working postures and reducing repetitive stress injuries.
- The HD11 XE features an ultra-bright, flickerless LCD flat panel display for reduced eye strain in rooms that are dark or bright.
- Users experience less fatigue – department productivity and workflow are optimized1.
- As the lightest and smallest system in its class, the HD11 XE system is the ultimate for portability—no more moving the most challenging patients to take advantage of advanced imaging capabilities on larger high performance machines.
- Up to five available ports reduce bending to switch out transducers.
- Advanced circuitry helps keep users and patients more comfortable by promoting a quiet and cool scanning environment.
- The integrated footrest allows correct posture, reducing stress on the spine [50].

D.3.2 Applications

- Pediatric
- Breast
- Vascular
- Transesophageal
- Musculoskeletal
- Orthopedics
- Doppler
- Cardiac

D.3.3 Transducer

- The HD11 XE system supports over 20 transducers, including many from the Explora line, for flexibility in meeting most any clinical need.
- New superflex cable technology is extremely flexible and lightweight, dramatically easing wrist strain.
- Explora transducers feature new low-loss lens design and next generation microelectronics to deliver maximum acoustic efficiency for greater penetration and resolution [50].

L12-5 50 mm

- Fine pitch, 256 elements, high resolution linear array
- 12 to 5 MHz extended operating frequency range
- 50mm effective aperture length
- 10 degrees of trapezoidal imaging
- Steerable pulsed wave, color Doppler, and Color Power Angio, Panoramic, SonoCT , XRES and harmonic imaging
- High resolution superficial applications including vascular, small parts, breast, and musculoskeletal imaging
- Supports stainless steel, reusable biopsy guides (up to 14 gauge)

D.4.4 Price

The Price of the Philips HD 11 XE ultrasound system is $75,000.

D.4 Siemens Sonoline G20 ultrasound System

The SONOLINE G20™ ultrasound system, shown in figure D.3, quickly distances itself from the competition with next-generation all-digital system architecture that utilizes Siemens technology migration. Individual imaging parameters have been optimized for a wide variety of clinical applications and patient types [48].

- All-digital signal processing technology creates excellent image quality.
- State-of-the-art beamforming provides a wide acoustic aperture, improved image resolution, uniformity and penetration for difficult-to-image patients.
- All-digital G20 system architecture enables seamless integration of advanced capabilities including DICOM connectivity solutions, Tissue Harmonic Imaging (THI) and TGO™ tissue grayscale optimization technology.
- Ongoing performance enhancements, which require only simple, cost-effective software upgrades, protect your initial investment into the future.
- Slim, lightweight design with small footprint and four swivel wheels makes the system ideally suited for use in tight workspaces and easily maneuverable from suite to suite and patient to patient.
- Intuitive interface with the familiar Windows®-based operating system promotes efficient and ergonomic system control via on-screen menus and proprietary ReadySet™ workflow shortcuts.
- The operating system software supports all standard applications, exam specific imaging presets, measurements, pictograms, annotations, reports, worksheets and system diagnostics
- QuickSet™ user programmable system parameters and integrated cine review streamline exams and enhance workflow
- TGO technology for instantaneous, one-button image optimization
- Tissue Harmonic Imaging (THI) is available to enhance visualization, particularly in difficult-to-image patients
- MultiHertz™ multiple frequency imaging optimizes penetration and resolution to expand the clinical versatility of each transducer [48].

Figure D.3: Sonoline G 20 Ultrasound, gray scale imaging

D.4.1 Specifications:

- Ultrasound imaging system supporting linear and convex transducers in the frequency range of 2.8 to 10.0 MHz.
- Imaging modes of B, M, A and their combinations. Field size (depth) from 3 cm to 24 cm. Comprehensive measurement, calculation and report packages integrated.
- Monitor 12 Inch (non-interlaced).
- DIMAQ Integrated Ultrasound Workstation standard.
- CD-RW for Patient Studies, Presets, Quicksets, reports, system software.

D.4.2 Applications:

- Small Parts
- Breast
- Vascular
- Musculoskeletal
- Orthopedics

D.4.3 Transducers

The 7.5L75S linear array transducer uses ultra-sensitive wideband 128-element technology for improved resolution and penetration. User-selectable MultiHertz multiple-frequency imaging expands its clinical versatility.

Features include:

- 2D, M-Mode frequency range: 5-8 MHz
- Doppler frequency range: 7 - 5 MHz
- Active field of view: 67 mm
- Optional stainless steel biopsy attachment [48]

D.4.4 Price:

The total equipment cost around $24, 860 including

1) SONOLINE G20 Ultrasound system with operating system
2) 7.5L75S Linear Array Transducer
3) Mitsubishi B&W Thermal Printer

More information can be found on:
http://www.medical.siemens.com/siemens/en_AU/gg_us_FBAs/files/brochures/Sonoline/G20Brochure.pdf#search=%22sonoline%20g20%20specifications%22

D.5 Aloka

The ProSound SSD-4000, shown in figure D.4 utilizes the most advanced acoustic technologies available today, and its multidisciplinary technology architecture enables it to offer great versatility and flexibility over a wide range of clinical applications.
The system employs a Pure Harmonic Detection (PureHD) feature to create exceptionally clear images—artifact free and with a higher signal-to-noise ratio. This is especially useful when scanning traditionally difficult-to-scan patients (e.g., the aged or the obese).
The PureHD technology enables distortion-free fundamental frequency transmission as well, which makes harmonic images much clearer. This maximizes the affect of both the Tissue and the Contrast harmonic echo by providing excellent contrast and spatial resolution [47].

Figure D.4: Aloka SSD 4000 Utrasound System

D.5.1 Specifications

Scanning Method

- Electronic Convex Sector
- Electronic Linear
- Electronic Phased Array Sector

Image Display Modes

- B: gray-scale imaging
- M
- Flow: Color Doppler and Power Flow imaging
- Dual B
- B and M
- B and D
- B(Flow)
- Dual B(Flow)
- M(Flow)
- B(Flow) and M(Flow)
- B(Flow) and D
- Triplex mode: B, Flow, and PW Doppler simultaneous real-time display
- Dual Dynamic Display (DDD): B and B(Flow) simultaneous real-time display

System Dynamic Range

- 172 dB

Number of Processing Channels

- 256 channels

Frame Rate

- Max. 500 frames/sec or more [47].

D.5.2 Pricing

The equipment costs $96,300.00, which includes

1) SSD-4000 Surgery Color Console with Harmonic Imaging
2) UST-579T-7.5 Side Fire T-Shaped Linear Probe (60 mm aperture)
3) 1 UP-895MD Sony B/W Printer

More information can be found on:
http://www.aloka.com/products/view_system.asp?id=4

D.6 Pyramid

The Pyramid 800 shown in figure D.5 is designed to enable improved ultrasonic diagnosis of the musculoskeletal system. It is a portable scanner utilizing a smaller monitor for improved contrast resolution of bones, muscles and tendons. High resolution 7.5 Mhz linear array imaging, with electronic focussing, makes this the ideal musculoskeletal system.

Figure D.5: Pyramid 800 Ultrasound System

D.6.1 Specifications

Probe Frequency: 3.5 to 7.5 MHz
Scanning System: Electronic Convex and Linear Scanning
Scanning Mode: B and M Mode
Image processing: Pre-processing, Correlation-Processing, Interpolation
Zooming: $^{x}1$, $^{x}1.2$, $^{x}2$ as well as depth shift
Measuring & Calculation: Distance, Area, Circumference, Heart Rate

Character Display: ID, Date, Time, Frequency, Gain, Zoom, Focus, Comments (with keyboard), etc.
Power Requirements: 110V/220V, 140VA [46].

D.6.2 Price:
The total equipment costs only $9,500.00. This includes

1) Main unit with digital scan converter
2) 7.5 MHz Linear array probe
3) Alpha-Numeric Keyboard
4) Accessories : Dust-proof cover, Cables and Operation Manual
5) Extra Accessories (not included in price):
    - 3.5MHz Linear Probe EZU-PL21
    - 5.0MHz Linear Probe EZU-PL22
    - 5.0MHz Transvaginal EUP-V12B
    - 5.0MHz Convex Probe EZU-PC2B
    - 5.0MHz Microconvex Probe EZU-PC4B
    - Sony Video Printer B/W UP-890
    - Trolley/Mobile Cart
    - 9 inch monitor [46].

More information on this system can be found at: http://www.pyramidmed.com/pms-ultrasoundsystems.html

D.7 TeraRecon

The UF-850XTD shown in figure D.6 from TeraRecon is a mid-range ultrasound system. This is ideally suited for musculoskeletal imaging applications. TeraRecon's XTrillion image processing chip technology provides the underlying foundation for achieving high frame rates and high definition imaging [49].

Figure D.6: Cart Base Ultrasound system UF-850XTD from TeraRecon

D.7.1 Clinical Benefits:

- View soft tissue above and between underlying bones.
- Assess complete and partial tears in tendons, ligaments, and muscles in a dynamic state by viewing pathology missed by static imagery or more expensive CT and MR.
- Image superficial skeletal structures, muscle fibers, and nerves in the wrist.
- Image discontinuity of cortical bone, bony spurs, and septic arthritis.
- Visualize carotid artery stenosis, deep venous thrombosis, and peripheral arterial disease.
- Assess abdominal pathology such as aortic aneurysm, liver pathology, gallstones, and kidney diseases.

D.7.2 Specifications:

- It has a footprint of 19"W x 32"D) featuring a Dual Receiving Digital Beam former with multi-frequency Transducer.
- Features Digital storage on integrated high capacity hard disk or CDR/ RW or USB memory.
- Features a 15-inch TFT Color LCD monitor, (DICOM 3.0 Connectivity, Print & Worklist capabilities are available options)

D.7.3 Scanning Modes:

Standard capabilities include B-Mode (2-D), M-Mode and Color M-Mode, Color Flow Mapping PW Power Doppler, Triplex mode and Tissue Harmonic Imaging and basic measurements and reporting packages. Fully Digital Platform Architecture and software oriented features allows for flexible expandability.

D.7.4 Transducers:

1) Linear Probe 38mm 6.0/7.5/9.0 MHz
2) Linear Probe 30mm 8.0/10.0/14.0 MHz [49].

D.7.5 Price:

This total equipment costs $41,200.00. This includes

1) UF-850XTD Multi-function, All Digital Color Doppler Ultrasound System
2) Linear Probe 30mm 8.0/10.0/14.0 MHz - FUG-LG308-16A – (for UF-850XTD)
3) Linear Probe 38mm 6.0/7.5/9.0 MHz - FUT-LG386-9A – (for UF-850XTD)
4) Mitsubishi P-93W A6 Monochrome Thermal Printer – P-93W

More information can be found on: http://www.terarecon.com/products/us_prod.html

D.8 Comparison:

The table D.1 shows the comparison of all the commercially available ultrasound system we have researched.

	GE	Siemens	Pyramid	Aloka	TeraRecon	Philips
Price	$39,040	$24, 860	$9,500	$96,300	$41,200	$70,000
Type of Probes	Linear	Linear	Linear	Linear	Linear	Linear,
Aperture Length	39 mm	75 mm	38 mm	60 mm	38mm	50 mm
Application	Abdominal, obstetrics, gynecology, vascular, musculoskeletal, small parts, pediatric and neonatal	Small Parts, Breast,Vascular ,Musculoskeletal,Orthopedics	Musculoskeletal	Cardiac,Abdominal, obstetrics, gynecology, vascular, musculoskeletal, urology and many more	Musculoskeletal, muscle fibers,nerves in the wrist, abdominal pathology, liver pathology, gallstones, and kidney diseases	Pediatric, Breast, Vascular, Transesophageal, Musculoskeletal, Orthopedics, Doppler, Cardiac,Abdominal, Liver pathology, Muscles, obstetrics, and gynecology
Cart base or Laptop Based	Laptop	Cart	Cart	Cart	Cart	Cart
Availability in US	Yes	Yes	Yes	Yes	Yes	Yes
Screen	High Resolution 10.4 inch Color LCD	12 Inch	9 Inch	15 inch	15-inch	15 inch
Display	Color	Gray Scale	Gray Scale	Color	Color	Color and grayscale
Operating Modes	B-Mode, M-Mode, Color Flow Mode (CFM), Power Doppler Imaging (PDI), Pulse Wave Doppler(PWD).	B, M, A and their combinations.	B and M	B: gray-scale imaging, M Flow: Color Doppler, PowerFlow imaging, Dual B, B and M, B and D, B(Flow), M(Flow), and D Triplex mode: B, Flow, and PW, Doppler simultaneous real-time display, Dual Dynamic Display.	B-Mode (2-D), M-Mode and Color M-Mode, Color Flow Mapping PW Power Doppler, Triplex mode and Tissue Harmonic Imaging and basic measurements and reporting packages	B-Mode (2D), M-Mode, Doppler, Power and Color Imaging, 2D Contrast Specific Imaging, 2D Pulse Inversion Harmonic Imaging, Tissue Doppler Imaging, Color Power Angio, Power Motion Imaging, ECG

Table D.1: Comparison of Ultrasound Systems

APPENDIX E

These are the web references used in this research work:

34. http://www.naturalcareli.com/flexion.html

35. http://www.spineuniverse.com/displayarticle.php/article897.html

36. http://www.logan.edu/pages/chiro_tech_cox.asp

37. http://www.ndt-ed.org/

38. http://www.kettering.edu/~drussell/Demos/waves/wavemotion.html

39. http://www.reedlink.com/ProductInfo~Productid~39528~ProductName~Ultrasonic-Transducers.html

40. http://www.imasonic.com/Industry/PAprinciple.php

41. http://www.spinalinjury.net/html/_anatomy_of_the_spinal_cord_co.html

42. University of Maryland Spine Center, www.umm.edu/spinecenter/education

43. www.spineuniversity.com

44. http://www.gehealthcare.com/company/docs/ultrasound4.pdf

45. http://www.gehealthcare.com/usen/ultrasound/products/lbook_index.html

46. http://www.pyramidmed.com/pms-ultrasoundsystems.html

47. http://www.aloka.com/products/view_system.asp?id=4

48. http://www.medical.siemens.com/webapp/wcs/stores/servlet/ProductDisplay~q_catalogId~e_-1~a_catTree~e_100001,12805,12761~a_langId~e_~a_level~e_0~a_productId~e_138562~a_storeId~e_10001.htm

49. http://www.terarecon.com/products/us_prod.html

50. http://www.medical.philips.com/main/products/ultrasound/general/hd11_xe/index.htm

51. www.usultratek.com , USUltratek

52. www.magma.com , MAGMA.